

Running coupling and power corrections in nonlinear evolution at the high-energy limit

Einan Gardi^{1,2}, Janne Kuokkanen³, Kari Rummukainen^{3,4}, and Heribert Weigert⁵

¹ Cavendish Laboratory, University of Cambridge, J J Thomson Avenue, Cambridge CB3 0HE, UK

² Department of Applied Mathematics & Theoretical Physics, Wilberforce Road, Cambridge CB3 0WA, UK

³ Department of Physical Sciences, University of Oulu, P.O. Box 3000, FI-90014 Oulu, Finland

⁴ Department of Physics, Theory Division, CERN, CH-1211 Geneva, Switzerland

⁵ Department of Physics, The Ohio State University, Columbus, OH 43210, USA

A main feature of high-energy scattering in QCD is saturation in the number density of gluons. This phenomenon is described by non-linear evolution equations, JIMWLK and BK, which have been derived at leading logarithmic accuracy. In this paper we generalize this framework to include running coupling corrections to the evolution kernel. We develop a dispersive representation of the dressed gluon propagator in the background of Weizsäcker Williams fields and use it to compute $\mathcal{O}(\beta_0^{n-1}\alpha_s^n)$ corrections to the kernel to all orders in perturbation theory. The resummed kernels present infrared-renormalon ambiguities, which are indicative of the form and importance of non-perturbative power corrections. We investigate numerically the effect of the newly computed perturbative corrections as well as the power corrections on the evolution and find that at present energies they are both significant.

1 Introduction

Modern hadron collider experiments such as HERA, RHIC and especially the forthcoming LHC operate at high enough energies to observe new phenomenon associated with high gluon density. The principal characteristics of high-energy QCD scattering are the following: firstly, owing to Lorentz contraction, the configurations probed appear to be *frozen in time* compared to the natural time scales of the interaction. Secondly, the number density of soft gluons gets *saturated* at densities of the order of $1/g^2$. These features, which are usually referred to as the Color Glass Condensate (CGC), are a consequence of the non-Abelian nature of the interaction and of the fact that gluons are massless. These features are therefore unique to QCD.

At sufficiently high energy the dominant interaction between the projectile and the target can be described by ensembles of boost-enhanced field configurations, the “frozen” modes mentioned above. This has been extensively explored in the context of the McLerran–Venugopalan model [1–9]. This description is tailored for asymmetric situations in which the field of, say, the target can be argued to be much stronger than that of the projectile. High-energy scattering of a virtual photon on a large nucleus is the prototype example of this situation. Nonetheless, at sufficiently high energy this generic picture is applicable to nucleus–nucleus scattering as well.

Energy dependence can be incorporated into this picture by taking into account fluctuations that acquire properties of the previously frozen modes as one increases the collision energy. The relevant contributions are characterized by large logarithms $\ln(s)$ in the total invariant energy s in the collision. At low gluon densities, or weak fields, the resummation of high-energy logarithms has been formulated long ago as a *linear evolution equation* for the gluon distribution function, the BFKL equation [10–14]. However, at high densities the resummation of these logarithms leads instead to *non-linear evolution equations* for gauge field correlators. These can be formulated as a functional evolution equation known as the JIMWLK equation [6, 15–22], or equivalently, as an infinite coupled hierarchy of evolution equations for field correlators known as the Balitsky hierarchy [23–25]. A truncation of this hierarchy that retains most of its essential properties is known as the BK equation [23–27]. This equation describes high-gluon-density dynamics in terms of dipole degrees of freedom. In Refs. [26, 27] the BK equation has been derived from Mueller’s dipole model [28–31], using nuclear enhancement as a tool to trace the dominant field configurations. This extends the ideas of the dipole model beyond the mere onset of saturation effects [32].

The most prominent feature of the solutions of these non-linear evolution equations is the emergence of an energy-dependent transverse correlation length R_s , or saturation scale $Q_s \sim 1/R_s$, which, asymptotically, encodes all the energy dependence of the cross section. The saturation scale characterizes the transverse momentum scales of radiated gluons that contribute to the evolution at any given energy. Modes much softer than Q_s decouple: the number densities of soft gluons are saturated, so they remain constant as the energy increases. Independently of the initial condition, at sufficiently high energies the saturation scale increases rapidly with the energy. Therefore, Q_s can be considered a hard scale: $Q_s \gg \Lambda$.

The possibility to describe saturation by perturbative evolution equations is a highly non-trivial result, since the gauge field involved is necessarily strong. The evolution equation is derived perturbatively by expanding in small fluctuations on a strong background field. This is justified a posteriori: having found that soft modes do not contribute to the evolution, the equation is perturbatively consistent. This kind of infrared stability is a direct consequence of gluon saturation. It is therefore not shared by the linear BFKL equation, which is instead afflicted by diffusion into the infrared. As was beautifully illustrated in Ref. [33] it is the non-linearity of the JIMWLK and BK equations that makes them infrared stable. The presence of the nonlinearities and hence Q_s will also modify the rôle and influence of power corrections compared to the BFKL case discussed in Ref. [34].

Despite these strengths, JIMWLK and BK evolution suffer from a serious shortcoming: they are derived only at leading logarithmic accuracy, i.e. at fixed coupling. To partially compensate for this, all recent studies of the evolution have included running-coupling effects in some more or less ad hoc manner. There are several reasons why running-coupling effects are essential:

- Running-coupling effects are known [35–43] to provide a large part of the next-to-leading-

order (NLO) corrections to the evolution in the low density limit, where the description matches onto the BFKL equation.

- On the purely phenomenological side, for example in fits to HERA data [44], running coupling (or more precisely a dependence of the coupling on a scale involved in a single emission step, see below) is essential to slow down evolution by reducing gluon emission from small objects.
- Conceptually, it is understood that the evolution is dominated by scales of the order of Q_s . The non-linearity of the equation ensures that dipoles much larger than $1/Q_s$ are inherently suppressed through the evolution (the saturation mechanism). However, with strictly fixed coupling, dipoles *much smaller* than $1/Q_s$ still contribute to the evolution. As soon as the coupling depends on the size of the emitting dipole such contributions are also suppressed through the evolution [45].

Despite both the practical and conceptual importance of running-coupling effects in the nonlinear evolution equations, there has been no derivation of how they enter. All simulations done so far involved ad hoc prescriptions for the scale of the coupling, based on nothing more than educated guesswork.

In this paper we approach the problem on the more fundamental level. We show that the JIMWLK and BK equations can indeed be derived beyond the fixed coupling level. We find that the equations take a similar form to the fixed coupling case, while their kernel changes in a rather drastic way. For example, it does not naturally appear as a single scale-dependent coupling times the LO scale-invariant kernel. We explicitly compute running coupling $\mathcal{O}(\beta_0^{n-1}\alpha_s^n)$ corrections to the kernel to all orders and resum them by means of Borel summation. We find that the resummed kernel present infrared-renormalon ambiguities. These are indicative of the form and importance of non-perturbative power corrections.

In order to perform this calculation we develop a dispersive representation of the dressed gluon propagator *in the background of Weizsäcker-Williams fields*. This is a generalization of the well-known dispersive representation of the *free* dressed gluon propagator, a technique that has been used to compute running-coupling corrections and estimate power corrections in a variety of applications, see e.g. [46–55].

As in the BFKL case, the non-linear evolution equations are expected to receive additional sub-leading corrections, which are not related to the running of the coupling. In this paper we will not attempt to include such corrections. Some steps in this direction on the level of the BK equation have been taken in Ref. [56], or with an entirely different focus in Ref. [57], and can be combined with our treatment where desired.

The structure of the paper is as follows: in Sec. 2 we give a short introduction to the physics described by the JIMWLK equation, in order to establish the key ideas and the notation that will be used in the rest of the paper. For more detailed background we refer the reader to the original literature [6, 15–27] or review articles [58–61]. In Sec. 2.1 we briefly review the JIMWLK and BK equations and recall those details of their derivation that are needed in what follows. Sec. 2.2 is devoted to a discussion of running-coupling effects in JIMWLK and BK evolution, contrasting what has been done previously with what we want to achieve in this paper. This will be important also to clarify the terminology used in the remainder of the paper. Sec. 3 extends the derivation of the JIMWLK equation to the running-coupling case. It is divided into four subsections: Sec. 3.1

collects the tools of the conventional dispersive technique for the calculation of running-coupling corrections in the free field case. Sec. 3.2 generalizes these tools for use in the presence of the Weizsäcker-Williams background as needed in the derivation of the JIMWLK equation. Sec. 3.3 presents a re-derivation of the JIMWLK equation with a running coupling. Next, in Sec. 3.4 we formulate the newly computed corrections to the kernel as an all-order Borel sum. In Sec. 4 we discuss the convergence of perturbation theory. In Sec. 5 we use the renormalon singularities to determine the parametric form and the typical magnitude of power corrections affecting the kernel. Finally, in Sec. 6 we investigate numerically the effect of running coupling and power corrections on the BK evolution as a function of the saturation scale. In Sec. 7 we summarize our conclusions.

2 The physics of the JIMWLK equation

The key points can be most easily understood in the context of deep inelastic scattering (DIS) of leptons on protons or nuclei, where q and p are the momenta of the virtual photon and the target respectively. Here, two kinematic variables play a rôle: (1) the deeply-spacelike momentum $q^2 = -Q^2 < 0$ carried by the exchanged photon. This scale defines the transverse resolution of the probe and thereby the apparent size of the quarks and gluons encountered; and (2) Bjorken $x := Q^2/(2p \cdot q)$, which is inversely proportional to the total energy $s = (p + q)^2$ in the collision: $x \approx Q^2/s$. At high energy, the *rapidity* Y is directly related to Bjorken x via $Y = \ln(1/x)$. The rapidity is the natural evolution variable since $\ln(1/x) \approx \ln(s/Q^2)$ reflects the large hierarchy of scales in the high-energy limit, which appears with increasing powers in perturbation theory.

At large Q^2 with fixed x there are well-established methods to treat such a system based on the Operator Product Expansion (OPE), a short-distance expansion in powers of $1/Q^2$. Since Q^2 also controls the apparent size of the particles encountered, the OPE can be viewed as a small density expansion, despite the fact that particle numbers, driven by large logarithms in Q^2 , increase in parallel with increasing resolution. As a consequence the description at large Q^2 can be based entirely on single-particle properties such as quark and gluon distribution functions: particle correlations are not important. This restriction is a key ingredient of the derivation of the Dokshitzer-Gribov-Lipatov-Altarelli-Parisi (DGLAP) equations that describe the increase of particle numbers with Q^2 in this domain.

Going to small x at fixed Q^2 , no matter how large, one ends up in an entirely different domain, that of high densities, even if one starts out in a dilute situation. As the energy increases BFKL evolution keeps generating new particles (mostly gluons) which are all of effective size of $\mathcal{O}(1/Q^2)$, and so the density keeps increasing. Eventually the density reaches a level where particle correlations become essential [28–32] and a description in terms of distribution functions alone becomes untenable. Since the BFKL description is based on gluon distributions, this is also the point where this evolution equation ceases to be adequate. Appropriate degrees of freedom and more general evolution equations are needed to describe the system beyond this point. The most general of these existing to date are the JIMWLK equation, or, the completely equivalent Balitsky hierarchies, with their factorized truncation, the BK equation.

JIMWLK and BK equations are formulated in terms of path-ordered exponentials, as defined in Eq. (2) below, with paths collinear to the projectile direction, which can be interpreted as quark and gluon constituents of the projectile. The path-ordered exponentials encode the fact that, owing

to the high energy in the collision, these constituents penetrate the target without being deflected from their straight-line trajectories. The γ^*A cross section then reads

$$\sigma_{\text{DIS}}(Y, Q^2) = \text{Im} \left[\text{Diagram} \right] = \int d^2r |\psi|^2(r^2 Q^2) \int d^2b \left\langle \frac{\text{tr}(1 - U_{\mathbf{x}} U_{\mathbf{y}}^\dagger)}{N_c} \right\rangle (Y) \quad (1)$$

where $\mathbf{r} = \mathbf{x} - \mathbf{y}$ corresponds to the transverse size of a given $q\bar{q}$ dipole and $\mathbf{b} = (\mathbf{x} + \mathbf{y})/2$ to the impact parameter of this dipole relative to the target. $q^2 := -Q^2$ is the large spacelike momentum carried by the virtual photon. The square of the $q\bar{q}$ component of the photon wave function $|\psi|^2(r^2 Q^2)$ describes the probability to find a $q\bar{q}$ pair of size r inside the virtual photon and can be calculated in QED. It consists of a known combination of Bessel functions together with an integral over longitudinal momentum fractions already absorbed in the notation. The remaining factor, the expectation value of U -operators is usually called the dipole cross section $\sigma_{\text{dipole}}(Y, \mathbf{r})$ of the target in question. All the properties of this interaction — details of the target wave function, gluon exchange between the target and projectile etc. — are encoded in this expectation value. The leading-logarithmic corrections at small x appear in powers of $\alpha_s \ln(1/x)$. These corrections are resummed by the JIMWLK equation.

The dipole operator $\hat{N}_{\mathbf{x}\mathbf{y}} := \text{tr}(1 - U_{\mathbf{x}} U_{\mathbf{y}}^\dagger)/N_c$ itself is naturally bounded between zero and one. Typically, gluon densities grow towards large r , such that the expectation value of $\hat{N}_{\mathbf{x}\mathbf{y}}$ interpolates between 0 for infinitesimally small dipoles, and 1 for very large ones. This encodes the idea of color transparency at short distances and saturation at large distances where gluon densities grow up to $\mathcal{O}(1/g^2)$. The length scale that characterizes the transition between the two domains can be interpreted as the correlation length R_s of U -operators, or equivalently gluon fields. The corresponding momentum scale $Q_s \propto 1/R_s$ is usually called the saturation scale. Clearly, as more gluons are generated in JIMWLK evolution towards small x , the correlation length gets small and Q_s increases.

One key feature that emerges for this evolution is that details about the initial conditions are erased quickly and a universal scaling form of correlators such as the dipole cross section is reached. From then on, all x or Y dependence is carried by the saturation scale $Q_s(Y)$. Such behavior has been seen in HERA data (geometric scaling) [62–64] and has important consequences for RHIC (disappearance of Cronin enhancement from mid to forward rapidities) [65–69] and the LHC experiments where the energies are higher.

It had been noted early on in the context of the BK equation that a treatment at the strictly leading-logarithmic level is insufficient: running-coupling effects have a strong influence on the speed of evolution; quantities like the evolution rate $\lambda(Y) := \partial_Y \ln Q_s^2(Y)$ are reduced by more than 50% if running-coupling effects are introduced (in some heuristic way). Despite the explicit scale breaking introduced by the appearance of Λ_{QCD} in the running coupling, scaling of the dipole cross section with Q_s is retained to very good accuracy. In Ref. [45] it was emphasized that running-coupling effects are also conceptually important: only with running-coupling effects included does the phase-space region active in the evolution center around the physical scale Q_s . At strictly leading-logarithmic level — in the conformal limit for the evolution kernel — the evolution involves short-distance¹ contributions from more than 7 orders of magnitude away from the physical scale.

¹As explained above, the infrared is not a problem due to the presence of the correlation length R_s , which acts as an effective infrared cutoff.

Unlike the other evolution equations in QCD, such as DGLAP and BFKL, the JIMWLK and BK equations have been derived only at leading logarithmic accuracy. Only partial calculations of two-loop corrections to the BK equation are available [56] but they do not include any attempt to determine the running of the coupling. For our purposes, the existing results in the low-density limit for BFKL evolution are of limited use: they offer no hint as for how to extend or extrapolate the calculation into the high-density domain where non-linearities appear. A direct calculation in the context of the JIMWLK and BK equations is therefore necessary.

As announced in the introduction, in this paper we compute running-coupling corrections to the JIMWLK and BK equations. In Sec. 2.1 we briefly review the fixed-coupling derivation of the JIMWLK equation, by considering small fluctuations in a strong Weizsäcker-Williams field that is encoded in the eikonal factors of Eq. (1). This derivation will then be generalized to the running-coupling case in Sec. 3 using a dispersive representation of the dressed gluon propagator in such a background field. This will not only enable us to calculate running-coupling corrections, but also to explore non-perturbative effects in the evolution.

2.1 Evolution equations

The JIMWLK equation and the Balitsky hierarchies

The JIMWLK equation is a functional Fokker-Planck equation for the statistical weight $Z_Y[U]$ defining the Y -dependent averaging procedure $\langle \dots \rangle(Y)$ that determines the expectation value of operators $O[U]$ made of an arbitrary number of path-ordered exponentials U , where

$$U_{\mathbf{x}}^{-1} = P \exp \left\{ ig \int_{-\infty}^{\infty} dz^- \delta(z^-) \beta(\mathbf{x}) \right\} . \quad (2)$$

Such an average was already encountered above in Eq. (1) in the case of the dipole operator $\text{tr}(1 - U_{\mathbf{x}} U_{\mathbf{y}}^\dagger) / N_c$. To understand why these averages determine virtually all cross sections at small x , recall the origin of the path-ordered exponentials (2): they encode the interaction of fast moving quarks and gluons in the projectile wave function with the target field. It is the high energy of the collision that allows the description of this interaction in terms of the eikonal factors U , that at leading order follow perfectly straight, lightlike worldlines. We have chosen a frame where these trajectories extend along the minus light-cone direction at $x^+ = 0$. Each particle is then characterized by the remaining coordinates, namely its transverse location \mathbf{x} . The leading contribution comes from interaction with the non-Abelian Weizsäcker-Williams field of the target, A^+ . It takes the form

$$A^+(x) = b^+(x^-, \mathbf{x}) + \delta A(x), \quad b^+(x^-, \mathbf{x}) = \delta(x^-) \beta(\mathbf{x}) \quad (3)$$

where b^+ , or more specifically $\beta(\mathbf{x})$, is the single leading degree-of-freedom, a strong field, while δA is a small fluctuation in which we will expand. The $\delta(x^-)$ reflects the lack of resolution in longitudinal direction: no internal details of the field of the target are probed. The independence on x^+ reflects the fact that the target wave function is frozen during the interaction, an extreme time dilation. At fixed rapidity all dominant contributions are determined by the background field $b^+ = \delta(x^-) \beta(\mathbf{x})$. Moreover, they only enter in a very specific form, via the Wilson lines U .

For some generic operator made of these Wilson–line fields, $O[U]$, the average of Eq. (1) will be written as

$$\langle O[U] \rangle_Y := \int \hat{D}[U] O[U] Z_Y[U] \quad (4)$$

where $\hat{D}[U]$ is a functional Haar-measure and $Z_Y[U]$ contains the detailed physics beyond the eikonal approximation already incorporated by selecting U as the relevant degrees-of-freedom: $Z_Y[U]$ is the statistical weight for all possible field configurations.

Most of our knowledge of $Z_Y[U]$ is perturbative: the JIMWLK equation² determines the Y dependence of this average:

$$\partial_Y \hat{Z}_Y[U] = -\mathcal{H}[U] Z_Y[U], \quad (5)$$

where the JIMWLK Hamiltonian $\mathcal{H}[U]$ is given by

$$\mathcal{H}[U] = -\frac{\alpha_s(\mu^2)}{2\pi^2} \mathcal{K}_{\mathbf{x}\mathbf{z}\mathbf{y}} \left[U_{\mathbf{z}}^{ab} (i\bar{\nabla}_{\mathbf{x}}^a i\nabla_{\mathbf{y}}^b + i\nabla_{\mathbf{x}}^a i\bar{\nabla}_{\mathbf{y}}^b) + (i\nabla_{\mathbf{x}}^a i\nabla_{\mathbf{y}}^a + i\bar{\nabla}_{\mathbf{x}}^a i\bar{\nabla}_{\mathbf{y}}^a) \right], \quad (6)$$

with the LO kernel:

$$\mathcal{K}_{\mathbf{x}\mathbf{z}\mathbf{y}} = \frac{(\mathbf{x} - \mathbf{z}) \cdot (\mathbf{z} - \mathbf{y})}{(\mathbf{x} - \mathbf{z})^2 (\mathbf{z} - \mathbf{y})^2} = -\frac{\mathbf{r}_1 \cdot \mathbf{r}_2}{r_1^2 r_2^2}, \quad (7)$$

where \mathbf{x} , \mathbf{y} and \mathbf{z} are transverse coordinates. Here we also introduced a shorthand notation for the vectors connecting the points in the transverse plain:

$$\mathbf{r} = \mathbf{x} - \mathbf{y}, \quad \mathbf{r}_1 = \mathbf{x} - \mathbf{z}, \quad \mathbf{r}_2 = \mathbf{y} - \mathbf{z}, \quad (8)$$

and their lengths: $r_1 := |\mathbf{r}_1|$, etc. The notation in (6) assumes an integration convention over repeated coordinates appearing as an index in $\mathcal{K}_{\mathbf{x}\mathbf{z}\mathbf{y}}$ and in the vector field operators $\nabla_{\mathbf{x}}^a$. The Hamiltonian $\mathcal{H}[U]$ is second order in left- and right-invariant vector fields $\nabla_{\mathbf{x}}^a$ and $\bar{\nabla}_{\mathbf{x}}^a$, which are Lie derivatives: they act on the Wilson–line variables $U_{\mathbf{x}}$ according to³

$$i\nabla_{\mathbf{x}}^a U_{\mathbf{y}} := -U_{\mathbf{x}} t^a \delta_{\mathbf{x}\mathbf{y}}^{(2)}; \quad i\bar{\nabla}_{\mathbf{x}}^a U_{\mathbf{y}} := t^a U_{\mathbf{x}} \delta_{\mathbf{x}\mathbf{y}}^{(2)}. \quad (9)$$

The terms in the square brackets on the r.h.s of Eq. (6) are grouped according to their origin in real–emission and virtual corrections, respectively: real–emission contributions involve an additional Wilson line $U_{\mathbf{z}}^{ab}$ at transverse location \mathbf{z} .

The full derivation of Eq. (5) has been presented exhaustively in Refs. [20–23]. We nevertheless need to recall here how the JIMWLK Hamiltonian relates to Feynman diagrams, in order to prepare its re-derivation with running–coupling corrections. Rapidity dependence of $Z_Y[U]$ at LO is driven by the lowest–order fluctuations δA around the background $\delta(x^-)\beta(\mathbf{x})$ of Eq. (3). In this sense, the LO JIMWLK Hamiltonian in Eq. (6) is *constructed* such that it adds the LO “exchange” and “self-energy” corrections to, say, an interacting $q\bar{q}$ pair, represented by its Wilson–line bilinear

²For a first derivation of this equation in its most compact form see Ref. [20]. The version presented here is based on Ref. [60].

³See Ref. [20] for more details.

$U_{\mathbf{x}} \otimes U_{\mathbf{y}}^\dagger$:

$$\ln(1/x) \mathcal{H}[U] U_{\mathbf{x}} \otimes U_{\mathbf{y}}^\dagger = \text{diag}_1 + \text{diag}_2 + \text{diag}_3 \quad (10)$$

The diagrams shown in (10) are Feynman diagrams where the gluon propagator of the fluctuations $\langle \delta A \delta A \rangle$ is taken in the background of the strong target field $\delta(x^-)\beta(\mathbf{x})$.

The correspondence to real and virtual diagrams becomes visible upon resolving the Feynman diagrams into x^- ordered diagrams of light-cone perturbation theory. For instance,

$$\text{diag}_1 = \text{diag}_{1a} + \text{diag}_{1b} + \text{diag}_{1c} + \text{diag}_{1d}, \quad (11)$$

where the diagrams on the r.h.s. should be interpreted as diagrams of light-cone perturbation theory. Light-cone time x^- runs from bottom right to top left, the two collinear⁴ Wilson lines in this direction represent the dipole (the projectile) and the target is shown as a perpendicular line at $x^- = 0$, from bottom left to top right. To be precise, the last two diagrams in (11) are a shorthand notation for a sum of two different x^- orderings each:

$$\text{diag}_{1c} = \text{diag}_{1c1} + \text{diag}_{1c2}; \quad \text{diag}_{1d} = \text{diag}_{1d1} + \text{diag}_{1d2}. \quad (12)$$

The factors of U , U^\dagger and U^{ab} representing the interactions of a projectile quark, antiquark and gluon, respectively, are indicated as large dots where these Wilson lines cross the target line. In a derivation of JIMWLK based on projectile wave functions⁵, the contribution of the first two diagrams of (11) are associated with a situation where the interacting gluon reaches the final state and in this sense they correspond to *real-emission* diagrams. Correspondingly, as indicated by the third dot, they contain an additional Wilson line for this produced, eikonally interacting gluon, which appears in (6) as U_z^{ab} . The remaining diagrams represent purely *virtual* contributions in which the number of Wilson lines does not change. Similarly, both real-emission and virtual corrections are present in the self-energy-like diagrams in (10).

⁴Note that these two lines are actually separated only in the transverse direction.

⁵See Refs. [28–31] for a derivation of JIMWLK based on projectile wave functions in the context of the dipole model, Refs. [26, 27] for the BK case, or Ref. [70] for a re-derivation of JIMWLK via amplitudes.

Note that in the absence of the target field (3), the eikonal factors become trivial: $U \rightarrow 1$, and then there is strictly no evolution. In this limit each individual diagram on the r.h.s. of (10) vanishes identically owing to exact real–virtual cancellation: in (11) the first two diagrams, corresponding to real gluon emission, cancel against the last two diagrams, which represent virtual corrections. Analogous cancellations occur in this limit in the light–cone perturbation theory decomposition of the self–energy–like diagrams in (10).

As a functional equation, Eq. (5) is equivalent to an infinite set of equations for n -point correlators of U and U^\dagger fields in any representation of $SU(N_c)$, called the Balitsky hierarchies [23]. In order to obtain the evolution equation for a correlator of a given composite operator $O[U]$ made of U -fields, one first takes the Y derivative of (4) and then uses (5) to replace the $\partial_Y \hat{Z}_Y[U]$ by $-\mathcal{H}[U] Z_Y[U]$, obtaining:

$$\partial_Y \langle O[U] \rangle (Y) = - \int \hat{D}[U] O[U] \mathcal{H}[U] Z_Y[U], \quad (13)$$

where the Hamiltonian still acts on $Z_Y[U]$. Using the self-adjoint nature of $\mathcal{H}[U]$ with respect to the Haar measure (as ensured by the Lie derivatives), one can then rewrite (13) as

$$\partial_Y \langle O[U] \rangle (Y) = - \langle (\mathcal{H}[U] O[U]) \rangle (Y). \quad (14)$$

Here the JIMWLK Hamiltonian acts on $O[U]$. Observing that $\mathcal{H}[U]$ explicitly contains a U -operator, and that the number of U -operators remains invariant when acted upon by the Lie derivatives $\nabla_{\mathbf{x}}^a$ (see Eq. (9)) one understands that the evolution equation for $\langle O[U] \rangle$ must involve operators with more U fields than the original operator $O[U]$. Thus, the nonlinear nature of $\mathcal{H}[U]$ implies that the r.h.s. of the equation depends on a new type of correlator of U fields. To determine the rapidity dependence of $\langle O[U] \rangle (Y)$ one will therefore need also the evolution equation of this new correlator, which in turn will couple to yet higher composite operators containing more U fields. Continuing the process one ends up with an infinite hierarchy of equations, defined by the operator $O[U]$ used to start the process. The derivation of the BK equation shown below provides a simple example for such a hierarchy.

Truncation and the BK equation

As the simplest correlator with immediate phenomenological relevance we consider the two–point function of the dipole operator⁶:

$$N_{Y, \mathbf{x} \mathbf{y}} := \langle \hat{N}_{\mathbf{x} \mathbf{y}} \rangle (Y) \quad \hat{N}_{\mathbf{x} \mathbf{y}} := \frac{\text{tr}(1 - U_{\mathbf{x}}^\dagger U_{\mathbf{y}})}{N_c}. \quad (15)$$

Using Eq. (14) in the case of $\hat{N}_{\mathbf{x} \mathbf{y}}$ with the explicit expressions corresponding to the diagrams in Eq. (10), one immediately obtains:

$$\partial_Y \langle \hat{N}_{\mathbf{x} \mathbf{y}} \rangle (Y) = \frac{\alpha_s N_c}{2\pi^2} \int d^2 z (2\mathcal{K}_{\mathbf{x} \mathbf{z} \mathbf{y}} - \mathcal{K}_{\mathbf{x} \mathbf{z} \mathbf{x}} - \mathcal{K}_{\mathbf{y} \mathbf{z} \mathbf{y}}) \langle \hat{N}_{\mathbf{x} \mathbf{z}} + \hat{N}_{\mathbf{z} \mathbf{y}} - \hat{N}_{\mathbf{x} \mathbf{y}} - \hat{N}_{\mathbf{x} \mathbf{z}} \hat{N}_{\mathbf{z} \mathbf{y}} \rangle (Y). \quad (16)$$

The linear combination of JIMWLK kernels \mathcal{K} that appear in this expression are in one-to-one correspondence with the three diagrams in (10). They combine into the very compact form of the

⁶Below we will often use a shorthand notation where the Y dependence is not explicitly indicated.

BK kernel $\tilde{\mathcal{K}}_{\mathbf{xzy}}$:

$$\tilde{\mathcal{K}}_{\mathbf{xzy}} := 2\mathcal{K}_{\mathbf{xzy}} - \mathcal{K}_{\mathbf{xzx}} - \mathcal{K}_{\mathbf{yzy}} = \frac{(\mathbf{x} - \mathbf{y})^2}{(\mathbf{x} - \mathbf{z})^2(\mathbf{z} - \mathbf{y})^2}. \quad (17)$$

Clearly the r.h.s. of Eq. (16) depends on a 3-point function containing operators with up to four $U^{(\dagger)}$ factors, that in general does not factorize into a product of two 2-point correlators:

$$\langle \hat{N}_{\mathbf{xz}} \hat{N}_{\mathbf{zy}} \rangle(Y) = \langle \hat{N}_{\mathbf{xz}} \rangle(Y) \times \langle \hat{N}_{\mathbf{zy}} \rangle(Y) + \text{corrections}. \quad (18)$$

To completely specify the evolution of $\langle \hat{N}_{\mathbf{xy}} \rangle(Y)$ one therefore need to know $\langle \hat{N}_{\mathbf{xz}} \hat{N}_{\mathbf{zy}} \rangle(Y)$. The latter, in its evolution equation, will couple to yet higher n -point functions and thus one is faced with an infinite hierarchy of evolution equations, as anticipated above. The entire hierarchy (as well as others, corresponding to other composite operators $O[U]$) is encoded in the single functional equation (5). If one drops the corrections in (16) and factorizes the correlators in the spirit of a large- N_c approximation, the hierarchy is truncated and reduces to a single equation. This truncation can be interpreted as an independent scattering approximation and it leads to the Balitsky-Kovchegov (BK) equation [24, 27]:

$$\partial_Y N_{Y, \mathbf{xy}} = \frac{\alpha_s(\mu^2) N_c}{2\pi^2} \int d^2 z \tilde{\mathcal{K}}_{\mathbf{xzy}} \left(N_{Y, \mathbf{xz}} + N_{Y, \mathbf{zy}} - N_{Y, \mathbf{xy}} - N_{Y, \mathbf{xz}} N_{Y, \mathbf{zy}} \right). \quad (19)$$

Generic features and infrared stability

Despite the complex nature of the evolution equation, it is possible to gain insight into some generic features. It can be proven [20] that the evolution equation possesses an attractive fixed point at $Y \rightarrow \infty$ at which the system has vanishing correlation length. For the evolution of a physical correlator, such as $N_{Y, \mathbf{xy}}$, this implies a generic trend as shown in Fig. 1 (a): with increasing Y saturation ($N_{Y, \mathbf{xy}} \rightarrow 1$) is reached at ever shorter distances. This leads to a further important property of the evolution equation, namely its infrared stability: the evolution is not affected by long-wavelength fluctuations beyond the characteristic correlation length (the inverse of the saturation scale Q_s) where $N_{Y, \mathbf{xy}} = 1$. In this way the saturation scale acts as an effective infrared cutoff. Fig. 1 (b) demonstrates that the modes that contribute to the evolution have momenta of order of $Q_s(Y)$. With increasing Y , the active region moves towards the ultraviolet.

2.2 What we mean by running coupling

Similarly to other evolution equations in QCD [71], the LO JIMWLK kernel is conformally invariant⁷. As usual, breaking of this symmetry is expected to appear through radiative corrections at $\mathcal{O}(\beta_0 \alpha_s^2)$ where β_0 is the leading coefficient of the β function,

$$\frac{d\alpha_s(\mu^2)/\pi}{d \ln \mu^2} = -\beta_0 (\alpha_s(\mu^2)/\pi)^2 - \beta_1 (\alpha_s(\mu^2)/\pi)^3 + \dots; \quad \beta_0 = \frac{11}{12} C_A - \frac{1}{6} N_f. \quad (20)$$

⁷Note that while the LO *kernel* is conformally invariant, the solution of the equation is not: it is characterized by a correlation length. This scale originates in the initial condition, and it is preserved owing to the non-linearity of the equation.

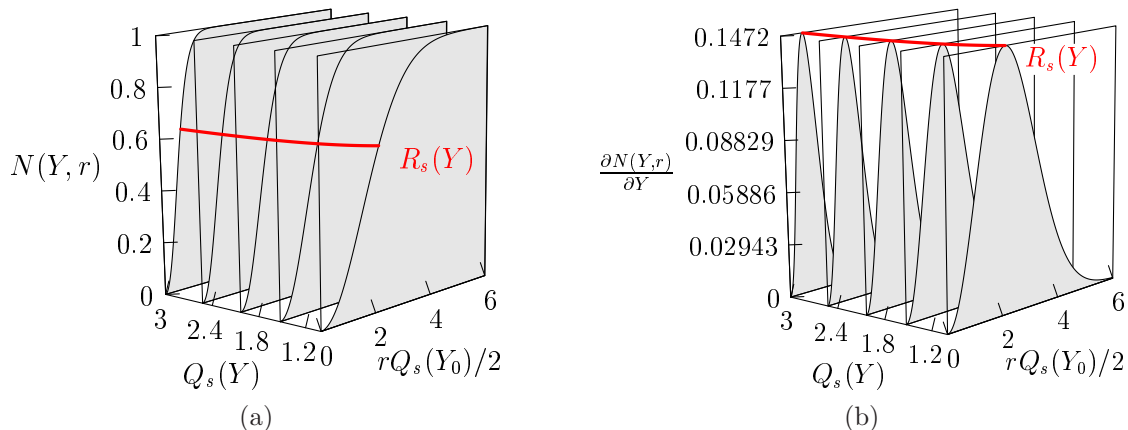


Figure 1: *Generic evolution trend for a single-scale dipole correlator. (a) shows $N(Y, r)$ as a function of the dipole size $r = |\mathbf{x} - \mathbf{y}|$ for several values of the saturation scale $Q_s(Y)$. Q_s increases with Y ; saturation then sets in at smaller distances. (b) shows $\partial_Y N$ and thus the activity in a given evolution step as a function of the same variables. With increasing $Q_s(Y)$ contributions are centered at ever shorter distances.*

At higher orders one expects corrections $\mathcal{O}(\beta_0^{n-1} \alpha_s^n)$, as well as ones associated with subleading coefficients of the β function, e.g. $\mathcal{O}(\beta_1 \beta_0^{n-3} \alpha_s^n)$. In Sec. 3 we compute these running-coupling corrections using a dispersive representation of the dressed gluon propagator in a background field. We will show that while the general structure of the evolution equation, namely Eq. (5), holds as at LO, the kernel itself changes drastically with respect to Eq. (7) — see Eq. (62) or (77) below. A similar generalization holds in the BK case, see Eqs. (91) and (92). JIMWLK and BK evolution with running-coupling is therefore qualitatively different from the fixed-coupling case in that at each step in the evolution the coupling depends on the details of the evolving configuration; moreover, different *final states*, that are characterized by different “daughter dipole” sizes, are weighted differently in the r.h.s. of the evolution equation.

Although all previous derivations of JIMWLK and BK evolution equations were restricted to the leading logarithmic approximation, it has been clear for quite a while that running-coupling corrections will be necessary to get quantitative results⁸. By making physically-motivated scale choices for the renormalization scale of the coupling, several authors found that the evolution rate $\lambda(Y)$ reduces by a factor of two or more compared to the fixed-coupling case.

It is important to make a clear distinction between the actual higher-order contributions to the kernel, which we compute in the following, and ad hoc choices of scale for the coupling, which have been often referred to as “running coupling”. Such prescriptions have been assumed in all numerical simulation of the BK equation [33, 45, 72–77]. Similar assumptions were used in the analytical estimates of Ref. [78], which agree well with numerical simulations [45]. To put the results of the present paper in context of previous work, we find it useful to further distinguish

⁸In Ref. [45] it has been further emphasized that running-coupling corrections, where the scale of the coupling depends on the scales involved in a *single* evolution step, are needed to reduce active phase space in the ultraviolet from about 6 orders of magnitude to about one. Despite this dramatic reduction of phase space, other qualitative features of the solution of JIMWLK or BK equations were found to be the same: for any set of initial conditions that interpolate between color transparency at short distance and saturation at large distance (as shown schematically in Fig. 1) the system approaches an asymptotic line where the dipole correlator reaches a near-scaling form.

between different categories of scale choices that were made in the literature:

1. **Fixed or essentially fixed coupling:** $\alpha_s(\mu^2)$ is treated as a constant or as a function of Y . Within this class, simulation results, starting from the same initial condition, can be related by re-scaling the evolution variable. For example, the scenario where the coupling depends on $Q_s(Y)$ can be related to the one where the scale of the coupling is fixed as some Q_0 through the change of variables (see also [79]):

$$Y' = \frac{\alpha_s(Q_s^2(Y))}{\alpha_s(Q_0^2)} Y.$$

Obviously, any ansatz of this sort would fail to capture the essential physics of running coupling, and would inherit the ultraviolet phase-space problem discussed in Ref. [45].

A non-trivial change in the shape of the solutions with respect to the fixed-coupling case occurs if the scale of the coupling is determined by the size of the “dipoles” involved in the evolution. In such cases the ultraviolet phase-space problem is generally removed, since emission from very small objects is suppressed by small coupling constants. The remaining two cases fall into this category.

2. **“Parent-dipole” running:** where the scale of the coupling on r.h.s. of the BK equation (19) is assumed to depend on the initial dipole size $r = |\mathbf{x} - \mathbf{y}|$, namely

$$\alpha_s(\mu^2) \tilde{\mathcal{K}}_{\mathbf{xzy}} \rightarrow \alpha_s(c^2/r^2) \tilde{\mathcal{K}}_{\mathbf{xzy}}, \quad (21)$$

where c is a dimensionless “scale factor” of order one⁹. This has been the most common ansatz in numerical simulations of the BK equation.

While this appears to be a natural ansatz in the context of the BK equation, it can not be easily reconciled with the JIMWLK equation. To see this, recall that (5) is a functional equation. Therefore, the Hamiltonian in Eq. (6) cannot depend on any scales characterizing a particular operator $O[U]$; all three transverse coordinates appearing in (6) are integrated over internally. When deriving the BK equation from JIMWLK as in (16) one obtains the BK kernel as a specific combination of the original JIMWLK kernel:

$$\alpha_s \tilde{\mathcal{K}}_{\mathbf{xzy}} \rightarrow 2\alpha_s(\mu_{\mathbf{xzy}}^2) \mathcal{K}_{\mathbf{xzy}} - \alpha_s(\mu_{\mathbf{zxz}}^2) \mathcal{K}_{\mathbf{zxz}} - \alpha_s(\mu_{\mathbf{yzy}}^2) \mathcal{K}_{\mathbf{yzy}}, \quad (22)$$

where each term corresponds to one of the diagrams in (10). Whatever one assumes of the functional dependence of $\mu_{\mathbf{xzy}}^2$ on the coordinates, since the self-energy-like diagrams are independent of the parent dipole size $|\mathbf{x} - \mathbf{y}|$, Eq. (22) does not lead to Eq. (21).

Even considering the BK case on its own, “parent-dipole” running may appear artificial: there is no reason why the sizes of the dipoles *produced* in the same step in the evolution, which can of course be quite different from the parent size, should not play an important rôle [77]. This leads us to the final category:

⁹It was often taken as $c \approx 4$, motivated by direct Fourier transform in the double logarithmic limit.

3. **Final-state-dependent evolution:** where the scale of the coupling on r.h.s. of the BK (19) or JIMWLK (6) equations is assumed to depend on all three distance scales present in a single evolution step, namely the “parent dipole” $r = |\mathbf{x} - \mathbf{y}|$ and the two newly produced “daughter dipoles”, $r_1 = |\mathbf{x} - \mathbf{z}|$ and $r_2 = |\mathbf{y} - \mathbf{z}|$. Obviously, in this case the coupling affects the weight of different final states, depending on the transverse location of the emitted gluon (the coordinate \mathbf{z}) that is integrated over.

Several such models were proposed, e.g. $\sqrt{\alpha_s(c^2/r_1^2)} \sqrt{\alpha_s(c^2/r_2^2)}$ or $\alpha_s(\max\{c^2/r_1^2, c^2/r_2^2\})$, and found to be in fair agreement with “parent-dipole” running, see e.g. [77]. As already mentioned, no deep justification of any of these models has been provided.

In the next section we compute running-coupling corrections to the JIMWLK equation. In Sec. 6 shall use this result to derive the corrections for the BK case and study the consequences numerically. As we will see, these corrections *do* depend on the details of the final state at each evolution step and involve all three scales. Moreover, in neither of the two equations do these corrections naturally reduce to a single scale-dependent coupling times the LO kernel.

3 Derivation of JIMWLK evolution with running coupling

3.1 Running coupling, Borel transform and the dispersive approach

We are interested in improving the leading-logarithmic result of the JIMWLK and BK equations by including running-coupling effects, namely corrections associated with the renormalization-group equation (20). In general, running-coupling corrections are important in QCD, for two reasons:

- They usually constitute a large part of the higher-order (notably NLO) corrections [48, 49, 52, 80–84]. The main reasons for this are: (1) the average virtuality of gluons is usually different (typically much lower) than the principal hard scale, which is often used as the default renormalization point; and (2) β_0 is sizeable. These effects are especially important when the hard scale is low, since then the coupling is large and its evolution (20) is fast.
- They dictate the large-order asymptotic behavior of the perturbative series, which is dominated by factorially increasing contributions, $\mathcal{O}(n! \beta_0^{n-1} (\alpha_s/\pi)^n)$, the renormalons [85, 86]. In this way the resummation provides some insight into the non-perturbative side of the problem: the *ambiguity* in summing the perturbative expansion, which is expected to cancel in the full theory, indicates the parametric dependence of non-perturbative corrections on the hard scales (power-suppressed corrections) and provides some clue on the potential size of these corrections [87–90]; for a review see Refs. [91, 92].

Both these aspects are relevant in non-linear evolution. As demonstrated in Sec. 2.2, the multi-scale nature of the problem calls for a systematic study.

In this section we wish to briefly recall some basic ideas and techniques for resummation of running-coupling corrections that will be generalized and applied to the JIMWLK case in what follows. To this end, consider some perturbatively calculable (infrared and collinear safe) quantity, $R(Q^2/\Lambda^2)$,

depending, for simplicity, on a single external scale Q^2 and having an expansion starting at order $\alpha_s(\mu^2)/\pi$ with the LO coefficient normalized¹⁰ to $c_{00} \equiv 1$:

$$R(Q^2/\Lambda^2) = \frac{\alpha_s(\mu^2)}{\pi} + \left[\left(c_{11} + \ln \frac{\mu^2}{Q^2} \right) \beta_0 + c_{10} \right] \left(\frac{\alpha_s(\mu^2)}{\pi} \right)^2 + \dots, \quad (23)$$

where β_0 is defined in (20) and the c_{10} term is a conformal coefficient, not associated with the running coupling. We will work in the large- β_0 limit, where the c_{10} term is formally subleading. The well-known BLM prescription [80] absorbs the NLO contribution that is leading in β_0 into the LO by a scale choice: $\mu_{\text{BLM}}^2 = Q^2 \exp\{-c_{11}\}$. In this way also higher-order corrections often become smaller. This becomes intuitive upon looking at the momentum integral that is approximated by $\alpha_s(\mu_{\text{BLM}}^2)/\pi$, where μ_{BLM}^2 acquires the interpretation of the average gluon virtuality. The all-order resummation of running-coupling effects in the single dressed gluon approximation,

$$R(Q^2/\Lambda^2)|_{\text{large } \beta_0} = \left(\frac{\alpha_s(Q^2)}{\pi} \right) \left[1 + \sum_{n=1}^{\infty} c_{nn} \times \left(\beta_0 \frac{\alpha_s(Q^2)}{\pi} \right)^n \right], \quad (24)$$

can be viewed as a generalization of this procedure, where instead of a single optimal scale choice, the proper (observable-dependent) weight is given to any specific gluon virtuality. In the context of the dispersive approach presented below (see Eq. (36)), this weight function is called the ‘‘characteristic function’’ [50].

Technically, the resummation of all $\mathcal{O}(\beta_0^{n-1} \alpha_s^n)$ higher-order corrections becomes feasible in QCD, owing to its simple relation with the resummation of diagrams with an arbitrary number of fermion-loop insertions. Because β_0 is linear in N_f , one can simply compute the fermion-loop chain diagrams and then replace N_f by the non-Abelian value of $-6\beta_0$, according to (20). In more formal terms, one begins by considering the large- N_f limit with fixed $N_f \alpha_s$, the leading term in the flavor expansion. Clearly this limit itself is not physically interesting, it just provides a tool to identify running-coupling contributions in the approximation where the non-Abelian β function (20) is one loop, the so-called large- β_0 limit.

The calculation of a gluon propagator, dressed by fermion-loop insertions is simplified by the fact that the fermion loop itself is transverse,

$$\Pi_{\mu\nu}(k^2) = \left(g_{\mu\nu} - \frac{k_\mu k_\nu}{k^2} \right) k^2 \Pi(k^2),$$

and therefore, in any gauge such insertions affects only the propagating particle pole $1/k^2$. The all-order sum builds up a geometric series giving rise to a factor $1/(1 + \Pi(k^2))$. The resummed propagator takes the form¹¹:

$$\text{covariant gauges:} \quad \frac{1}{k^2} \frac{1}{1 + \Pi(k^2)} \left(g_{\mu\nu} - \frac{k_\mu k_\nu}{k^2} \right) + \xi \frac{1}{k^2} \frac{k_\mu k_\nu}{k^2} \quad (25a)$$

$$\text{strict axial gauge:} \quad \frac{1}{k^2} \frac{1}{1 + \Pi(k^2)} \left(g_{\mu\nu} - \frac{k_\mu n_\nu + n_\mu k_\nu}{k \cdot n} + \frac{k_\mu k_\nu n^2}{(k \cdot n)^2} \right), \quad (25b)$$

¹⁰Using this normalization $R(Q^2/\Lambda^2)$ can also be interpreted as an ‘‘effective charge’’ [93].

¹¹Note that the ξ term in (25a) is not affected as it does not describe a physical mode. ξ is the width of a Gaussian approximation to a functional δ -function that is meant to implement the covariant gauge $\partial_\mu A^\mu = 0$. Only for vanishing width, $\xi = 0$, do all gauge fields obey the gauge condition strictly. The axial propagator is written for vanishing width, i.e. the strict gauge condition. That is why the resummed terms multiply the whole structure.

with

$$\Pi(k^2)|_{\text{one-loop}} = \frac{\alpha_s(\mu^2)\beta_0}{\pi} \ln\left(-k^2 e^{-\frac{5}{3}}/\mu^2\right), \quad (26)$$

where the renormalization of the fermion-loop $\Pi(k^2)$ was done in the $\overline{\text{MS}}$ scheme¹² and where we already made the replacement: $N_f \rightarrow -6\beta_0$.

The next step would be to insert the dressed propagator into the relevant Feynman diagrams and perform the momentum integration, d^4k . Since the sum over any number of $\Pi(k^2)$ insertions has already been done, by performing the k -integration one would hope to get directly the *resummed* physical quantity $R(Q^2/\Lambda^2)$ in (24). Observing that the resummed propagator with (26) has a Landau singularity, one realizes that this direct all-order calculation cannot be done. As we explain below, a regularization of the sum is required even if the coefficients c_{nn} are all finite¹³. The simplest and most familiar way to see this is to represent the effective running coupling¹⁴ *that includes the dressing*, as a Borel sum:

$$\frac{\alpha_s^V(-k^2 - i0)}{\pi} := \frac{\alpha_s(\mu^2)}{\pi} \frac{1}{1 + \Pi(k^2)} = \frac{1}{\beta_0} \int_0^\infty du T(u) \left(-k^2 e^{-\frac{5}{3}}/\Lambda^2\right)^{-u}, \quad (27)$$

where for one-loop running coupling¹⁵, namely upon using (26), one simply gets

$$\frac{\alpha_s^V(-k^2 - i0)}{\pi} \Big|_{\text{one-loop}} = \frac{1}{\beta_0} \frac{1}{\ln\left(-k^2 e^{-\frac{5}{3}}/\Lambda^2\right)},$$

and therefore $T(u) \equiv 1$. It is now possible to proceed with the calculation of the Feynman diagrams where the only change is that the particle pole is modified into a cut:

$$\frac{1}{-k^2 - i0} \rightarrow \frac{1}{(-k^2 - i0)^{1+u}}, \quad (28)$$

This modification of the propagator is known as Borel or analytic regularization.

The all-order resummation of a given quantity R in the large- β_0 limit can therefore be done using (27) by first performing the momentum integration with the modified propagator (28), which directly yields the Borel representation of the sum in the single dressed gluon approximation, namely:

$$R(Q^2/\Lambda^2)|_{\text{large } \beta_0} = \frac{1}{\beta_0} \int_0^\infty du T(u) (Q^2/\Lambda^2)^{-u} B(u). \quad (29)$$

Upon performing the momentum integration for a typical observable in QCD one would find that $B(u)$ has singularities along the positive real axis, which is the integration axis. This obviously

¹²We denote the $\overline{\text{MS}}$ coupling $\alpha_s^{\overline{\text{MS}}}(\mu^2)$ by $\alpha_s(\mu^2)$.

¹³This is indeed the case if R is an observable, i.e. it requires no additional renormalization and has no infrared divergencies.

¹⁴It is convenient to absorb the factor $e^{-\frac{5}{3}}$ from the renormalization of the fermion loop in (26) into the definition of the coupling. We follow this convention and define α_s^V as the coupling in the V scheme, which is related to the $\overline{\text{MS}}$ scheme by $\Lambda_V^2 = e^{\frac{5}{3}}\Lambda^2$.

¹⁵Although we restrict the calculation to one-loop coupling where $T(u) \equiv 1$, we will keep writing $T(u)$ in any Borel representation: this allows for a straightforward generalization to two-loop running coupling following [94,95].

means that Eq. (29) is ill-defined as it stands. The obstructing singularities are called infrared renormalons, and they merely reflect the fact that the series for R in (24) and thus also in (23), is non summable. The problem only becomes manifest if one attempts to sum the series: any finite order expansion — here all the coefficients c_{nn} in (24) — are well-defined and finite. They can be obtained by expanding $B(u)$ under the integral,

$$B(u) = \sum_{n=0}^{\infty} \frac{c_{nn}}{n!} u^n. \quad (30)$$

The Borel function typically has a finite radius of convergence u_0 , so c_{nn} grow as $n!/u_0^n$ at high orders¹⁶; in the case of infrared renormalons in QCD, the singularity is at $u = u_0 > 0$, so the coefficients all have the same sign¹⁷. In terms of the momentum integration these large perturbative coefficients are associated with extremely small virtualities $k^2 \rightarrow 0$, namely soft modes whose dynamics is non-perturbative. Thus, the non-existence of the sum is a reflection of the fact that perturbation theory does not fully describe the dynamics, and the observable is sensitive to some extent to non-perturbative contributions. The ambiguity can therefore be resolved by a proper separation prescription between perturbative and non-perturbative corrections, either by an infrared curoff, or by other means, for example by modifying the integration contour of the Borel integral (29) in a particular way or by taking its principal value. The same prescription must then be applied to regularize the non-perturbative contribution.

An additional, general property is that the singularities in $B(u)$ occur at integer — and sometimes half integer — values of u . This corresponds to the fact that alternative definitions of the sum of the series (that arise e.g. by modifying the integration contour in (29)) differ by integer — or half integer — powers of Λ^2/Q^2 . These ambiguities must be cancelled by non-perturbative power corrections, and they can therefore serve as a perturbative probe of such effects. In cases where an operator product expansion applies, one can get a direct interpretation of the source of each ambiguity in terms of local operators of higher dimension (or twist) [87, 89]. In such cases it is also possible to trace the cancellation of ambiguities [91, 96, 97]. In the absence of an operator product expansion, the renormalon technique often provides a unique window into the non-perturbative regime: by identifying the ambiguities in summing the perturbative series one learns about the parametric dependence of power corrections on the hard scales and about their potential size [46–55, 87–91, 96–99].

Computing directly the Borel function $B(u)$ using (28) may sometimes present technical difficulties. One of the most effective techniques to deal with this problem is the dispersive technique, which has been used in a variety of applications, see e.g. [46–55, 98, 99]. In the next sections we shall generalize this technique to the case of Weizsäcker-Williams background fields, in order to use it in the re-derivation of the JIMWLK equation. Let us therefore review here the basic idea, and collect the necessary formulae.

The dispersive method, see e.g. [49, 84, 98], recasts the dressed gluon propagator, and thus the running coupling of (27) as a dispersive integral. As we shall see, this allows one to compute a generic quantity $R(Q^2/\Lambda^2)$ to all orders in the large- β_0 limit, by simply replacing the massless

¹⁶This asymptotic behavior can be modified by additional factors of the form n^{γ/β_0} , depending on the structure of the Borel singularity. For simplicity we assume here simple poles.

¹⁷In contrast, for ultraviolet renormalons in QCD $u_0 < 0$, so there is sign oscillation at high order.

gluon pole by a massive one, namely:

$$\frac{1}{-k^2 - i0} \rightarrow \frac{1}{m^2 - k^2 - i0}, \quad (31)$$

instead of (28).

The dispersive representation takes the form

$$\frac{\alpha_s^V(-k^2 - i0)}{\pi} = \frac{\alpha_s(\mu^2)}{\pi} \frac{1}{1 + \Pi(k^2)} = \frac{1}{\beta_0} \int_0^\infty dm^2 \frac{\rho_V(m^2)}{m^2 - k^2 - i0}, \quad (32)$$

where ρ_V is the discontinuity of the coupling on the time-like axis,

$$\rho_V(m^2) := -\frac{\beta_0}{\pi} \text{Im} \{ \alpha_s^V(-m^2 - i0)/\pi \} = \frac{1}{\pi} \frac{\beta_0 \alpha_s(\mu^2)}{\pi} \frac{\text{Im} \{ \Pi(m^2) \}}{|1 + \Pi(m^2)|^2}. \quad (33)$$

Alternatively, it is convenient to express Eq. (32) in terms of the “effective¹⁸ time-like coupling”,

$$\frac{\alpha_s^V(-k^2 - i0)}{\pi} = \frac{1}{\beta_0} \int_0^\infty dm^2 \frac{\rho_V(m^2)}{m^2 - k^2 - i0} = \frac{1}{\beta_0} \int_0^\infty \frac{dm^2}{m^2} A_{\text{eff}}^V(m^2) \left[-m^2 \frac{d}{dm^2} \frac{1}{k^2 - m^2} \right], \quad (34)$$

where $A_{\text{eff}}^V(m^2)$ is defined by

$$\rho_V(m^2) =: m^2 \frac{d}{dm^2} A_{\text{eff}}^V(m^2). \quad (35)$$

The explicit expression for $A_{\text{eff}}^V(m^2)$ in the case of a one-loop running-coupling (namely (32) with (26)) takes the form:

$$A_{\text{eff}}^V(m^2)|_{\text{one-loop}} = \frac{1}{2} - \frac{1}{\pi} \arctan \left(\frac{1}{\pi} \ln \frac{m^2}{\Lambda_V^2} \right).$$

A two-loop expression for $A_{\text{eff}}^V(m^2)$ can be found in Ref. [99].

The all-order resummation of R in the large- β_0 limit can now be done using (34) by first performing the momentum integration with a massive gluon (i.e. with the replacement of Eq. (31)) leaving the dispersive integral over the mass undone. This leads to¹⁹

$$\begin{aligned} R(Q^2/\Lambda^2)|_{\text{large } \beta_0} &= \frac{1}{\beta_0} \int_0^\infty \frac{dm^2}{m^2} A_{\text{eff}}^V(m^2) \left[-m^2 \frac{d}{dm^2} \mathcal{F}(m^2/Q^2) \right] \\ &= \frac{1}{\beta_0} \int_0^\infty \frac{dm^2}{m^2} \rho_V(m^2) [\mathcal{F}(m^2/Q^2) - \mathcal{F}(0)], \end{aligned} \quad (36)$$

¹⁸Let us emphasize that we do *not* make any use of the dispersive representation to impose analyticity and regularize the Landau singularity, as done for example in Ref. [100]. We merely use the dispersive method to compute the Borel function, which serves as a generating function for the perturbative coefficients according to (30) and as a tool to analyze infrared renormalon ambiguities.

¹⁹Note that we ignore pure power correction terms (Λ^2/Q^2) which distinguish this integral from the Borel sum we eventually compute. These will be totally irrelevant here. The interested reader is referred to [49, 51, 52].

where in the $m^2 \rightarrow 0$ limit $\mathcal{F}(m^2/Q^2)$ yields the LO coefficient, $\mathcal{F}(0) = c_{00} = 1$. By definition, $\mathcal{F}(m^2/Q^2)$ depends on the specific quantity computed and it encodes perturbative as well as power-correction information (see e.g. [49,84]). $\mathcal{F}(m^2/Q^2)$ is therefore called the “characteristic function” of the quantity or process under consideration. Upon expanding the effective coupling $A_{\text{eff}}^V(m^2)$ in (36) in powers of $\ln(m^2/\Lambda^2)$ and integrating term by term (log moments) one obtains the perturbative coefficients c_{nn} . On the other hand, expanding $\mathcal{F}(m^2/Q^2)$ at small m^2 and extracting the non-analytic terms [84] one obtains information on renormalon ambiguities and thus on power corrections in Λ^2/Q^2 .

As explained above, the perturbative and power-correction information encoded in the characteristic function can be conveniently extracted from the Borel representation (29). The Borel formulation also offers a natural definition of the sum, using the principal value (PV) prescription. The PV Borel sum can be related to a Euclidian-cutoff regularization [52], and it has good analytic properties as a function of the hard scales [54,101], e.g. it has no Landau singularities and it is real-valued. In order to relate the dispersive and the Borel formulations, (36) and (29), respectively, one first computes the Borel representation of the discontinuity of the coupling by using (27) in (33); a straightforward calculation yields:

$$\rho_V(m^2) = - \int_0^\infty du T(u) \frac{\sin \pi u}{\pi} e^{\frac{5}{3}u} (m^2/\Lambda^2)^{-u}. \quad (37)$$

Next, by substituting (37) in (36) and changing the order of integration one recovers the Borel representation (29) with

$$B(u) = -e^{\frac{5}{3}u} \frac{\sin \pi u}{\pi} \int_0^\infty d\zeta \zeta^{-1-u} [\mathcal{F}(\zeta) - \mathcal{F}(0)] = -e^{\frac{5}{3}u} \frac{\sin \pi u}{\pi u} \int_0^\infty d\zeta \zeta^{-u} \frac{d\mathcal{F}(\zeta)}{d\zeta}. \quad (38)$$

In the following we will use this formula to compute the Borel function $B(u)$ from $\mathcal{F}(\zeta)$.

Finally, it should be emphasized that the resummed result for $R(Q^2/\Lambda^2)$, computed with a single dressed gluon, is exactly renormalization-scale invariant, despite using just a subset of all perturbative corrections. At power level, we shall define the sum using the principal value prescription of (29) and use the renormalon poles to analyze non-perturbative power corrections.

3.2 The dressed propagator in the background field

At this point, we have described the method used to derive the JIMWLK equation at fixed coupling (Sec. 2.1) and the generic tools used to promote a one-loop calculation to one with a dressed gluon (Sec. 3.1). These need now to be combined. Since all the diagrams in (10) involve a single gluon, the dispersive technique should be applicable. The crucial step is to construct a propagator that is both in the background of Weizsäcker-Williams field *and* is dressed by running-coupling corrections. This is the main goal of this section.

Independently of the particular technique adopted, the calculation of running-coupling corrections to the kernel involves a subtlety which is associated with the presence of new production channels, namely the production of a well separated $q\bar{q}$ pair or a pair of gluons, starting at NLO. These processes involve *two* additional Wilson lines — not one — on the r.h.s of the evolution equation,

namely an entirely new contribution to the JIMWLK Hamiltonian (6). Obviously, these contributions should not be considered a running-coupling correction, and we do not aim to compute them here. As explained in Sec. 3.1 running-coupling corrections are usually identified by considering diagrams with fermion-loop insertions, namely considering the formal large- N_f limit with fixed $N_f\alpha_s$ (the flavor expansion), and then making the substitution $N_f \rightarrow -6\beta_0$. However, in the present case this criterion is insufficient: similarly to running-coupling corrections, $q\bar{q}$ pair production appears at LO in the flavor expansion, as can be seen in Fig. 2. Moreover, the running-coupling correc-

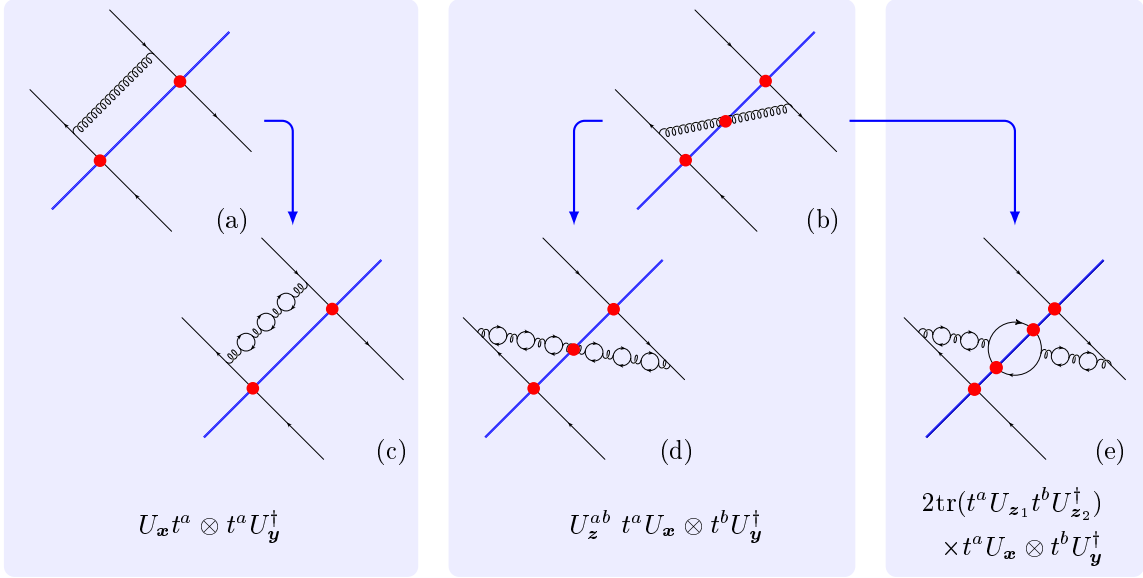


Figure 2: *Virtual and real contributions at LO (a), (b) and NLO (c), (d) and (e). Vertically (as delineated by the background shading) they are grouped by the Wilson line structure induced by the target interaction. The latter are indicated on the diagrams via large solid dots, their analytical form is listed at the bottom. Diagram (e) induces a new structure via a $q\bar{q}$ loop that interacts with the target.*

tions and $q\bar{q}$ pair production are physically distinct only if the transverse separation of the pair is non-vanishing. Therefore, the identification of running-coupling corrections to the kernel requires a separation prescription. As we shall see below, the use of the dressed propagator in the background field automatically implements such a prescription.

A related complication arises in the derivation of the JIMWLK Hamiltonian with running coupling because of the possibility of interaction between the background field and a produced $q\bar{q}$ pair. Dressing the *virtual* diagram, shown in Fig. 2 (a), poses no problems, since the gluon itself does not interact with the target²⁰. For each LO virtual contribution in (11), as well as their self-energy-like analogues, there is just one type of dressed virtual counterpart; e.g. in Fig. 2, diagram (c) corresponds to dressing of diagram (a). The eikonal interactions with the target field remain

²⁰At this point one might be worried that some of intermediate quark-gluon vertices (whose location is to be integrated over) might lie on different sides of the target line – this is precluded by causality since the interaction is restricted to the light-like support of the target field $b^+ = \delta(x^-)\beta(\mathbf{x})$. Even the dressed gluon line cannot propagate back and forth across this hyperplane. This will be borne out by the explicit calculation.

unaffected by the dressing. The dressed propagator in (c) reduces to the dressed propagator in the absence of the target field, and the running-coupling corrections may be directly obtained using the tools of Sec. 3.1.

On the other hand, real-emission diagrams, such as the diagram in Fig. 2 (b), lead to two physically different generalizations upon inserting fermion loops; these are shown in diagrams (d) and (e), respectively. Diagram (d) contains the same eikonal factors as the LO diagram, while diagram (e) contains a new channel: the production of a well separated $q\bar{q}$ -pair, which interacts with the target field at two *distinct* points on the transverse plane \mathbf{z}_1 and \mathbf{z}_2 . Instead of the single gluonic eikonal factor $U_{\mathbf{z}}$ as in diagrams (b) and (d), in diagram (e) one encounters a factor $2\text{tr}(t^a U_{\mathbf{z}_1} t^b U_{\mathbf{z}_2}^\dagger)$. The distinction between the two, however, is lost if the transverse separation of the $q\bar{q}$ -pair (or the invariant mass of the pair) becomes small: in this limit the $q\bar{q}$ -pair in the final state becomes indistinguishable from a gluon. This (by necessity) is mirrored in the eikonal structure associated with the diagrams:

$$\lim_{\mathbf{z}_1, \mathbf{z}_2 \rightarrow \mathbf{z}} 2\text{tr}(t^a U_{\mathbf{z}_1} t^b U_{\mathbf{z}_2}^\dagger) = U_{\mathbf{z}}^{ab} . \quad (39)$$

Therefore, while in the virtual diagrams running-coupling corrections can be reconstructed solely from bubble sums as in Fig. 2 (c), in the real-emission diagrams these corrections are associated with both Fig. 2 (d) and the local limit of (e). However, real and virtual contributions are related by the requirement of probability conservation: in the absence of interactions the dressed virtual terms must cancel the dressed real contributions exactly. In the following we show that it is possible to generalize the LO calculation of Sec. 2.1 in a way that manifestly implements all these requirements. Specifically, the separation prescription between the running-coupling corrections that we compute and the $q\bar{q}$ production channel that we neglect, simply amounts to the replacement of $2\text{tr}(t^a U_{\mathbf{z}_1} t^b U_{\mathbf{z}_2}^\dagger)$ of diagram (e) by its local limit of (39), namely $U_{\mathbf{z}}^{ab}$. As announced, this is automatically realized upon using the dressed propagator in the background field to compute the diagrams of Eq. (10).

The main ingredient in the LO calculation in [20] is the propagator of the fluctuation δA in the presence of the background field b^+ . The calculation sketched in Sec. 2.1 was performed in the $A^- = 0$ axial gauge in order to reduce the number of diagrams that contribute. These diagrams are shown in Eq. (10). The eikonal nature of the interaction in these diagrams implies that one only needs the “++” component of the fluctuation propagator, $\langle \delta A_x^+ \delta A_y^+ \rangle^{ab}$. This remains true for the dressed propagator.

At LO, the gluon propagator can be expressed (see Eq. (45) below) in terms of an external tensor structure and the propagator $iG_0^{ab}(x', y')$ of a massless scalar field in the adjoint color representation, propagating through the target field [3]. Our generalization will involve its massive counterpart $iG_m^{ab}(x', y')$. Since the structure of the propagator has been discussed extensively in the literature [3, 102], we only describe here the key ingredients that will be needed to apply the dispersive method and re-derive the JIMWLK equation with running coupling.

Massive scalar propagator in the background field

The starting point is a spectral representation of the massive scalar propagator

$$G_m^{ab}(x, y) := \int \frac{d^4 k}{(2\pi)^2} \frac{1}{k^2 - m^2 + i0} [\phi_k(x) \phi_k^\dagger(y)]^{ab} , \quad (40)$$

where we have combined a spectral integral over the virtuality $\int dk^2$, and the sum over all states at fixed virtuality, $\int d^2 k_\perp dk^- / (2k^+)$, into one 4-dimensional integral $\int d^4 k$.

Here $\phi_k^{ac}(x)$ are the solutions of the Klein-Gordon equation at virtuality $k^2 = 2k^+k^- - \mathbf{k}^2$ in the background field b^+ of Eq. (3):

$$(-D[b]^2 - k^2)^{ab} \phi_k^{bc}(x) = 0, \quad (41)$$

where a and b are color indices and c is a basis label. $D_\mu[b] = \partial_\mu - igb_\mu$ is the (adjoint) covariant derivative in the background field (3). Explicitly,

$$\phi_k^{ab}(x) = \frac{1}{(2\pi)^2} \int d^4 p e^{-ip \cdot x} \delta(p^2 - k^2) \delta\left(1 - \frac{p^-}{k^-}\right) \int d^2 z e^{-i(\mathbf{p}-\mathbf{k})\mathbf{z}} [U_{x^-, -\infty}^{-1}(\mathbf{z})]^{ab}, \quad (42)$$

reflecting the fact that the interaction with the background field can transfer *transverse* momentum from the target, while it cannot modify the conserved k^- component nor the virtuality k^2 . The color structure in (42) is carried by the adjoint eikonal factor $[U_{x^-, y^-}^{-1}(\mathbf{z})]^{ab}$ defined by

$$[U_{x^-, y^-}^{-1}(\mathbf{z})]^{ab} := \left[\text{P exp} \left\{ ig \int_{y^-}^{x^-} dz^- \delta(z^-) \beta(\mathbf{z}) \right\} \right]^{ab}. \quad (43)$$

A straightforward calculation using (42) in (40) yields:

$$G_m^{ab}(x, y) = \int \frac{dk^-}{2k^-(2\pi)^3} [\theta(x^- - y^-)\theta(k^-) - \theta(y^- - x^-)\theta(-k^-)] \int d^2 p_\perp d^2 q_\perp \times \left[e^{-ip \cdot x} \int \frac{d^2 z_\perp}{(2\pi)^2} e^{-i(\mathbf{p}-\mathbf{q})\mathbf{z}} [U_{x^-, y^-}^{-1}(\mathbf{z})]^{ab} e^{iq \cdot y} \right], \quad (44)$$

where the 4-momenta p and q obey the constraints

$$p^+ = \frac{\mathbf{p}^2 + m^2}{2k^-}; \quad q^+ = \frac{\mathbf{q}^2 + m^2}{2k^-}; \quad p^- = q^- = k^-.$$

Eq. (44) differs from the free massive propagator by the Wilson line (43) that represents the interaction with the target field. Since the interaction in (43) is localized at $z^- = 0$, this Wilson line reduces to $U_{\mathbf{z}}$ (defined in (2)) if $x^- > 0 > y^-$, to $U_{\mathbf{z}}^\dagger$ if $x^- < 0 < y^-$ and to 1 otherwise. This implies [3, 102] free propagation²¹ when the endpoints x^- and y^- are both on the same side of the $z^- = 0$ hyperplane, while if they lie on opposite sides one encounters a three-step process: free propagation from the initial point onto the hyperplane, a current interaction with the background field, and free propagation again from there to the endpoint. Only in the latter case does the background field induce a change of the transverse momentum in the propagator. It is important to note that these features carry over to the fluctuations propagator $\langle \delta A_x^+ \delta A_y^+ \rangle^{ab}$ in both the massless and the massive case.

²¹With $U = 1$ there is no obstacle to performing the \mathbf{z} integration in (44).

Massive gauge–field propagator in the background field

The relevant, “++” component of the fluctuation propagator at LO is expressed in terms of the scalar–field propagator $iG_0^{ab}(x', y')$ as

$$\langle \delta A_x^+ \delta A_y^+ \rangle^{ab} = - \left[\frac{1}{\partial^-} \right]_{xx'} \left\{ -D^2[B]_{x'} iG_0^{ab}(x', y') + \overrightarrow{\partial}_{x'}^j iG_0^{ab}(x', y') \overleftarrow{\partial}_{y'}^j \right\} \left[\frac{1}{\partial^-} \right]_{y'y}. \quad (45)$$

Here an integration convention over 4-vector coordinates x' and y' is implied. Note that one may simplify the first term in this expression using the defining equation for G_0 , namely

$$D^2[b]_{x'} G_0^{ab}(x', y') = \delta^{(4)}(x' - y').$$

We have chosen not to do this since $G_0^{ab}(x', y')$ represents the propagating particle pole that will be affected by the dressing, while the remainder of the expression will not change. To illustrate that this is indeed the right procedure let us connect back to the free case, or alternatively restrict ourselves to virtual diagrams such as Fig. 2 (c), by replacing

$$D^2[b]^{ab} \longrightarrow \square_{x'} \quad iG_0^{ab}(x, y) \longrightarrow \frac{i}{\square}(x, y) \delta^{ab} \quad (46)$$

to obtain

$$\langle \delta A_x^+ \delta A_y^+ \rangle_{\text{free}}^{ab} = - \left[\frac{1}{\partial^-} \right]_{xx'} \left\{ -\square_{x'} \left[\frac{i}{\square} \right]_{x'y'} + \overrightarrow{\partial}_{x'}^j \left[\frac{i}{\square} \right]_{x'y'} \overleftarrow{\partial}_{y'}^j \right\} \left[\frac{1}{\partial^-} \right]_{y'y} \delta^{ab}. \quad (47)$$

This coordinate–space expression may be readily Fourier–transformed and shown to coincide with the “++” component of the free axial–gauge propagator²² of (25b), which is $(1/k^2) 2k^+/k^-$. One can in fact relate the two terms in (47) respectively, to the contributions of longitudinal and transverse polarizations in the conventions of light–cone perturbation theory. To this end let us define transverse polarizations by

$$\epsilon_T^{\mu\lambda} := \left(\frac{\mathbf{k} \cdot \epsilon_T^\lambda}{k^-}, \epsilon_T^\lambda, 0 \right) \quad \text{based on } \epsilon_T^\lambda := (1, i(-1)^{\lambda+1})/\sqrt{2} \quad \text{with } \lambda = 1, 2.$$

Here we used the notation $(+, \perp, -)^\mu$ for the components of a four–vector. We may then recast Eq. (25b) (before dressing the propagator), for our light–cone gauge (where $n^2 = 0$), as

$$\frac{1}{k^2} \left(g_{\mu\nu} - \frac{n^\mu k^\nu + k^\mu n^\nu}{k \cdot n} \right) = -\frac{n^\mu n^\nu}{(k \cdot n)^2} k^2 \frac{1}{k^2} - \sum_{\lambda=1,2} \frac{\epsilon_T^{*\mu\lambda} \epsilon_T^{\nu\lambda}}{k^2}. \quad (48)$$

This uniquely identifies the second term in (47) with transverse polarizations while the first term is related to longitudinal contributions.

In (47) the factors $\frac{i}{\square}(x, y)$ correspond to the propagating particle pole $1/k^2$ in (25b), which get multiplied by $1/(1 + \Pi(k^2))$ upon dressing the gluon. The point of separating the simple tensor structure of $(1/k^2) 2k^+/k^-$ by polarizations into two terms as in (45) and (47) is that the separation

²²For our purposes the gauge vector n projects out the minus component of a vector: $n \cdot a = a^-$.

helps to extract the leading small- x contribution: when used in the diagrams of Eq. (10), only the second term contributes a logarithm in $1/x$, while the first term is subleading.

Eq. (47) offers a straightforward route to apply the dispersive method for *virtual* diagrams such as Fig. 2 (c). As explained above, in this case the dressed propagator does not interact with the target field, so the standard dispersive method described in Sec. 3.1 directly applies. Following Eq. (31) one replaces $1/k^2$ by $1/(k^2 - m^2)$ or, in coordinate language

$$\left[\frac{i}{\square}\right]_{x'y'} \rightarrow \left[\frac{i}{\square + m^2}\right]_{x'y'}.$$

After making this replacement in (47) the first term may be further split according to

$$-\square_{x'} \left[\frac{i}{\square + m^2}\right]_{x'y'} = -i\delta_{x'y'}^{(4)} + m^2 \left[\frac{i}{\square + m^2}\right]_{x'y'}, \quad (49)$$

so the massive propagator finally takes the form

$$\langle \delta A_x^+ \delta A_y^+ \rangle_m^{ab} |_{\text{free}} = - \left[\frac{1}{\partial^-}\right]_{xx'} \left\{ -i\delta_{x'y'}^{(4)} + m^2 \left[\frac{i}{\square + m^2}\right]_{x'y'} + \overrightarrow{\partial}_{x'}^j \left[\frac{i}{\square + m^2}\right]_{x'y'} \overleftarrow{\partial}_{y'}^j \right\} \left[\frac{1}{\partial^-}\right]_{y'y} \delta^{ab}. \quad (50)$$

As we shall see below, the δ -function term does not generate a logarithm in $1/x$, while the other two terms do, and will therefore be relevant for the JIMWLK equation.

The dispersive representation of the dressing was derived in the free case and it therefore directly applies only to (50) and thus to the resummation of running-coupling corrections in the virtual diagrams in the JIMWLK Hamiltonian. Nevertheless, a similar procedure can be applied to real-emission diagrams, where it provides a natural *definition* of the running-coupling contribution, whose separation from the $q\bar{q}$ -pair production channel is a priori ambiguous. To this end we construct the massive propagator in the background field by reversing the replacements (46) in (50):

$$\langle \delta A_x^+ \delta A_y^+ \rangle_m^{ab} = - \left[\frac{1}{\partial^-}\right]_{xx'} \left\{ -i\delta_{x'y'}^{(4)} + m^2 i G_m^{ab}(x', y') + \overrightarrow{\partial}_{x'}^j i G_m^{ab}(x', y') \overleftarrow{\partial}_{y'}^j \right\} \left[\frac{1}{\partial^-}\right]_{y'y}. \quad (51)$$

By using this propagator in *both* real and virtual diagrams, the real-virtual cancellation mechanism is in place, just as at LO. Thus, probability conservation is guaranteed. It is by this fundamental principal that the dressing of the *virtual* diagrams by fermion-loop insertions, which is uniquely determined by (50) using the dispersive method, essentially dictates the structure of running-coupling corrections in the JIMWLK kernel as a whole.

Generalization of the dispersive approach

To incorporate running-coupling corrections in the derivation of the JIMWLK equation, we will modify the fluctuation propagator in analogy with Eq. (36), namely

$$\frac{\alpha_s}{\pi} \langle \delta A_x^+ \delta A_y^+ \rangle^{ab} \rightarrow \frac{1}{\beta_0} \int_0^\infty \frac{dm^2}{m^2} \rho_V(m^2) \left[\langle \delta A_x^+ \delta A_y^+ \rangle_m^{ab} - \langle \delta A_x^+ \delta A_y^+ \rangle_0^{ab} \right], \quad (52)$$

where $\langle \delta A_x^+ \delta A_y^+ \rangle_m^{ab}$ is given in (51). Note this modification can be traced back to a substitution in the scalar propagator

$$\begin{aligned} \frac{\alpha_s}{\pi} G_0^{ab}(x, y) &= \frac{\alpha_s}{\pi} \int \frac{d^4 k}{(2\pi)^4} \frac{[\phi_k(x) \phi_k^\dagger(y)]^{ab}}{k^2 + i0} \quad \rightarrow \quad \int \frac{d^4 k}{(2\pi)^4} \frac{\alpha_s^V(-k^2 - i0)}{\pi} \frac{[\phi_k(x) \phi_k^\dagger(y)]^{ab}}{k^2 + i0} \quad (53) \\ &= \frac{1}{\beta_0} \int_0^\infty \frac{dm^2}{m^2} \rho_V(m^2) [G_m^{ab}(x, y) - G_0^{ab}(x, y)] , \end{aligned}$$

where in the final expression we used the dispersive representation of the running coupling (34). Restoring the tensor structure then yields (52).

As explained above, our procedure, which uses the propagator (51) for both virtual and real-emission diagrams guarantees probability conservation. Its diagrammatic interpretation at the level of fermion loops can be read off Fig. 2: in the absence of interaction, (the limit $U \rightarrow 1$), the sum of diagrams (d) and (e) reduces to diagram (c) and their cancellation is complete; as the interaction is turned on they become distinct and evolution takes place. At the same time a new channel, the production of a $q\bar{q}$ pair in diagram (e), opens up. Our procedure uses the leading- N_f corrections in the virtual diagrams to identify (define) running-coupling corrections. This amounts to a specific separation of the leading- N_f corrections in the real-emission diagrams into ones that are part of the running coupling and ones that constitute the new production channel of diagram (e). By virtue of Eq. (39) the local limit of diagram (e) is included in the running-coupling contribution. As a consequence, real-virtual cancellation holds *separately* for the running-coupling corrections, and the remainder, namely the new $q\bar{q}$ production channel can be computed separately: it is a well-defined NLO contribution to the kernel that is not associated with the running coupling. This is confirmed by an explicit calculation of the diagrams using light-cone perturbation theory [103].

Finally, let us briefly comment on the separate terms in Eq. (51). We begin by observing that, as in the LO case, the first term in (51), $-i\delta_{x'y'}^{(4)}$, is suppressed at large p^- and will therefore not contribute to the evolution equations. The two terms containing G_m , however, will generate ∂^- contributions in the numerator, and will therefore contribute to logarithmically-enhanced terms at small x through $\int dp^-/p^- = \ln(1/x)$. Next, we note that the two surviving terms are very different in nature: the last term is already present in the LO fixed-coupling calculation, while the middle term does not contribute there, as it vanishes in the $m \rightarrow 0$ limit. It starts contributing at NLO. This is in keeping with the different origin of the terms: the transverse partial derivatives in the last term reflect the Weizsäcker-Williams field structure of the LO emission kernel (55) that is entirely driven by transverse polarizations. The middle term, in contrast, arises entirely from longitudinal polarizations that are absent at leading order. As such it has an entirely new dependence on the transverse coordinates not present at LO. The corresponding diagrammatic calculation in [103] confirms this structure and the association of the terms with transverse and longitudinal polarizations; the latter enter there (starting at NLO) via instantaneous contributions.

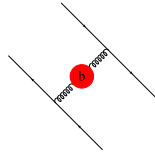
3.3 Application to JIMWLK

The dispersive method introduces running-coupling corrections by performing a direct replacement of the gluon propagator in the *leading-order calculation* according to (52). Therefore, the generalization of the JIMWLK equation to running coupling essentially constitutes of recalculating the

LO diagrams of (10) with the massive propagator of (51) instead of that of (45). In the following we first present an explicit calculation of one of the diagrams, and then generalize and derive the running-coupling corrections to the Hamiltonian $\mathcal{H}[U]$ in (6).

Let us first recapitulate the ingredients: in (10) we consider the calculation of the leading logarithmic correction to the propagation of a fast moving dipole, a $q\bar{q}$ -pair. As explained in Sec. 2, this object can be represented as a product of two Wilson lines along the classical trajectories of the quarks. We take the trajectories to lie along the minus light-cone direction at $x^+ = 0$. The pair is then characterized by the transverse locations \mathbf{x} and \mathbf{y} of the quark and antiquark, respectively.

The first diagram²³ in (10) contains all the information we need: the other two can be deduced from it. It describes the leading $\ln(1/x)$ contribution to the exchange of a gluon between the two quarks in the presence of Weizsäcker-Williams background field. The result (see [20, 23]) involves the fluctuation propagator and the Wilson lines that represent the external quark and antiquark:



$$= g^2 \int dx^- dy^- \langle \delta A_x^+ \delta A_y^+ \rangle_0^{ab} \\ \times \left(\theta(-x^-) U_{\mathbf{x}} t^a + \theta(x^-) t^a U_{\mathbf{x}} \right) \otimes \left(\theta(y^-) U_{\mathbf{y}}^\dagger t^b + \theta(-y^-) t^b U_{\mathbf{y}}^\dagger \right),$$

which, after some algebra involving the fluctuation propagator (45) (see below) may be recast as

$$= -\frac{\alpha_s}{\pi^2} \ln(1/x) \int d^2 \mathbf{z} \mathcal{K}_{\mathbf{xz}\mathbf{y}} \left([U]_{\mathbf{z}}^{ab} t^a U_{\mathbf{x}} \otimes t^b U_{\mathbf{y}}^\dagger + [U^\dagger]_{\mathbf{z}}^{ab} U_{\mathbf{x}} t^a \otimes U_{\mathbf{y}}^\dagger t^b \right. \\ \left. - \delta^{ab} [U_{\mathbf{x}} t^a \otimes t^b U_{\mathbf{y}}^\dagger + t^a U_{\mathbf{x}} \otimes U_{\mathbf{y}}^\dagger t^b] \right). \quad (54)$$

The four terms on the r.h.s are in one-to-one correspondence with the four diagrams in Eq. (11), and \mathcal{K} is a purely two-dimensional scale-invariant kernel, given by

$$\mathcal{K}_{\mathbf{xz}\mathbf{y}} = -\partial_x^j \partial_y^j \int \frac{d^2 p d^2 q}{(2\pi)^2} \frac{e^{i\mathbf{p}(\mathbf{x}-\mathbf{z})}}{p^2} \frac{e^{i\mathbf{q}(\mathbf{z}-\mathbf{y})}}{q^2} = \frac{(\mathbf{x}-\mathbf{z}) \cdot (\mathbf{z}-\mathbf{y})}{(\mathbf{x}-\mathbf{z})^2 (\mathbf{z}-\mathbf{y})^2} = -\frac{\mathbf{r}_1 \cdot \mathbf{r}_2}{r_1^2 r_2^2} = \frac{1}{2} \frac{r^2 - (r_1^2 + r_2^2)}{r_1^2 r_2^2}, \quad (55)$$

where we used the notation for “parent-” and “daughter-dipoles” introduced in (8). The last formula shows explicitly that this leading order kernel changes sign at a circle whose diameter is defined by the “parent.” To arrive at the final expression in (54) with the kernel of (55) we have performed the x^- and y^- integrals, using (45) with the explicit formula for $G_0^{ab}(x, y)$, given by (44) with $m = 0$. These integrations give rise to factors $2p^-/p^2$ and $2q^-/q^2$, respectively. The minus momentum components in the numerator compensate the explicit ∂^- in the denominator in (45), while the additional $\int_0^\infty dk^-/k^-$ in $G_0^{ab}(x, y)$ leads to the factor $\ln(1/x)$ upon imposing cutoffs in x . Note that the first term in the curly brackets in (45) reduces to $-i\delta_{x'y'}^{(4)}$ and it does not contribute to the equation since it is suppressed at large p^- .

Eqs. (54) and (55) summarize the result for one of the diagrams in (10) used in deriving the JIMWLK equation [20]. As announced we will now use this diagram to demonstrate how the

²³This quantity was called $\bar{\chi}_{\mathbf{x}\mathbf{y}}^{q\bar{q}}$ in [20].

JIMWLK equation can be promoted to running coupling by means of the dispersive method. To this end we use the substitution (52) obtaining

$$\frac{\alpha_s}{\pi} \text{diagram} \rightarrow \frac{1}{\beta_0} \int_0^\infty \frac{dm^2}{m^2} \rho_V(m^2) \left(\text{diagram}(m) - \text{diagram}(m=0) \right). \quad (56)$$

Recall that $\rho_V(m^2)$ is a universal object, the discontinuity of the coupling on the time-like axis, defined in (33). To compute running-coupling corrections using (56) we need to repeat the calculation of the diagram, but now with the massive propagator of (51) instead of the massless one (45). Doing this we find that Eq. (54) is unmodified while $\mathcal{K}_{\mathbf{xzy}}$ is replaced by its massive counterpart:

$$\mathcal{K}_{\mathbf{xzy}} \rightarrow \mathcal{K}_{\mathbf{xzy}}^m = -(\partial_x^j \partial_y^j + m^2) \int \frac{d^2 p d^2 q}{(2\pi)^2} \frac{e^{i\mathbf{p}(x-z)}}{\mathbf{p}^2 + m^2} \frac{e^{i\mathbf{q}(z-y)}}{\mathbf{q}^2 + m^2}, \quad (57)$$

where the two terms $\partial_x^j \partial_y^j$ and m^2 originate in the last and the middle terms in Eq. (51), respectively. As in the LO case, the $-i\delta_{x'y'}^{(4)}$ term in Eq. (51) does not contribute in the small- x limit.

Let us now compute the integrals in (57) explicitly. Denoting the “daughter dipoles” respective lengths by $r_i := |\mathbf{r}_i|$ ($i = 1, 2$) we obtain:

$$\mathcal{K}_{\mathbf{xzy}}^m = \mathcal{K}_{\mathbf{xzy}} r_1 m K_1(r_1 m) r_2 m K_1(r_2 m) - m^2 K_0(r_1 m) K_0(r_2 m) \quad (58)$$

where $\mathcal{K}_{\mathbf{xzy}}$ is the LO kernel of (55) and $K_0(x)$ and $K_1(x) = -dK_0(x)/dx$ are K -Bessel functions. These functions depend only on the lengths of the vectors \mathbf{r}_i , not on the angles — a direct consequence of the angular integration in (57). Angular dependence appears here *only* through the derivative $\partial_x^j \partial_y^j$, giving rise to the factor $\mathcal{K}_{\mathbf{xzy}}$ in the first term in (58), just as at LO.

The next observation is that upon applying the dispersive method to the self-energy diagrams in Eq. (10), in analogy with (56), one recovers again the LO result with the kernel of (57). Thus, *all* the diagrams share the same massive kernel $\mathcal{K}_{\mathbf{xzy}}^m$ of Eq. (58). Since also the dispersive integral of Eq. (56) is common to all three diagrams, running-coupling corrections to the JIMWLK Hamiltonian $\mathcal{H}[U]$ of (6) appear through the replacement:

$$\frac{\alpha_s}{\pi} \mathcal{K}_{\mathbf{xzy}} \rightarrow \mathcal{K}_{\mathbf{xzy}} \frac{1}{\beta_0} \int_0^\infty \frac{dm^2}{m^2} \rho_V(m^2) [\mathcal{F}(\mathbf{r}_1 m, \mathbf{r}_2 m) - 1], \quad (59)$$

where we defined the “characteristic function” $\mathcal{F}(\mathbf{r}_1 m, \mathbf{r}_2 m)$, following the general discussion in Sec. 3.1, by extracting the LO kernel:

$$\begin{aligned} \mathcal{K}_{\mathbf{xzy}}^m &=: \mathcal{K}_{\mathbf{xzy}} \mathcal{F}(\mathbf{r}_1 m, \mathbf{r}_2 m) = \mathcal{K}_{\mathbf{xzy}} \left[\mathcal{F}^T(\mathbf{r}_1 m, \mathbf{r}_2 m) + \mathcal{F}^L(\mathbf{r}_1 m, \mathbf{r}_2 m) \right], \\ \mathcal{F}^T(\mathbf{r}_1 m, \mathbf{r}_2 m) &= r_1 m K_1(r_1 m) r_2 m K_1(r_2 m), \\ \mathcal{F}^L(\mathbf{r}_1 m, \mathbf{r}_2 m) &= m^2 \frac{r_1^2 r_2^2}{\mathbf{r}_1 \cdot \mathbf{r}_2} K_0(r_1 m) K_0(r_2 m), \end{aligned} \quad (60)$$

and used the fact that $\lim_{m \rightarrow 0} \mathcal{F}(\mathbf{r}_1 m, \mathbf{r}_2 m) = 1$. Here \mathcal{F}^T and \mathcal{F}^L correspond to the first and second terms in (58), which in turn originate in the $\partial_x^j \partial_y^j$ and m^2 terms in (57), respectively. As mentioned

in Sec. 3.2 (see Eq. (51) there) these terms are associated with transverse (T) and longitudinal (L) gluons, respectively, which explains the notation in (60). As we see, these two contributions to $\mathcal{K}_{\mathbf{xzy}}^m$ are rather different in nature: the first can be naturally written as a product of the scale-invariant kernel $\mathcal{K}_{\mathbf{xzy}}$ times a function of the lengths of the “daughter dipoles”, while the second brings in an entirely new structure that does not share the angular dependence of the LO kernel.

We also introduce a notation for the “effective charge”

$$R(\mathbf{r}_1\Lambda, \mathbf{r}_2\Lambda) := \frac{1}{\beta_0} \int_0^\infty \frac{dm^2}{m^2} \rho_V(m^2) \left[\mathcal{F}(\mathbf{r}_1 m, \mathbf{r}_2 m) - 1 \right], \quad (61)$$

which plays the rôle of a scale-dependent α_s/π in all our calculations: the substitution of

$$\frac{\alpha_s}{\pi} \mathcal{K}_{\mathbf{xzy}} \rightarrow \mathcal{M}_{\mathbf{xzy}} := R(\mathbf{r}_1\Lambda, \mathbf{r}_2\Lambda) \mathcal{K}_{\mathbf{xzy}} \quad (62)$$

in (6) promotes all the fixed coupling diagrams entering the JIMWLK equation to running coupling. The running coupling corrected JIMWLK Hamiltonian then reads

$$\mathcal{H}[U] = -\frac{1}{2\pi} \mathcal{M}_{\mathbf{xzy}} \left[U_{\mathbf{z}}^{ab} (i\bar{\nabla}_{\mathbf{x}}^a i\nabla_{\mathbf{y}}^b + i\nabla_{\mathbf{x}}^a i\bar{\nabla}_{\mathbf{y}}^b) + (i\nabla_{\mathbf{x}}^a i\nabla_{\mathbf{y}}^a + i\bar{\nabla}_{\mathbf{x}}^a i\bar{\nabla}_{\mathbf{y}}^a) \right]. \quad (63)$$

All other ingredients in the JIMWLK equation (5) and the definition of correlator averages (4) remain unchanged. Eq. (62), and with it (63), is our key result that fully implements running coupling in the JIMWLK equation.

3.4 Borel representation of the resummed kernel

To systematically define the perturbative sum and analyze power corrections in the JIMWLK kernel $\mathcal{M}_{\mathbf{xzy}}$, it is convenient to write a Borel representation of the “effective charge” R , in the form of Eq. (29):

$$\mathcal{M}_{\mathbf{xzy}} = \mathcal{K}_{\mathbf{xzy}} R(\mathbf{r}_1\Lambda, \mathbf{r}_2\Lambda) = \frac{1}{\beta_0} \int_0^\infty du T(u) \left(\frac{\mu^2}{\Lambda^2} \right)^{-u} \mathcal{K}_{\mathbf{xzy}} B(u, \mathbf{r}_1\mu, \mathbf{r}_2\mu), \quad (64)$$

where the Borel function is related to the characteristic function \mathcal{F} (see Eq. (38)) by

$$B(u, \mathbf{r}_1\mu, \mathbf{r}_2\mu) = -e^{\frac{5}{3}u} \frac{\sin \pi u}{\pi} \int_0^\infty \frac{dm^2}{m^2} \left(\frac{m^2}{\mu^2} \right)^{-u} \left[\mathcal{F}(\mathbf{r}_1 m, \mathbf{r}_2 m) - 1 \right]. \quad (65)$$

Owing to the different nature of the transverse and longitudinal contributions to \mathcal{F} , it is convenient to deal with them separately also on the level of the Borel function. To this end we write

$$B(u, \mathbf{r}_1\mu, \mathbf{r}_2\mu) = B^T(u, \mathbf{r}_1\mu, \mathbf{r}_2\mu) + B^L(u, \mathbf{r}_1\mu, \mathbf{r}_2\mu), \quad (66)$$

corresponding to the two terms in (60). Below we present explicit expressions for these functions in both momentum and coordinate space. Using (57) and (65) we obtain the following expressions

as Fourier transformations from momentum space:

$$\begin{aligned}
\mathcal{K}_{\mathbf{xzy}} B^T(u, \mathbf{r}_1\mu, \mathbf{r}_2\mu) &= -e^{\frac{5}{3}u} \frac{\sin \pi u}{\pi} \int \frac{d^2p d^2q}{(2\pi)^2} e^{i\mathbf{p}\cdot\mathbf{r}_1} e^{-i\mathbf{q}\cdot\mathbf{r}_2} \\
&\quad \times \int_0^\infty \frac{dm^2}{m^2} \left(\frac{m^2}{\mu^2}\right)^{-u} (-1) \left[\frac{\mathbf{p}\cdot\mathbf{q}}{(\mathbf{p}^2+m^2)(\mathbf{q}^2+m^2)} - \frac{\mathbf{p}\cdot\mathbf{q}}{\mathbf{p}^2\mathbf{q}^2} \right] \\
&= -e^{\frac{5}{3}u} \int \frac{d^2p d^2q}{(2\pi)^2} e^{i\mathbf{p}\cdot\mathbf{r}_1} e^{-i\mathbf{q}\cdot\mathbf{r}_2} \frac{\mathbf{p}\cdot\mathbf{q}}{\mathbf{p}^2\mathbf{q}^2} \frac{\mathbf{q}^2 \left(\frac{\mathbf{p}^2}{\mu^2}\right)^{-u} - \mathbf{p}^2 \left(\frac{\mathbf{q}^2}{\mu^2}\right)^{-u}}{\mathbf{q}^2 - \mathbf{p}^2}, \quad (67a)
\end{aligned}$$

$$\begin{aligned}
\mathcal{K}_{\mathbf{xzy}} B^L(u, \mathbf{r}_1\mu, \mathbf{r}_2\mu) &= -e^{\frac{5}{3}u} \frac{\sin \pi u}{\pi} \int \frac{d^2p d^2q}{(2\pi)^2} e^{i\mathbf{p}\cdot\mathbf{r}_1} e^{-i\mathbf{q}\cdot\mathbf{r}_2} \\
&\quad \times \int_0^\infty \frac{dm^2}{m^2} \left(\frac{m^2}{\mu^2}\right)^{-u} \frac{-m^2}{(\mathbf{p}^2+m^2)(\mathbf{q}^2+m^2)} \\
&= -e^{\frac{5}{3}u} \int \frac{d^2p d^2q}{(2\pi)^2} e^{i\mathbf{p}\cdot\mathbf{r}_1} e^{i\mathbf{q}\cdot\mathbf{r}_2} \frac{\left(\frac{\mathbf{p}^2}{\mu^2}\right)^{-u} - \left(\frac{\mathbf{q}^2}{\mu^2}\right)^{-u}}{\mathbf{p}^2 - \mathbf{q}^2}. \quad (67b)
\end{aligned}$$

These expressions assume a perhaps more familiar form if we restrict ourselves to one-loop running, where, with $T(u) = 1$, expanding under the Borel integral amounts to replacing the powers of the momenta $\mathbf{k} = \mathbf{p}, \mathbf{q}$, i.e. $(\mathbf{k}^2/\mu^2)^{-u}$ by the corresponding geometric series according to

$$\left(\frac{\mathbf{k}^2}{\mu^2}\right)^{-u} \rightarrow \frac{\alpha_s(\mu^2)}{\pi} \frac{1}{1 + \frac{\beta_0\alpha_s(\mu^2)}{\pi} \ln(\mathbf{k}^2/\mu^2)}. \quad (68)$$

In fact, using (64) and (68), the expressions in (67) can be directly mapped onto the expressions derived diagrammatically in [103].

We note that in the purely virtual case of Fig. 2 (c) the result simplifies in the expected manner: there the \mathbf{z} integral may be performed and, in the absence of interaction with the target, it sets $\mathbf{q} = \mathbf{p}$. Then the *sum* of the integrands of transverse and longitudinal contributions (67) yields

$$\underbrace{\frac{1}{\mathbf{p}^2} \left(\frac{\mathbf{p}^2}{\mu^2}\right)^{-u}}_{\text{from } \mathcal{K} B^T} (1+u) - \underbrace{\frac{1}{\mathbf{p}^2} \left(\frac{\mathbf{p}^2}{\mu^2}\right)^{-u}}_{\text{from } \mathcal{K} B^L} u = \frac{1}{\mathbf{p}^2} \left(\frac{\mathbf{p}^2}{\mu^2}\right)^{-u}. \quad (69)$$

Via (68), this corresponds to $(1/\mathbf{p}^2)\alpha_s(\mathbf{p}^2 e^{-\frac{5}{3}})/\pi$, which is the expected contribution of a gluon of transverse momentum \mathbf{p}^2 that does not interact with the background field. Note that there is an important cancellation at NLO (and beyond) between the separate contributions of transverse and longitudinal gluons. On the level of the dispersive integrals used to define B^T and B^L this cancellation is even more obvious: for $\mathcal{K}_{\mathbf{xzy}}^m$ (c.f. Eq. (57)) it takes the form

$$\frac{\mathbf{p}\cdot\mathbf{q} + m^2}{(\mathbf{p}^2+m^2)(\mathbf{q}^2+m^2)} \xrightarrow{\mathbf{q}\rightarrow\mathbf{p}} \frac{1}{\mathbf{p}^2+m^2}, \quad (70)$$

which has exactly the same interpretation.

Direct Fourier integration of the perturbative sum obtained through (68) is not well defined owing to the Landau pole. In this respect these all-order expressions are largely symbolic. Correspondingly, the Borel integrals of both (67a) and (67b) converge for $u \rightarrow \infty$ only when the momenta are larger than the QCD scale Λ . Thus, when we exchange the order of integrations and perform the Borel integration *after* the Fourier transforms, the Borel integral will no longer be unambiguous for any value of the coordinates. As we shall see explicitly below, the coordinate-space Borel function exhibits poles along the integration path, at positive integer values of u . This reflects ambiguities in summing the series, which are indicative of power corrections (see the general discussion in Sec. 3.1). Knowing the location of the poles and the parametric dependence of their residues on the hard scales involved, one can estimate the effect of non-perturbative power corrections. It is the advantage of the Borel method to expose these power corrections in such a clear and concise way.

With this in mind we now perform the Fourier transformation of the Borel functions. The all-order expressions lead to infinite sums that can be recast in terms of hypergeometric functions. The calculation is done using integral representations of the Bessel functions. The integrals over the dispersive mass intertwine the parameter integrations so that it becomes necessary to use Mellin-Barnes representations to decouple them. The Mellin-Barnes integrals are done last and lead to infinite sums of residues. Details of the rather involved algebra are given separately for B^T and B^L in Appendix A and B, respectively.

To express the results in a compact manner we define

$$r_> := \max\{r_1, r_2\}; \quad r_< := \min\{r_1, r_2\}; \quad \xi := \frac{r_<}{r_>}. \quad (71)$$

We present two versions for each of the results for B^T and B^L , as a series in ξ^2 and in $1 - \xi^2$, respectively. This is important for numerical implementations near $\xi = 0$ and $\xi = 1$, respectively, and will be used in Sec. 6.1 below. In addition, the first form conveniently displays the singularity structure and the functional form of the residues, while the second form is convenient for performing an expansion in u , in order to extract the perturbative coefficients.

The coordinate-space result for B^T is:

$$\begin{aligned} \mathcal{K}_{\mathbf{xzy}} B^T(u, \mathbf{r}_1\mu, \mathbf{r}_2\mu) &= \frac{\mathbf{r}_1 \cdot \mathbf{r}_2}{r_1^2 r_2^2} \left(\frac{4e^{-\frac{5}{3}}}{r_>^2 \mu^2} \right)^{-u} \frac{\sin(\pi u)}{\pi} \left\{ \Gamma(1-u)\Gamma(-u) \right. \\ &\quad + \sum_{k=0}^{\infty} (\xi^2)^{1+k} \frac{\Gamma(2-u+k)\Gamma(1-u+k)}{\Gamma(1+k)\Gamma(2+k)} \\ &\quad \left. \times \left(\Psi(2-u+k) + \Psi(1-u+k) - \Psi(2+k) - \Psi(1+k) + \ln \xi^2 \right) \right\}, \end{aligned} \quad (72a)$$

which can be recast in terms of a hypergeometric series ${}_2F_1$ using 15.3.11 of [104]

$$\begin{aligned} &= - \frac{\mathbf{r}_1 \cdot \mathbf{r}_2}{r_1^2 r_2^2} \left(\frac{4e^{-\frac{5}{3}}}{r_>^2 \mu^2} \right)^{-u} \frac{\sin(\pi u)}{\pi} \frac{u(1-u)\Gamma^2(-u)\Gamma^2(1-u)}{\Gamma(2-2u)} \\ &\quad \times {}_2F_1 \left(\begin{matrix} 1-u, -u \\ 2-2u \end{matrix} \middle| 1-\xi^2 \right). \end{aligned} \quad (72b)$$

A useful alternative expression to (72b) can be obtained using the identity:

$${}_2F_1\left(\begin{matrix} 1-u, -u \\ 2-2u \end{matrix} \middle| 1-\xi^2\right) = \xi^2 \left[1 - \frac{1-\xi^2}{1-u} \frac{d}{d\xi^2} \right] {}_2F_1\left(\begin{matrix} 1-u, 1-u \\ 2-2u \end{matrix} \middle| 1-\xi^2\right). \quad (73)$$

The result for B^L is:

$$\begin{aligned} \mathcal{K}_{\mathbf{xz}\mathbf{y}} B^L(u, \mathbf{r}_1\mu, \mathbf{r}_2\mu) &= -\frac{\sin(\pi u)}{\pi} \frac{1}{\mathbf{r}_>^2} \left(\frac{4e^{-\frac{5}{3}}}{\mathbf{r}_>^2\mu^2} \right)^{-u} \sum_{k=0}^{\infty} \left(\frac{\Gamma(k+1-u)}{\Gamma(k+1)} \right)^2 (\xi^2)^k \\ &\quad \times \left(\ln(\xi^2) - 2\Psi(k+1) + 2\Psi(k+1-u) \right), \end{aligned} \quad (74a)$$

which again can be expressed in terms of a hypergeometric function, this time using 15.3.10 of [104],

$$= +\frac{\sin(\pi u)}{\pi} \frac{1}{\mathbf{r}_>^2} \left(\frac{4e^{-\frac{5}{3}}}{\mathbf{r}_>^2\mu^2} \right)^{-u} \frac{\Gamma^4(1-u)}{\Gamma(2-2u)} {}_2F_1\left(\begin{matrix} 1-u, 1-u \\ 2-2u \end{matrix} \middle| 1-\xi^2\right). \quad (74b)$$

The result is fully symmetric in \mathbf{r}_1 and \mathbf{r}_2 , in particular all coefficients in an expansion in powers of u (or α_s) have this property.

Our expressions for B^T and B^L can be put to use in several ways. The first two pertain to obtaining information on the perturbation theory:

- *A generating function* for the perturbative expansion in powers of $\alpha_s(\mu^2)$ (at a fixed scale). To this end one expands the results for the Borel function around $u = 0$ and then integrates over u in (64) term by term. Assuming one-loop coupling ($T(u) = 1$) this amounts to the replacement:

$$u^n \longrightarrow n! \left(\beta_0 \frac{\alpha_s(\mu^2)}{\pi} \right)^{n+1}. \quad (75)$$

- Knowing the analytic structure of the Borel function, which has a leading renormalon singularity at $u = 1$, it is clear that the expansion: (1) does not converge, and (2) it is not Borel summable; *A definition of the sum* in (64) is required. Starting from the expansion, a natural prescription is to truncate the sum at the minimal term. A more systematic regularization, which has been found useful in several applications in QCD, see e.g. [52, 54, 101], is the Principal Value (PV) of the Borel integral in (64).

In the next section (Sec. 4) we will perform the perturbative expansion of the JIMWLK kernel, study numerically its apparent convergence in the first few orders, and compare it to the PV Borel sum. We also examine the approximation of the sum by scale setting. These issues are revisited in Sec. 6 where we examine the effect of the newly computed higher-order corrections on the evolution in the case of the BK equation.

The third application goes beyond perturbation theory; we can extract information on the power corrections from the integrand: in (64):

- The renormalon poles at positive integer u in B^T and B^L can be used to infer the parametric form and significance of non-perturbative power corrections that are expected to affect the evolution kernel.

This is discussed in Sec. 5 for a single evolution step and re-visited in Sec. 6 when solving the evolution equations numerically.

4 Perturbation theory

Having computed the Borel function $B(u)$ entering Eq. (64), we have essentially determined the expansion coefficients for $R(\mathbf{r}_1\Lambda, \mathbf{r}_2\Lambda)$, and thus for the JIMWLK evolution kernel, to all orders in the large- β_0 limit. To get the coefficients one expands the expressions for $B^T(u, \mathbf{r}_1\mu, \mathbf{r}_2\mu)$ and $B^L(u, \mathbf{r}_1\mu, \mathbf{r}_2\mu)$ in Sec. 3.4 under the integral in (64),

$$B^T(u, \mathbf{r}_1\mu, \mathbf{r}_2\mu) = 1 + \sum_{n=1}^{\infty} b_n^T(\mathbf{r}_1\mu, \mathbf{r}_2\mu)u^n; \quad B^L(u, \mathbf{r}_1\mu, \mathbf{r}_2\mu) = \sum_{n=1}^{\infty} b_n^L(\mathbf{r}_1\mu, \mathbf{r}_2\mu)u^n \quad (76)$$

and integrates over the Borel variable term by term²⁴, to obtain:

$$\mathcal{M}_{\mathbf{xzy}} = R(\mathbf{r}_1\Lambda, \mathbf{r}_2\Lambda)\mathcal{K}_{\mathbf{xzy}} = \mathcal{K}_{\mathbf{xzy}} \frac{\alpha_s(\mu^2)}{\pi} \left(1 + \sum_{n=1}^{\infty} n! \left(\beta_0 \frac{\alpha_s(\mu^2)}{\pi} \right)^n b_n(\mathbf{r}_1\mu, \mathbf{r}_2\mu) \right), \quad (77)$$

with

$$b_n(\mathbf{r}_1\mu, \mathbf{r}_2\mu) := b_n^T(\mathbf{r}_1\mu, \mathbf{r}_2\mu) + b_n^L(\mathbf{r}_1\mu, \mathbf{r}_2\mu). \quad (78)$$

The purpose of this section is to study the effect of these perturbative corrections to the JIMWLK evolution kernel.

Explicit expressions for the expansion coefficients will be presented in Eqs. (80) and (82) below. Before looking into the details, let us briefly recall what one expects on general grounds following the discussion in Sec. 3.1:

- **The all-order sum is renormalization scale invariant:** Eq. (64) is renormalization-scale invariant. This means that also (77) shares this property, if it is formally considered to all orders. However, the choice of the expansion parameter would make any finite-order partial sum scale dependent.
- **The series in non-summable owing to infrared renormalons, which amount to power-suppressed ambiguities:** Going beyond the level of a finite-order partial sum, in an attempt to compute $R(\mathbf{r}_1\Lambda, \mathbf{r}_2\Lambda)$ to all orders, one finds infrared renormalon ambiguities. Let us explain how they arise here: since $B(u)$ in (64) has a finite radius of convergence ($u = 1$), b_n in (77) are characterized at high orders by geometrical progression with no sign oscillation. With the explicit $n!$ growth in (77), it is obvious that the series would not converge, but instead reach a minimal term, and then start diverging. An optimal perturbative

²⁴Since we are using one-loop running coupling, this amounts to making the replacement of Eq. (75).

approximation may be defined by truncation at the minimal term. This, however, is inconvenient since the truncation order may (and in our case does) depend on all the scales in the problem (in our case r^2 , r_1^2 and r_2^2). A more systematic definition of the sum can be made using the Borel sum (80). This integral does not exist as it stands, since the poles appear at real positive values of u , on the integration path. One can *define* the sum by shifting the contour above or below the real axis, or by choosing the Principal Value (PV) prescription. The differences between these choices are *power-suppressed* in the hard scales: they scale as integer powers of $\Lambda^2 r^2$, $\Lambda^2 r_1^2$ and $\Lambda^2 r_2^2$ (up to logarithms, see Sec. 5). The size of this ambiguity is obviously controlled by the residues of $B(u)$ in (80) and can therefore be explicitly computed. It is also similar to the magnitude of the minimal term in the series. Since these ambiguities are expected to cancel against non-perturbative power corrections, they provide important information on such corrections to the kernel, that are otherwise unknown. We will return to discuss these corrections in detail in Sec. 5.

Our default choice for defining the all-order sum of the series is the PV prescription. Having made this choice, we will examine the convergence of the perturbative expansion in the first few orders, and demonstrate (Fig. 3) the dependence of this (apparent) convergence on the region of phase space as well as on the choice of the expansion parameter.

Technically, the implementation of the PV regularization in the present case is complicated by the fact that Eqs. (72) and (74) contain terms with double poles²⁵ in u . We cope with this in the standard technique by isolating the double pole contributions and using integration by parts. The explicit expressions used in defining R are given in Appendix E; they are in turn based on the explicit expression for the first- and second-order poles extracted in Appendices C and D.

The numerical result for the PV Borel sum is shown in Fig. 3. To appreciate the qualities of this prescription as means of defining the all-order sum, it is useful to compare it with increasing-order partial sums. The expansion of the Borel functions can be conveniently obtained starting with expressions (74b) for B^L and (72b) with (73) for B^T , which involve ${}_2F_1\left(\begin{smallmatrix} 1-u, 1-u \\ 2-2u \end{smallmatrix} \middle| 1-\xi^2\right)$, a special case of the type E function expanded in [107] (see Eq. (4.29) there). It is convenient to define the dimensionless variable

$$\Omega := \frac{4 e^{-\frac{\xi}{3}-2\gamma_E}}{r_{>}^2 \mu^2}, \quad (79)$$

which appears as the argument of the logarithms in the coefficients. The expansion for B^T takes the form

$$\mathcal{K}_{\mathbf{xzy}} B^T(u, \mathbf{r}_1\mu, \mathbf{r}_2\mu) = \frac{1}{2} \frac{r^2 - (r_1^2 + r_2^2)}{r_1^2 r_2^2} \left[1 + \sum_{n=1}^{\infty} b_n^T(\mathbf{r}_1\mu, \mathbf{r}_2\mu) u^n \right], \quad (80a)$$

where

$$b_1^T(\mathbf{r}_1\mu, \mathbf{r}_2\mu) = -\ln(\Omega) - \frac{\xi^2 \ln(\xi^2)}{1-\xi^2}, \quad (80b)$$

²⁵The current example is by no means unique in this regard. The same occurs also in the absence of large target fields, e.g. for the well-studied example of the Adler function $D(Q^2) = 4\pi^2 d\Pi(Q^2)/dQ^2$, see [91, 105, 106].

$$b_2^T(\mathbf{r}_1\mu, \mathbf{r}_2\mu) = \frac{1}{2} \left(b_1^T(\mathbf{r}_1\mu, \mathbf{r}_2\mu) \right)^2 - \frac{\pi^2}{6} - \frac{1}{2} \frac{\left(\xi^2 \ln(\xi^2) \right)^2}{(1 - \xi^2)^2} + \frac{1 + \xi^2}{1 - \xi^2} \text{Li}_2(1 - \xi^2), \quad (80c)$$

$$b_3^T(\mathbf{r}_1\mu, \mathbf{r}_2\mu) = \frac{1}{1 - \xi^2} \left\{ -\frac{1}{6}(1 - \xi^2) \ln^3(\Omega) - \frac{1}{2} \ln^2(\Omega) \xi^2 \ln(\xi^2) \right. \\ \left. + \left[(\xi^2 + 1) (\ln(1 - \xi^2) \ln(\xi^2) + \text{Li}_2(\xi^2)) - \frac{\xi^2 \pi^2}{3} \right] \ln(\Omega) \right. \\ \left. + 2 \xi^2 \ln^2(\xi^2) \ln(1 - \xi^2) + 3 \xi^2 \ln(\xi^2) \text{Li}_2(\xi^2) + (2 \xi^2 + 2) \text{Li}_3(1 - \xi^2) \right. \\ \left. - 2 \xi^2 \text{Li}_3(\xi^2) + \left(-\frac{4}{3} + \frac{10 \xi^2}{3} \right) \zeta_3 - 4 \xi^2 (1 - \xi^2) \frac{dS_{2,2}(z)}{dz} \Big|_{z=1-\xi^2} \right\}. \quad (80d)$$

$dS_{2,2}(z)/dz$ in (80d) is the first occurrence of a Nielsen polylogarithm,

$$S_{a,b}(z) := \frac{(-1)^{a+b-1}}{(a-1)!b!} \int_0^1 \frac{d\xi}{\xi} \ln^{a-1}(\xi) \ln^b(1 - \xi z). \quad (81)$$

At higher orders in the expansion one encounters [107] higher Nielsen polylogarithms, as well as other harmonic polylogarithms [108].

The longitudinal part, B^L starts at order u , corresponding to $\mathcal{O}(\beta_0 \alpha_s^2)$. The expansion takes the form:

$$\mathcal{K}_{\mathbf{xzy}} B^L(u, \mathbf{r}_1\mu, \mathbf{r}_2\mu) = \sum_{n=1}^{\infty} \mathcal{K}_{\mathbf{xzy}} b_n^L(\mathbf{r}_1\mu, \mathbf{r}_2\mu) u^n, \quad (82a)$$

where, from (74b), we find

$$\mathcal{K}_{\mathbf{xzy}} b_1^L(\mathbf{r}_1\mu, \mathbf{r}_2\mu) = -\frac{1}{r_{>}^2} \frac{\ln(\xi^2)}{1 - \xi^2}, \quad (82b)$$

$$\mathcal{K}_{\mathbf{xzy}} b_2^L(\mathbf{r}_1\mu, \mathbf{r}_2\mu) = +\frac{1}{r_{>}^2} \frac{\ln(\xi^2) \ln(\Omega) + 2 \text{Li}_2(1 - \xi^2)}{1 - \xi^2}, \quad (82c)$$

$$\mathcal{K}_{\mathbf{xzy}} b_3^L(\mathbf{r}_1\mu, \mathbf{r}_2\mu) = -\frac{1}{r_{>}^2} \frac{1}{1 - \xi^2} \left[\ln(\xi^2) \text{Li}_2(\xi^2) - 2 \text{Li}_3(\xi^2) + 2 \zeta_3 - 4 \text{Li}_3(1 - \xi^2) \right. \\ \left. + \frac{1}{2} \ln(\xi^2) \ln^2(\Omega) + 2 \ln(\Omega) \text{Li}_2(1 - \xi^2) \right]. \quad (82d)$$

It is interesting to note that there is a qualitative difference between the leading behavior of the transverse and the longitudinal contributions, respectively. The sign of the LO, transverse contribution to the kernel $\mathcal{M}_{\mathbf{xzy}}$ in (77) can be directly read of Eq. (55); it is

$$\begin{aligned} \mathcal{M}_{\mathbf{xzy}}^T &> 0 && \text{inside the circle: } r_1^2 + r_2^2 < r^2 \\ \mathcal{M}_{\mathbf{xzy}}^T &< 0 && \text{outside the circle: } r_1^2 + r_2^2 > r^2, \end{aligned} \quad (83)$$

while the NLO longitudinal contribution to $\mathcal{M}_{\mathbf{xzy}}$, in (82b), is *always* positive.

With the explicit expressions of (80) and (82) we can now study the convergence of the perturbative series in (77) and compare the finite-order results to the PV definition of the all-order sum. Of course, at this point we must²⁶ make a choice of scale μ . Since $\mathcal{M}_{\mathbf{xzy}} = R(\mathbf{r}_1\Lambda, \mathbf{r}_2\Lambda)\mathcal{K}_{\mathbf{xzy}}$ is renormalization invariant (i.e. μ -independent) one may choose *any* function of r_1 , r_2 and r as long as the convergence of the perturbative series is good enough. As we shall see, this choice makes a significant difference for the apparent convergence at the first few orders.

A priori, a natural choice (see Sec. 2.2) may be the “parent dipole” size: $\mu^2 = c/r^2$. A posteriori, knowing the coefficients in (80) and (82), one can optimize the scale to reduce the size of subleading corrections. One possibility is to introduce BLM scale setting [80] by requiring that the entire NLO coefficient $b_1(\mathbf{r}_1\mu, \mathbf{r}_2\mu)$ would vanish identically²⁷:

$$\begin{aligned} \mathcal{K}_{\mathbf{xzy}}b_1^T(\mathbf{r}_1\mu, \mathbf{r}_2\mu) + \mathcal{K}_{\mathbf{xzy}}b_1^L(\mathbf{r}_1\mu, \mathbf{r}_2\mu) &= 0 \\ \implies \mu_{\text{BLM}}^2 &= \frac{4}{r_{>}^2} \exp\left\{-\frac{5}{3} - 2\gamma_E + \frac{\xi^2 \ln(\xi^2)}{1 - \xi^2} \left(1 + \frac{2r_{>}^2}{r^2 - r_{>}^2 - r_{<}^2}\right)\right\}. \end{aligned} \quad (84)$$

In our case, however, this approach is too simplistic: since the leading-order kernel vanishes on the circle $r_1^2 + r_2^2 = r^2$, as implied by (83), while the NLO contribution associated with B^L does not, (84) develops an artificial singularity *within the perturbative region*. Consequently, with this particular choice of scale, higher-order terms would not be bounded on the circle, while no special difficulty would arise there otherwise. While better possibilities for optimizing the scale exist — for example, setting the BLM scale such that the NLO *transverse* contribution would vanish $b_1^T(\mathbf{r}_1\mu, \mathbf{r}_2\mu) = 0$ — we will not take this avenue here. Let us just note in passing that the multi-scale nature of the problem, which is reflected in the dependence on the parent and daughter dipoles — or in momentum space by the separate Borel powers of the transverse momentum before and after the interaction with the target (Eq. (67)) — renders any scale-setting procedure in terms of a *single* coupling unnatural. Further progress in this direction will be reported in Ref. [103]. Here we consider a couple of simple examples for the scale:

$$\mu^2 = \frac{4e^{-5/3-2\gamma_E}}{r^2} \quad \text{and} \quad \mu^2 = \frac{8e^{-5/3-2\gamma_E}}{r_1^2 + r_2^2}. \quad (85)$$

The choice of the constant $4e^{-5/3-2\gamma_E} \approx 0.24$ is motivated by Eq. (84).

In Fig. 3 we show a numerical comparison of the order-by-order expansion with the PV Borel sum. As expected, at short distance scales perturbation theory is well-behaved²⁸: the first few orders in (64) gradually approach the PV Borel sum. For larger distances, the corrections become large, and the minimal term in the series is reached sooner (see Fig. 3 (b)). Eventually, for $r_1\Lambda$ of order of a few times 10^{-1} , the series diverges right from the start. Note that even in that region the PV Borel sum is uniquely defined, but as we shall see in the next section, power corrections are large as well.

²⁶To avoid the ultraviolet problems of a conventional fixed-coupling calculation one in fact needs to choose μ as *some* function of r_1 , r_2 and r instead of a single homogeneous scale independent of the configuration encountered [45].

²⁷To express the $\mathcal{K}_{\mathbf{xzy}}$ in the transverse part in terms of dipole lengths only we substitute: $-\mathbf{r}_1 \cdot \mathbf{r}_2 = (r^2 - r_1^2 - r_2^2)/2$, as in (55) above.

²⁸If we allow the constant in (85) to vary significantly compared the choice indicated, the convergence in both Figs. 3 (a) and (b) becomes appreciably worse, an obvious consequence of the logarithmic terms in the coefficients, see (80) and (82).

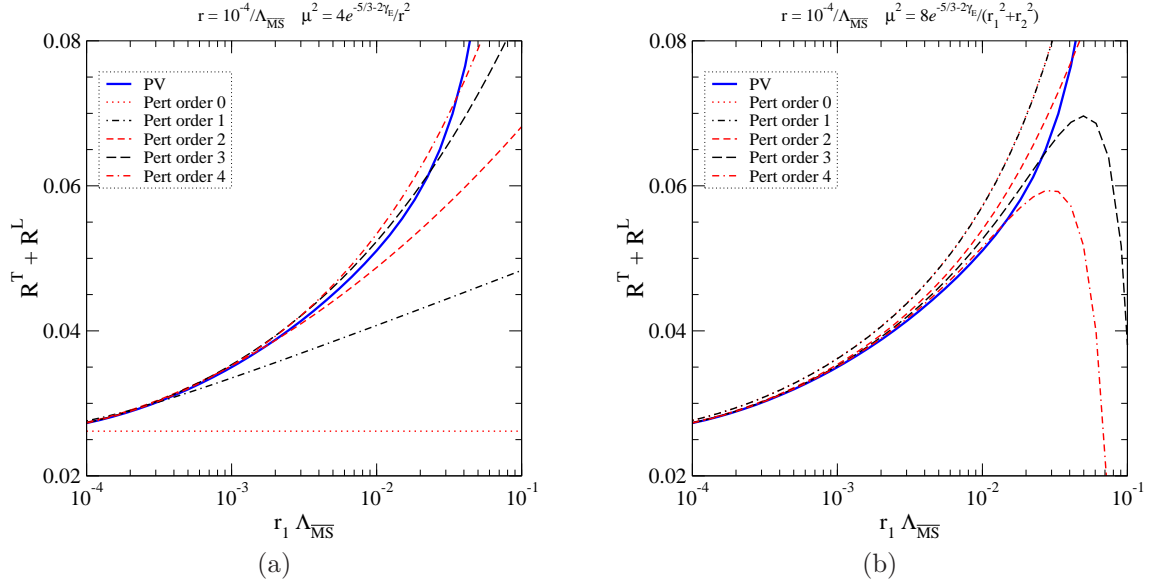


Figure 3: $R(r_1\Lambda, r_2\Lambda)$ as defined with a PV regularization of the Borel sum (64), and the convergence of perturbation theory at the first few orders, according to (77), with $\mu^2 = 4 \exp(-\frac{5}{3} - 2\gamma_E)/r^2$ (in (a)) and $\mu^2 = 8 \exp(-\frac{5}{3} - 2\gamma_E)/(r_1^2 + r_2^2)$ (in (b)). R is shown as a function of r_1 , with $r\Lambda = 10^{-4}$, $\mathbf{r} \parallel \mathbf{r}_1 \parallel \mathbf{r}_2$ and $r_2 = r_1 + r$.

It is interesting to further observe that there is a significant difference in the apparent convergence in the first few orders between Figs. 3 (a) and (b): the “parent dipole” scale setting in Fig. 3 (a) has significant corrections even at short distances, while with the scale choice of Fig. 3 (b) the first few orders provide a better approximation. It should be emphasized though that Fig. 3 shows a particular situation where $r_1, r_2 \gg r$. If the dipole sizes are of comparable magnitude, there is no significant difference between these two choices of scale²⁹. The fact that “parent dipole” running fails to approximate the kernel for $r_1, r_2 \gg r$, makes a difference for evolution when $R_s \gg r_1, r_2 \gg r$. We observe that parent dipole running in this region generically underestimates the perturbative sum. Accordingly, in Sec. 6.2, we will see that evolution is slower with the “parent dipole” ansatz than with the Borel sum.

In Fig. 4 we compare the PV Borel sum with two ad hoc running–coupling formulae, the “parent dipole” running and the “square–root daughter–dipole” running:

$$R_{\text{parent}} = \alpha_s^{\overline{\text{MS}}}(c^2/r^2)/\pi = \frac{1}{\beta_0 \ln(c^2/(r^2\Lambda^2))}; \quad R_{\text{sqrt}} = \left[\alpha_s^{\overline{\text{MS}}}(c^2/r_1^2) \alpha_s^{\overline{\text{MS}}}(c^2/r_2^2) \right]^{1/2}/\pi. \quad (86)$$

In these expressions we fix the scale $c^2 = 4e^{-\frac{5}{3} - 2\gamma_E}$, as motivated by Eq. (85). This ensures that these couplings would match the PV Borel sum soon enough when both $r_2, r_1 \ll 1/\Lambda$. This is shown on the right panel of Fig. 4. We note here that c^2 here is much smaller than the value $c^2 = 4$ arising

²⁹For clarity, let us comment that we have chosen to show the function R with \mathbf{r}_1 parallel to \mathbf{r}_2 . This avoids the apparent divergence $(\mathbf{r}_1 \cdot \mathbf{r}_2)^{-1}$ in the definition of R^L ; this divergence is exactly canceled in the BK kernel when R is multiplied by $K_{\mathbf{xzy}}$.

from a Fourier transform in the double logarithmic limit. From Fig. 4 it is clear that different

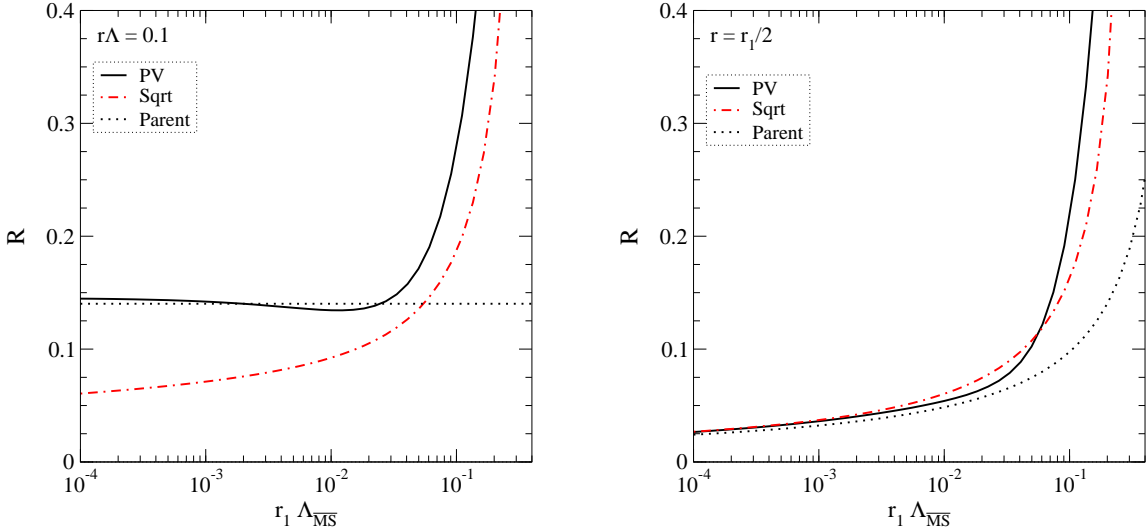


Figure 4: Comparison of ad hoc implementations for effective couplings R calculated with the principal value (PV) prescription, the “square root” prescription $[\alpha_s(c^2/r_1^2) \alpha_s(c^2/r_2^2)]^{1/2}/\pi$, and the parent dipole running $\alpha_s(c^2/r^2)/\pi$. On the left panel the size of the parent dipole is fixed, $r\Lambda = 0.1$ (and $r_2 = r_1 + r$); on the right panel the ratio of the dipole sizes is fixed, $r_1 = 2r$, $r_2 = 3r$.

definitions of running coupling can be made to match reasonably well at small enough dipole sizes, at least in parts of phase space, if the scales are chosen appropriately. On the other hand, at small dipole sizes, already at $0.1\text{--}0.3 \times 1/\Lambda$ the coupling diverge strongly. This related of course to the smallness of the effective scale at which the coupling is evaluated, $\mu_{\text{eff}}^2 \sim 4 e^{-\frac{5}{3}-2\gamma_E}/r^2$. As we shall see below, the effect of this divergence on the evolution rate (in the BK approximation) is somewhat less important than for R . This is to be expected, as evolution rate is an inclusive observable, and as such has reduced sensitivity to the phase-space region where the effective coupling is large.

5 Non-perturbative power corrections

After discussing the perturbative features in some detail, let us now turn to estimates the non-perturbative corrections to the JIMWLK kernel $\mathcal{M}_{\mathbf{xy}}$. The renormalon poles in R allow us to determine the type of power corrections, and their parametric form, based on the singularities of B^T and B^L . The original expressions in (72) and (74) have simple and double poles at integer values of u . As explained in the Appendices C and D, we perform integration by parts over the double pole terms to arrive at a representation of the Borel integral where the integrand is composed of simple poles only; in this way the double poles have been converted into a simple ones accompanied by a logarithmic-enhancement factor, $\ln(\Omega)$ where Ω is given in Eq. (79). In this representation,

the explicit expressions for the renormalon poles are the following:

$$\begin{aligned}
\mathcal{K}_{\mathbf{xzy}} B^T(u, \mathbf{r}_1 \mu, \mathbf{r}_2 \mu) &= \mathcal{K}_{\mathbf{xzy}} \left\{ \left(\frac{4e^{-\frac{5}{3}}}{r_{>}^2 \mu^2} \right)^{-1} \frac{-2 + (1 - \xi^2)}{u - 1} \right. \\
&+ \sum_{m=2}^{\infty} \sum_{n=2(m-1)}^{\infty} \frac{(-1)^m (1 - \xi^2)^n}{u - m} \frac{1}{\Gamma(n+1)} \left(\frac{4e^{-\frac{5}{3}}}{r_{>}^2 \mu^2} \right)^{-m} \frac{\Gamma(1 - m + n)}{\Gamma(n - 2(m-1)) \Gamma(m-1)} \\
&+ \sum_{m=2}^{\infty} \sum_{n=2}^{m-1} \frac{(1 - \xi^2)^n}{\Gamma(n+1)} \frac{2(-1)^{m-n}}{(u - m)} \\
&\times \frac{d}{dm} \left[\left(\frac{4e^{-\frac{5}{3}}}{r_{>}^2 \mu^2} \right)^{-m} \frac{\Gamma(2m - (n+1))}{\Gamma(m) \Gamma(m-1) \Gamma(m-n) \Gamma(m+1-n)} \right] \left. \right\} \\
&+ \text{regular contributions} \tag{87a}
\end{aligned}$$

and

$$\begin{aligned}
\mathcal{K}_{\mathbf{xzy}} B^L(u, \mathbf{r}_1 \mu, \mathbf{r}_2 \mu) &= - \sum_{m=1}^{\infty} \sum_{n=m}^{\infty} \frac{-(-1)^m}{u - m} \frac{1}{r_{>}^2} \left(\frac{4e^{-\frac{5}{3}}}{r_{>}^2 \mu^2} \right)^{-m} \frac{(1 - \xi^2)^n}{\Gamma(n+1)} \frac{(\Gamma(n+1-m))^2}{(\Gamma(m))^2 \Gamma(n+2-2m)} \\
&- \sum_{m=1}^{\infty} \sum_{n=0}^{m-1} \frac{2(-1)^{m-n}}{u - m} \frac{(1 - \xi^2)^n}{\Gamma(n+1)} \frac{1}{r_{>}^2} \frac{d}{dm} \left[\left(\frac{4e^{-\frac{5}{3}}}{r_{>}^2 \mu^2} \right)^{-m} \frac{\Gamma(2m - (n+1))}{(\Gamma(m))^2 (\Gamma(m-n))^2} \right] \\
&+ \text{regular contributions} . \tag{87b}
\end{aligned}$$

To determine the ambiguity associated with each renormalon we should first sum transverse and longitudinal contributions, and then isolate the residue at fixed $u = m$.

Power corrections are expected to follow this ambiguity structure. Let us therefore introduce a non-perturbative parameter C_m , of order 1, relating each power correction to the corresponding renormalon residue. The underlying assumption is that genuine non-perturbative effects would be of the same order as the ambiguities. The parametric dependence of the corrections on the hard scales then follow directly from the residues in Eq. (87): they are written as powers of $r_{>}^2 \Lambda^2$ times some function of ξ^2 , with additional logarithmic terms in Ω . The dependence soft scales is subsumed in the coefficients C_m . In doing so we write the full kernel $\mathcal{M}_{\mathbf{xzy}}$ as a sum of perturbative contributions $\mathcal{M}_{\mathbf{xzy}}^{\text{PV}}$ and power corrections $\delta \mathcal{M}_{\mathbf{xzy}}^{(m)}$:

$$\mathcal{M}_{\mathbf{xzy}} = \mathcal{M}_{\mathbf{xzy}}^{\text{PV}} + \sum_{m=1}^{\infty} \delta \mathcal{M}_{\mathbf{xzy}}^{(m)} . \tag{88}$$

As an example we explicitly present the power correction $\delta \mathcal{M}_{\mathbf{xzy}}^{(1)}$ corresponding to the leading $u = 1$ renormalon:

$$\delta \mathcal{M}_{\mathbf{xzy}}^{(1)} = C_1 \frac{\pi}{\beta_0} \left\{ \mathcal{K}_{\mathbf{xzy}} (1 + \xi^2) - \frac{1}{r_{<}^2} \left[\ln(\xi^2) - 2 \ln \left(\frac{4e^{-\frac{5}{3} - 2\gamma_E}}{r_{>}^2 \Lambda^2} \right) \right] \right\} \frac{1}{4} r_{>}^2 \Lambda^2 e^{\frac{5}{3}} . \tag{89}$$

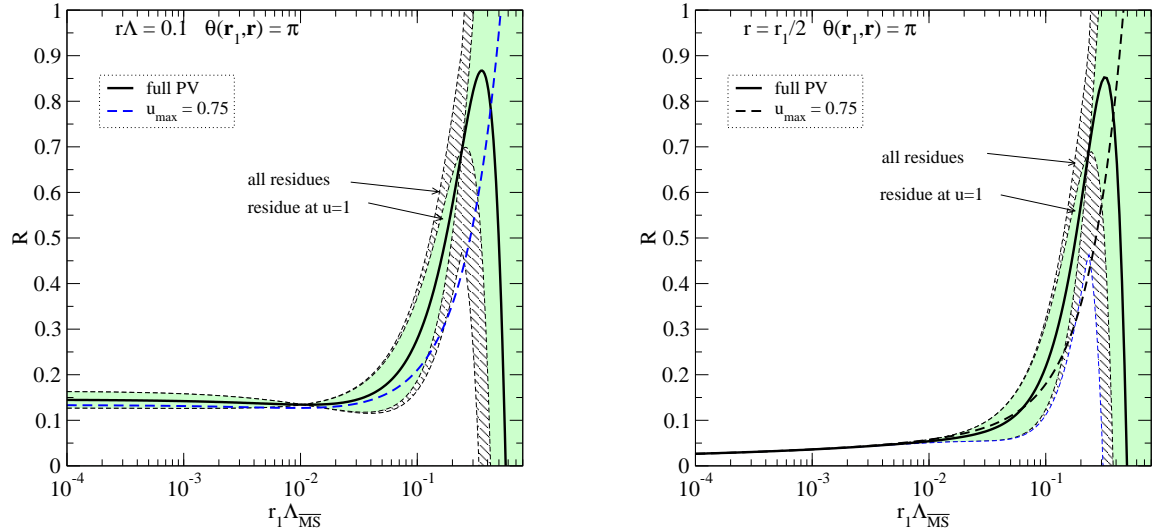


Figure 5: R_{PV} and the expected range of power corrections for fixed $r\Lambda = 0.1$ (left panel), and fixed ratio $r_1 = 2r$, $r_2 = 3r$ (right panel) with r_1 parallel to r_2 . The central solid line corresponds to the principal value result. The shaded regions estimate the relevance of power corrections by adding and subtracting $\pi|\text{residue}|(u = m)$. The inner band takes the first residue at $u = 1$, and the outer hashed band is the sum of absolute values of contributions from all residues. The dashed line shows the result when the u -integral has been cut at $u_{\text{max}} = 0.75$, before the first pole is encountered.

Fig. 5 shows R and the expected size of power corrections as functions of r_1 , for fixed parent dipole $r = 0.1/\Lambda$, and for fixed ratio of dipole sizes $r_2 = r_1/2$ (here $r_2 = r_1 + r$ and r_2 is parallel to r_1). The power corrections are assumed here to be of the order of the ambiguity in choosing an integration contour in the Borel plane, π times the absolute value of the residues at $u = m = 1, 2, 3, \dots$. The relative importance of renormalon poles can be seen from the width of the error band in Fig. 5. The contribution from the pole at $u = 1$, Eq. (89), is shown separately. It is evident that this first pole strongly dominates, except very close to $1/\Lambda$, as expected from the hierarchy of powers in the analytical expressions.

The key feature of the power corrections in Fig. 5 is the fact that they quickly die away at small scales³⁰. This feature is very robust and it does *not* depend on the detailed prescriptions used to estimate the size of the power corrections. Just to give an example, one might estimate the uncertainty by cutting off the u integral at some value $u_{\text{max}} < 1$, before one encounters the first renormalon pole. This is shown in Fig. 5 for $u_{\text{max}} = 0.75$ with dashed lines. Clearly this prescription leads to an alternative estimate for the perturbative sum for R which is roughly within the error band of the full PV integral.

From Fig. 5 it becomes strikingly clear that the poles limit the precision of our knowledge of the (non-perturbative) evolution kernel at large distances. We will see in Sec. 6, when we discuss evolution in the context of the BK equation, that for Q_s near $1 - 2\text{GeV}$, where large dipoles contributes significantly to the evolution, power corrections *must* be taken into account if one wants to quantitatively determine the evolution. If we wish to apply JIMWLK or BK evolution

³⁰Note that on the left panel of Fig. 5 r_2 approaches $r = 0.1/\Lambda$ as $r_1 \rightarrow 0$.

starting from Q_s -values in this range, both the evolution rate and the generic functional form of the initial condition for the dipole cross section $N_{Y_0, \mathbf{x}\mathbf{y}}$ receive sizeable non-perturbative contributions.

6 Evolution in the BK approximation

Our discussion so far focused on the *kernel* of the JIMWLK equation. We computed and resummed running-coupling corrections to the kernel and extracted an estimate for non-perturbative power corrections. All these affect only the “effective charge” in front of the leading-order kernel, although in a way that strongly depends on the size of the evolving dipole, and that varies significantly over the transverse phase space of the newly produced dipoles. In order to explore the consequences of these results on the *evolution*, one should clearly consider the solution of the equation over a sufficiently large range in rapidity. Only in this way would it be possible to examine the sensitivity of observable quantities, such as the rate of evolution, to the corrections computed.

The purpose of the present section is to perform a first exploration of this kind, by considering the evolution in the case of the BK equation. To this end, let us repeat the derivation of the BK equation, as described in Sec. 2.1, starting with the JIMWLK equation with the Hamiltonian of Eq. (63), which includes running-coupling corrections. A simple way to see the way the corrections enter is to first write the leading-order BK equation with the kernel separated according Eq. (10) into exchange and self-energy-like diagrams:

$$\begin{aligned} \partial_Y N_{Y, \mathbf{x}\mathbf{y}} = \frac{N_c}{2\pi} \int d^2 z \left[2 \frac{\alpha_s(\mu^2)}{\pi} \mathcal{K}_{\mathbf{x}\mathbf{z}\mathbf{y}} - \frac{\alpha_s(\mu^2)}{\pi} \mathcal{K}_{\mathbf{x}\mathbf{z}\mathbf{x}} - \frac{\alpha_s(\mu^2)}{\pi} \mathcal{K}_{\mathbf{y}\mathbf{z}\mathbf{y}} \right] \\ \times \left(N_{Y, \mathbf{x}\mathbf{z}} + N_{Y, \mathbf{z}\mathbf{y}} - N_{Y, \mathbf{x}\mathbf{y}} - N_{Y, \mathbf{x}\mathbf{z}} N_{Y, \mathbf{z}\mathbf{y}} \right). \end{aligned} \quad (90)$$

The result obtained using (63) by repeating the steps of Sec. 2.1 simply amounts the substitution (62), separately for each of the three terms in (90):

$$\frac{\alpha_s}{\pi} \tilde{\mathcal{K}}_{\mathbf{x}\mathbf{z}\mathbf{y}} \rightarrow \tilde{\mathcal{M}}_{\mathbf{x}\mathbf{z}\mathbf{y}} = 2 R(\mathbf{r}_1 \Lambda, \mathbf{r}_2 \Lambda) \mathcal{K}_{\mathbf{x}\mathbf{z}\mathbf{y}} - R(\mathbf{r}_1 \Lambda, \mathbf{r}_1 \Lambda) \mathcal{K}_{\mathbf{x}\mathbf{z}\mathbf{x}} - R(\mathbf{r}_2 \Lambda, \mathbf{r}_2 \Lambda) \mathcal{K}_{\mathbf{y}\mathbf{z}\mathbf{y}} \quad (91)$$

where the vectors \mathbf{r}_i are defined in (8). Our final result for the resummed BK equation is then written as

$$\partial_Y N_{Y, \mathbf{x}\mathbf{y}} = \frac{N_c}{2\pi} \int d^2 z \tilde{\mathcal{M}}_{\mathbf{x}\mathbf{z}\mathbf{y}} \left(N_{Y, \mathbf{x}\mathbf{z}} + N_{Y, \mathbf{z}\mathbf{y}} - N_{Y, \mathbf{x}\mathbf{y}} - N_{Y, \mathbf{x}\mathbf{z}} N_{Y, \mathbf{z}\mathbf{y}} \right). \quad (92)$$

6.1 Numerical implementation

The numerical solution of the BK evolution equation (92) requires care. In the following we briefly describe the choices we made in our implementation. Firstly, we consider only translationally-invariant and spherically-symmetric solutions; we set $\mathbf{x} \rightarrow 0$ and $N_{\mathbf{x}\mathbf{y}} \rightarrow N_{|\mathbf{y}|}$. Despite this, the \mathbf{z} -integral in Eq. (92) renders the evolution equation in essence two-dimensional. The simplest way to perform this integral is to discretize the two-dimensional space using a finite regular square lattice. This was used in [45] in order to compare BK with JIMWLK evolution. This approach, however, restricts the ratio of ultraviolet and infrared cutoffs (the ratio of the lattice size to the

lattice spacing) to, at most, $\sim 10^4$, and hence strongly limits the Y range over which the shrinking correlation length $R_s(Y)$ can be resolved on such a lattice. A solution to this problem is to use discretization with higher resolution power at small distances, as was done in [77].

To achieve this we discretize N_r on an even logarithmic scale, $r_n = r_0 \exp(n\Delta)$, using ~ 250 points with $r_{\min} = e^{-22}/\Lambda$ and $r_{\max} = 1/\Lambda$. The two-dimensional integral in Eq. (92) is evaluated using nested Simpson integrations in the $(\log|z|, \arg z)$ coordinates. While the values of $|z|$ and $|\mathbf{y}|$ are restricted to discrete r_n -values, $|z - \mathbf{y}|$ is not. Thus, it is necessary to interpolate the value of $N_{|z-\mathbf{y}|}$ in Eq. (92) using the known points N_{r_n} . We have checked the stability of the simulation by changing the number of discretization points, and verified that this leads to a negligible change in the results.

In order to evaluate the R -functions in the kernel $\tilde{\mathcal{M}}$ of (91), we need to integrate over the Borel function $B(u)$. However, as described in Sec. 4, one cannot directly use the expressions in Eqs. (72a) to (74b) when integrating over the positive real axis, because of the presence of single and double infrared renormalon poles there. As described in App. E, the double poles were converted analytically into simple ones by means of integration by parts. The integration over the simple poles was performed by a numerical implementation of the Principal Value prescription. This implementation is based on different analytic formulae, depending on the value of $\xi = r_</r_>$: for $\xi^2 < 0.8$ we use (123a) and (123b) for R^T and R^L , switching over to (124) and (125) when $\xi^2 > 0.8$. The integrals are completely stable when the threshold value of ξ^2 is changed within the interval $(0.01, 0.99)$, and our default value of 0.8 is chosen to optimize the evaluation speed. The numerical evaluation of the kernel is further stabilized by pulling the integrands of the three R -functions appearing in (91) under a single integral.

If the parent dipole is much smaller than the daughter dipoles, $r \ll r_1 \sim r_2$, the kernel $\tilde{\mathcal{M}}$ contains large terms that cancel each other almost completely, leading to numerical difficulties. This can be dealt with by recognizing that the large contributions arise in fact from the leading terms in the series expressions of Borel functions Eqs. (124) and (125) appearing in (92) (in this parameter region $1 - \xi^2 \approx 0$). Combining the first terms analytically stabilizes the evaluation of the series.

The evolution in rapidity Y is performed with the second-order Runge-Kutta method, with a “time” step of $\delta Y = 0.05 \dots 0.1$. Again, we observed no significant difference in the results upon varying the step size.

6.2 Simulation results

The key feature of JIMWLK and BK evolution is scaling of the solutions with $Q_s(Y)$ after the initial-state effects have died out. This scaling is exact in the fixed-coupling limit and has been shown to be retained to a very good approximation in simulations with ad hoc implementations of running coupling. Also our all-order resummation result shows this feature, as is demonstrated in Fig. 6.

The initial state in our simulations is $N_{\text{ini}}(r) = 1 - \exp[-r^2/r_0^2]$, where r_0 sets the initial scale. The evolution tends to flatten $N(Y, r)$ until the scaling shape has been reached. However, the shape remains considerably steeper than with fixed coupling, see Fig. 6 (b). From this plot we also see that the scaling shape is quite similar for the running coupling corrections computed in this paper and the ad hoc prescriptions shown. Thus, the asymptotic shape of $N(Y, r)$ is largely insensitive to the functional dependence of the scale of the coupling on the phase space.

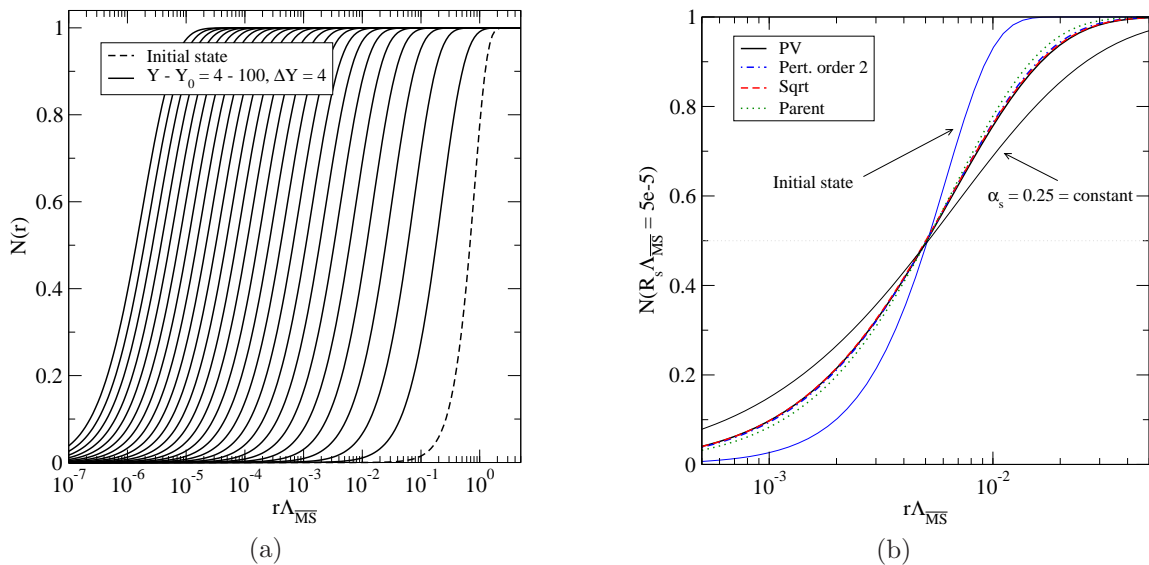


Figure 6: (a): The evolution of the function $N(r)$ as a function of $Y = \ln 1/x$, shown in intervals of $\Delta Y = 4$. After initial settling down the function evolves towards smaller r while approximately preserving its shape. The main effect of the running coupling is to slow down the evolution at small r . (b): The shape of $N(Y, r)$ using the computed running-coupling corrections (PV) as well as some running-coupling models, taken at Y where the saturation scale $R_s(Y) = 0.005/\Lambda$, where we define R_s through $N(Y, R_s) = 1/2$. Different running-coupling forms display similar shapes for $N(r)$, albeit slightly steeper for the parent-dipole running; much shallower than the initial state $N_{\text{ini}} = 1 - e^{-r^2/r_0^2}$, but much steeper than the fixed coupling shape shown for comparison.

In Fig. 7 (a) we show the evolution of the saturation scale $R_s\Lambda$ as a function Y ; here the full PV Borel sum result is compared with the parent-dipole running and the “sqrt” ansatz of (86). The correlation length R_s characterizes the scale where $N(Y, r)$ is changing and saturation sets in; here we define $R_s(Y)$ through the condition $N(Y, R_s(Y)) = 1/2$. The initial $R_s(Y = Y_0)$ is $\approx 0.1/\Lambda$. We see that $R_s(Y)$ rapidly evolves towards smaller values.

We note that a different definition of $R_s(Y)$ would naturally give somewhat different curves. However, when the system has evolved sufficiently long so that it reaches the scaling form, all reasonable definitions should yield $R_s(Y)$ values that differ only by a constant factor. Above all, the evolution speed

$$\lambda(Y) = \frac{1}{Q_s^2(Y)} \frac{\partial Q_s^2(Y)}{\partial Y} = -\frac{1}{R_s^2(Y)} \frac{\partial R_s^2(Y)}{\partial Y}; \quad Q_s := 1/R_s \quad (93)$$

should be the same.

As with the ad hoc prescriptions, the most interesting consequence of running coupling on JIMWLK and BK evolution is the fact that it drastically slows down the evolution compared to the purely fixed-coupling case by restricting the active phase space to within one order of magnitude of the characteristic scale $Q_s(Y)$ [45]. This qualitative feature does not depend on the details of the implementation of the running-coupling effects. The precise value of the evolution speed, as expressed by the evolution rate $\lambda(Y)$ on the other hand, does depend on these details. For fixed coupling, scaling

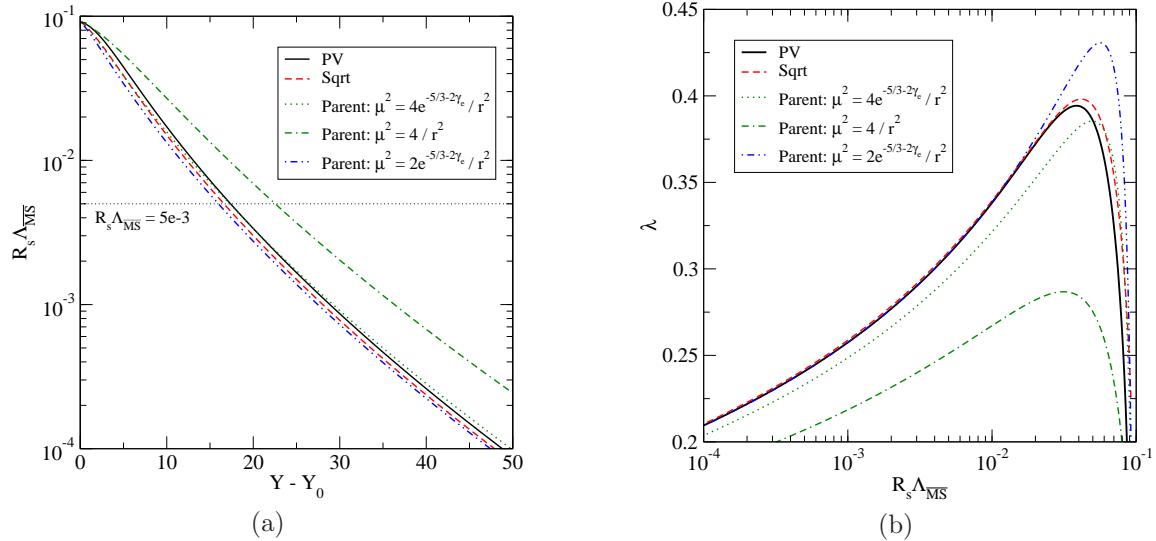


Figure 7: (a): the evolution of the saturation scale $R_s(Y)$ with the computed running-coupling corrections (PV), in comparison with a few different running-coupling models. The evolution starts at initial $R_s(Y = Y_0) \approx 0.1/\Lambda$. The horizontal dotted line shows the value of R_s where $N(r)$ was shown in Fig. 6. (b): the evolution speed $\lambda(Y)$ plotted against the saturation scale $R_s(Y)$. The evolution starts at large R_s values; the rapid increase at $R_s \Lambda \sim 0.1$ is an initial-state effect. Several choices of scale are presented for the “parent dipole”, demonstrating the sensitivity to the scale and the fact that upon tuning the scale, this model too can be made to agree with the resummed result for $\lambda(Y)$ at small R_s .

with Q_s is exact, and λ becomes a constant proportional to $\alpha_s(\mu^2)$ [79]. With running coupling, scaling is approximate, and λ becomes a function of Y that will receive both perturbative and non-perturbative corrections via $R(\mathbf{r}_1 \Lambda, \mathbf{r}_2 \Lambda)$, which we already examined numerically in Fig. 5.

While using Eq. (93) with $N(Y, R_s(Y)) = C$ (where $C = 1/2$ was used above) is certainly possible, during the initial stages of the evolution it is sensitive to the particular value of the constant C chosen. A more robust definition is the one used in [45], using a $1/r^2$ moment of the evolution equation as an operational definition of λ :

$$\lambda(Y) = \frac{N_c}{2\pi} \int \frac{d^2 r}{r^2} \int d^2 z \mathcal{M}_{\mathbf{xzy}} (N(Y, r_1^2) + N(Y, r_2^2) - N(Y, r^2) - N(Y, r_1^2)N(Y, r_2^2)) \quad (94)$$

We will follow this convention here.

Our results for $\lambda(Y)$ are shown in Fig. 7 (b). Here we plot λ against $R_s(Y)$; in this way the result is independent of the initial value for Y . The initial-state effects are visible as a very rapid increase of λ near the initial (large) R_s . As soon as these effects die out, the evolution approaches an initial-state-independent curve (see Fig. 8). On this curve $N(r)$ has reached the scaling shape shown in Fig. 6, and λ decreases slowly as R_s decreases at large Y . This is entirely driven by the logarithmic decrease of the coupling at short distances.

In this plot one can also observe the sensitivity of the evolution rate to running-coupling corrections. We show the resummed result computed by the PV prescription (full line) in comparison with LO

evolution where the scale is set in variety of ways. LO parent–dipole running with $\mu^2 = 4/r^2$ strongly under–estimates the evolution rate *even* at very small correlation lengths R_s . This clearly demonstrates the significance of higher–order running–coupling corrections, which are included in the PV Borel sum.

Interestingly, as seen in Fig. 7 (b), one can approximate the PV Borel sum result (at sufficiently small R_s) with a variety of different functional forms, *provided* that an appropriate choice of scale is made. Thus, despite the large differences in the “effective charge” between the resummed result and the models considered — which are particularly significant for large dipoles — the differences in λ , at sufficiently small R_s , reduce to an overall phase–space independent multiplicative factor in the scale of the coupling. With the specific scales given in Eq. (85) the “square root” ansatz approximates the PV Borel sum well, whereas parent–dipole running slightly underestimates it. In the latter case, choosing $\mu^2 = 2e^{\frac{5}{3}-2\gamma_E}/r^2$ yields a very good approximation to λ for $R_s\Lambda \lesssim 10^{-2}$, but somewhat over–estimates it at larger R_s . The possibility to approximate λ in (94) well *as a function of the correlation length* (provided it is sufficiently small) in terms of a phase–space independent coupling, such as the parent–dipole one, is probably related to the scaling property of $N(Y, r)$, namely the fact that its shape, which determines the weight given to different final states in (94) is invariant.

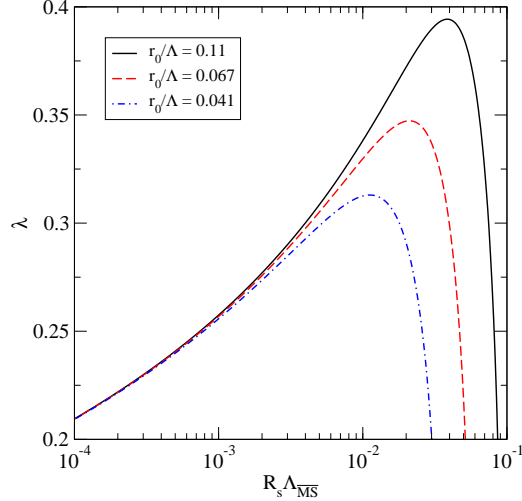


Figure 8: *The evolution speed $\lambda(R_s)$ for different initial conditions $N_{\text{ini}}(r) = 1 - \exp(-r^2/r_0^2)$, using the PV Borel sum. As the initial–state effects vanish, $\lambda(R_s)$ approaches a universal evolution trajectory.*

In Fig. 8 we show the evolution rate $\lambda(Y)$ as a function of R_s using different initial conditions. The trajectories approach a universal curve, which is independent of the initial condition.

In Fig. 9 (a) we show the evolution rate as a function of R_s using the perturbatively expanded kernel, Eq. (77) at different truncation orders. Here the scale of the coupling is chosen to be $\mu^2 = 8e^{-5/3-2\gamma_E}/(r_1^2 + r_2^2)$ as in (85). We note that in contrast with the Borel sum, the perturbative expansion suffers from a Landau pole when the daughter dipoles become too large. These Landau singularities obstruct the phase–space integration, so the large r_i region must be cut out. To avoid

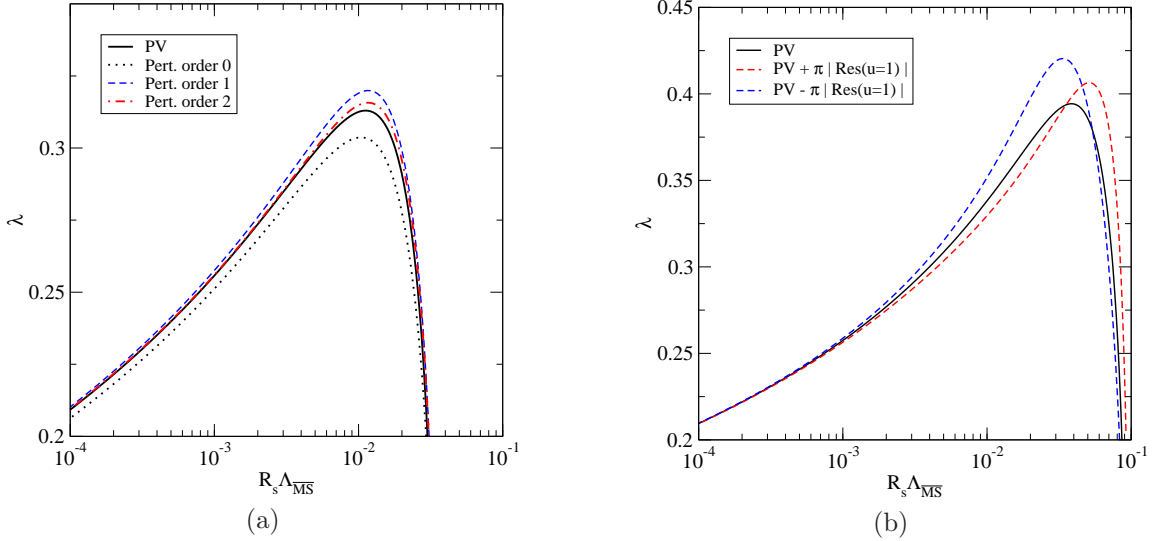


Figure 9: (a): Evolution using perturbatively expanded kernel, Eq. (77) with $\mu^2 = 8e^{-5/3-2\gamma_E}/(r_1^2 + r_2^2)$. (b): Estimating the non-perturbative influence on $\lambda(R_s)$ by adding and subtracting $\pi \times (\text{residue at } u=1)$ to the PV evolution kernel. The effect of the residue dies out quickly as R_s becomes smaller.

any visible effect by this cut we performed the simulation of Fig. 9 (a) with relatively small initial³¹ R_s . In the small R_s regime shown, one observe good convergence towards the PV Borel sum. At sufficiently small R_s only the leading-order result differs significantly from the PV one. This is of course specific to the (almost optimal) choice of scale made here. Much larger corrections appear for a generic scale choice as we have already seen in Fig. 7.

Fig. 9 (b) shows the effect of the estimated power corrections on evolution. The relative importance of the power corrections decrease with $Q_s(Y)$: the active phase follows $Q_s(Y)$ towards the ultraviolet. With increasing $Q_s(Y)$ the uncertainty induced by power corrections dies away very rapidly. Despite this general trend, it is apparent that a quantitative determination of evolution speed for current experiments where $Q_s = 1 - 2$ GeV, requires to take power corrections into account. To test the predictive power of the approach, it is important to compare several distinct observables, and address the universality of the relevant power corrections.

7 Conclusions

We have presented a first calculation of running-coupling corrections to both JIMWLK and BK equations. We have shown that both these equations, which were originally derived at leading logarithmic accuracy with strictly fixed coupling, can indeed be promoted to the running-coupling case: the general structure of the equations remains the same, while the kernel receives corrections. Running-coupling corrections are singled out from other radiative corrections in the following way:

³¹To study the fixed-order perturbative result at larger R_s with this or a similar phase-space dependent scale one would have to consider the effect of the cut or introduce another regularization of the Landau pole.

with or without running coupling, the r.h.s of the evolution equation of any correlation involves *just one* more Wilson line (the produced gluon) than the l.h.s (the evolving object); other radiative corrections entering at the NLO involve up to *two* more Wilson lines. The number of additional Wilson lines grows further at higher orders. It remains for future work to fully generalize the non-linear small- x evolution equations to NLO. Some work in this direction, which is complementary to ours, has already been done [56, 57, 76]. A full NLO generalization exists of course for the linear case of the BFKL equation, and our expectation is that it exists in the non-linear case as well. Since the BFKL equation is known in full at NLO, one can make a useful comparison. This goes beyond the scope of the present paper. One important fact, however, that we do learn from the BFKL limit, is that running-coupling corrections constitute a significant part of the total NLO correction. This, we expect holds also in the JIMWLK and BK cases.

The significance of the running coupling in the context of JIMWLK and BK evolution has been acknowledged long ago. For one thing, in fixed-coupling evolution the active phase space extends way into the ultraviolet, while practically any dependence of the coupling on the scales present at a single evolution step reduces the active phase space to within one order of magnitude around the correlation length R_s [45]. For this reason *all* simulations of JIMWLK or BK evolution have been performed with running coupling, implemented using some educated guess as to its scale dependence. The simulations presented in this paper are the first where the scale dependence is computed from QCD perturbation theory. While *qualitative* features of the effects of running coupling on the evolution — e.g. the decrease of the evolution rate $\lambda(Y)$ with decreasing correlation length $R_s(Y)$ at large Y — are similar to what has been observed before, the scale factor itself has been determined here for the first time. As shown in Fig. 7, using the correct scale is crucial in obtaining a quantitative estimate of the evolution rate. With this predictive power, we can hope that non-linear evolution equations with running coupling would become directly applicable to small- x phenomenology at LHC energies.

Technically, running-coupling corrections are computed, as usual, by focusing on a specific set of diagrams where a single gluon is dressed by fermion-loop insertions, making use of the linearity of β_0 in the number of flavors N_f . To perform this calculation we utilized in this paper the dispersive approach, where the all-order sum of vacuum-polarization insertions is traded for a dispersive integral in the “gluon mass”. While this technique has been used extensively in the past, using it to compute the diagrams entering the JIMWLK Hamiltonian is non-trivial for two reasons: first, the large- N_f limit by itself is not sufficient to disentangle running-coupling effects from the new production channel of a $q\bar{q}$ pair; second, the presence of the strong Weizsäcker-Williams background field may interfere with the “dressing” by interacting with the fermions. Guided by the correspondence between real and virtual corrections owing to conservation of probability, we could nevertheless disentangle running-coupling corrections from other contributions and generalize the dispersive technique to the case of the background field. To this end we derived a dispersive representation of the dressed gluon propagator in the background field. This formal development may well have other applications.

By computing the JIMWLK Hamiltonian using the dispersive technique we could go beyond the NLO $\mathcal{O}(\beta_0\alpha_s^2)$ running-coupling corrections to the kernel, and resum $\mathcal{O}(\beta_0^{n-1}\alpha_s^n)$ corrections *to all orders* in perturbation theory. Besides the obvious advantage of obtaining an exactly renormalization-scale invariant kernel, the all-order calculation offers a unique window into the non-perturbative side of the problem. The fact that infrared-finite evolution equations can be established in the high-energy limit, does not mean of course that the dynamics governing the

evolution is purely perturbative; non-perturbative dynamics affects the evolution through power-suppressed corrections. By performing an all-order resummation one can get access to this infrared sensitivity by looking at the ambiguity in separating perturbative and non-perturbative contributions; these are the infrared renormalons. Using Borel summation we identified explicitly the ambiguities in defining the perturbative sum, and in this way established an estimate for the parametric dependence of non-perturbative effects on the hard scales involved and the potential magnitude of these effects.

We find that both perturbative and non-perturbative corrections modify the evolution kernel in a non-trivial way. In particular, these corrections depend on all the different scales present: the “parent dipole” r as well as the two “daughter dipoles”, r_1 and r_2 . In this way different final states are weighted differently. An interesting feature at NLO and beyond is the appearance of two classes of contributions: one that is proportional to the LO kernel, which is associated uniquely with transversely polarized gluons, and one that is not, which is associated with longitudinal polarizations. Both perturbative and non-perturbative corrections to the kernel, propagate through the evolution and affect the rate at which the saturation scale $Q_s(Y)$ flows towards the ultraviolet with increasing energies. Conversely, the saturation scale itself determines the active phase space, leading to the decoupling of soft modes at large Y .

We studied here the effect of the newly computed corrections on two levels: first by looking at the “effective charge” controlling the contribution to the r.h.s. of the evolution equation, and then by solving the BK equation numerically and studying the effects on the evolution itself. We found, on both levels, that the running-coupling corrections are significant. Our simulations have shown that non-perturbative corrections are strongly suppressed at high energies, reflecting the fact that the increase of $Q_s(Y)$ with energy moves the active phase space along with it towards shorter distances. At presently accessible energies, where the saturation scale is estimated to be $Q_s(Y) \sim 1 - 2$ GeV, power corrections are definitely relevant. Going from high to low energies, one may view the breakdown of the perturbative evolution as the onset of the Soft Pomeron. If we accept this premise, our calculation opens a new way to think about the Soft Pomeron: as the energy is lowered the number of power-suppressed terms that need to be included in the evolution kernel increases. A possible determination of the power terms from data can thus be attempted at intermediate energies, before the power expansion breaks down. A detailed examination of this idea must address the distinction between the initial condition to the evolution and the corrections to the kernel itself.

In conclusion, we made an important step in extending the framework of non-linear evolution equations at small x to include running-coupling and power corrections. Nevertheless, this endeavor is by no means complete: small- x evolution at high densities presents many challenges, some of which we touched upon in this paper. This includes for example the generalization of the non-linear evolution equations to the NLO; the detailed comparison with the NLO BFKL kernel; understanding the relation with DGLAP evolution and higher-twist corrections to the twist expansion, gaining better understanding of the initial condition for the evolution; the development of (experimentally accessible!) observables of different degree of inclusiveness, which are sensitive to the dynamics underlying the evolution; and the determination of non-perturbative corrections affecting the small- x evolution.

Acknowledgments

E.G. wishes to thank Francesco Hautmann for illuminating discussions. H.W. is very grateful to Ian Balitsky for sharing his insights on computing running-coupling corrections to small- x evolution. H.W. also acknowledges extensive discussions with Yuri Kovchegov that lead to an independent investigation of this topic in terms of an explicit diagrammatic calculation presented in [103].

The work of H.W. is supported in part by the U.S. Department of Energy under Grant No. DE-FG02-05ER41377. JK and KR were partly supported by the Academy of Finland contract 104382.

A B^T in coordinate space

We begin with \mathcal{F}^T in d dimensional coordinate space. The regulator is only needed to have separately finite terms in (97) and may be removed once the cancellation of infinite contributions is manifest by setting $d \rightarrow 2$. The simplest way to obtain a dimensionally regulated expression for \mathcal{F}^T is to start from Eq. (57) and to promote the momentum integrals from 2 to d dimensions. One then exponentiates the denominators using two Schwinger parameters t_1 and t_2 . This leads to

$$\mathcal{F}^T(\mathbf{r}_1 m, \mathbf{r}_2 m) = \frac{1}{\Gamma^2(\frac{d}{2})} \left(\frac{r_1^2 r_2^2}{4 \ 4} \right)^{\frac{d}{2}} \int_0^\infty dt t^{-(d/2+1)} e^{-tm^2 - \frac{(r_1^2/4)}{t}} \int_0^\infty ds s^{-(d/2+1)} e^{-sm^2 - \frac{(r_2^2/4)}{s}} \quad (95)$$

and a d dimensional generalization of Eq. (60)

$$= \frac{2^{2-d}}{\Gamma^2(\frac{d}{2})} (r_1 m)^{\frac{d}{2}} K_{\frac{d}{2}}(r_1 m) (r_2 m)^{\frac{d}{2}} K_{\frac{d}{2}}(r_2 m) . \quad (96)$$

From here we obtain B^T according to (65):

$$B^T(u, \mathbf{r}_1 \mu, \mathbf{r}_2 \mu) = -e^{\frac{5}{3}u} \frac{\sin \pi u}{\pi} \int_0^\infty \frac{dm^2}{m^2} \left(\frac{m^2}{\mu^2} \right)^{-u} [\mathcal{F}^T(\mathbf{r}_1 m, \mathbf{r}_2 m) - 1] . \quad (97)$$

We will first perform the m^2 integral by using (95):

$$\begin{aligned} \int_0^\infty \frac{dm^2}{m^2} \left(\frac{m^2}{\mu^2} \right)^{-u} [\mathcal{F}^T(\mathbf{r}_1 m, \mathbf{r}_2 m) - 1] &= \int_0^\infty \frac{dm^2}{m^2} \left(\frac{m^2}{\mu^2} \right)^{-u} \\ &\times \left[\frac{1}{\Gamma^2(\frac{d}{2})} \left(\frac{r_1^2 r_2^2}{4 \ 4} \right)^{\frac{d}{2}} \int_0^\infty dt_1 t_1^{-(d/2+1)} e^{-t_1 m^2 - \frac{(r_1^2/4)}{t_1}} \int_0^\infty dt_2 t_2^{-(d/2+1)} e^{-t_2 m^2 - \frac{(r_2^2/4)}{t_2}} - 1 \right] . \end{aligned}$$

The $\mathcal{F} - 1$ structure serves to regulate at $m = 0$. To capture its effect it is expedient to make use of $\frac{e^{-m^2(t_1+t_2)} - 1}{m^2} = - \int_0^{t_1+t_2} d\alpha e^{-m^2\alpha}$ to decouple the m^2 and t_i integrals

$$\begin{aligned}
&= - \frac{1}{\Gamma^2(\frac{d}{2})} \left(\frac{r_1^2}{4} \frac{r_2^2}{4} \right)^{\frac{d}{2}} \int_0^\infty dt_1 t_1^{-(d/2+1)} e^{-\frac{(r_1^2/4)}{t_1}} \int_0^\infty dt_2 t_2^{-(d/2+1)} e^{-\frac{(r_2^2/4)}{t_2}} \\
&\quad \times \int_0^{t_1+t_2} d\alpha \underbrace{\int_0^\infty dm^2 \left(\frac{m^2}{\mu^2} \right)^{-u} e^{-m^2\alpha}}_{(\mu^2)^u \alpha^{u-1} \Gamma(1-u)}. \tag{98}
\end{aligned}$$

The m^2 integral converges only if $\text{Re}(u) < 1$. $u = 1$ will be the location of the first renormalon pole. At this point we may set $d = 2$ since all expressions are now explicitly finite:

$$= - (\mu^2)^u \frac{r_1^2}{4} \frac{r_2^2}{4} \int_0^\infty dt_1 t_1^{-2} e^{-\frac{(r_1^2/4)}{t_1}} \int_0^\infty dt_2 t_2^{-2} e^{-\frac{(r_2^2/4)}{t_2}} \frac{(t_1 + t_2)^u}{u} \Gamma(1 - u). \tag{99}$$

One might guess that the poles of $\Gamma(1 - u)$ reflect the location of the renormalon poles, but this is not true: once one restores the pre-factor to recover B , $\Gamma(1 - u)$ is actually canceled by $\sin(\pi u)$:

$$\begin{aligned}
B^T(u, \mathbf{r}_1 m, \mathbf{r}_2 m) &= \frac{e^{\frac{5}{3}u} (\mu^2)^u}{\Gamma(u+1)} \left(\frac{r_1^2}{4} \frac{r_2^2}{4} \right)^{\frac{d}{2}} \int_0^\infty dt_1 t_1^{-(d/2+1)} e^{-\frac{(r_1^2/4)}{t_1}} \int_0^\infty dt_2 t_2^{-(d/2+1)} e^{-\frac{(r_2^2/4)}{t_2}} \\
&\quad \times (t_1 + t_2)^u \tag{100}
\end{aligned}$$

which would be completely regular if not the t integrations expose poles at positive u .

This can be uncovered by using a Mellin-Barnes representation for the $(t_1 + t_2)^u$ factor in this expression (see [109] for a textbook on applications of the Mellin-Barnes technique in field theory). We write

$$(t_1 + t_2)^u = \frac{1}{2\pi i} \int_\gamma d\nu \frac{\Gamma(-u + \nu) \Gamma(-\nu)}{\Gamma(-u)} \frac{t_1^\nu}{t_2^{-u+\nu}}, \tag{101}$$

where the path γ connects $-\eta - i\infty$ to $\eta + i\infty$ (η real and infinitesimal) in such a way that it separates *all* left from *all* right poles of the integrand. [To recall the definition: poles originating from factors $\Gamma(a + \nu)$ and $\Gamma(a - \nu)$ are called left and right poles respectively. The left hand side is recovered as a series in either t_1/t_2 or t_2/t_1 by summing residues. The sign of $\ln(t_1/t_2)$ determines which way to close the contour and in turn the form of the series by selecting the relevant residues.] This decouples the t integrations which provide additional ν dependent Γ functions allows us to write B^T as

$$B^T(u, \mathbf{r}_1 \mu, \mathbf{r}_2 \mu) = -e^{\frac{5}{3}u} \frac{(r_2/4)^u}{\Gamma(u+1)\Gamma(-u)} \frac{1}{2\pi i} \int_{-\eta-i\infty}^{-\eta+i\infty} d\nu \left(\frac{r_1^2}{r_2^2} \right)^\nu \frac{\Gamma^2(1-u+\nu)}{-u+\nu} \frac{\Gamma^2(1-\nu)}{\nu}. \tag{102}$$

The integral can now be done by summing residues. We have to distinguish two cases: the sign of $\ln(r_1^2/r_2^2)$ determines where to close the contour. It proves useful to emphasize the symmetry of this procedure by expressing the result via $r_<$, $r_>$ and $\xi^2 = r_<^2/r_>^2$:

- $\ln(r_1^2/r_2^2) < 0$, closing to the right:

$$(102) \rightarrow \frac{\sin(\pi u)}{\pi} \left(\frac{4e^{-\frac{5}{3}}}{r_{>}^2 \mu^2} \right)^{-u} \left\{ u\Gamma^2(-u) - \sum_{n=0}^{\infty} \frac{(n+1)(\xi^2)^{n+1} \Gamma^2(2+n-u)}{(n+1-u)\Gamma^2(n+2)} \right. \\ \left. \times \left[-\frac{(2+2n-u)}{(n+1)(n+1-u)} + \ln(\xi^2) - 2(\psi(n+1) - \psi(n+2-u)) \right] \right\} \quad (103)$$

- $\ln(r_1^2/r_2^2) > 0$, closing to the left:

$$(102) \rightarrow \frac{\sin(\pi u)}{\pi} \left(\frac{4e^{-\frac{5}{3}}}{r_{<}^2 \mu^2} \right)^{-u} \left\{ u\Gamma^2(-u) (\xi^2)^{-u} - \sum_{n=0}^{\infty} \frac{(n+1)(\xi^2)^{(n+1)-u} \Gamma^2(2+n-u)}{(n+1-u)\Gamma^2(n+2)} \right. \\ \left. \times \left[-\frac{(2+2n-u)}{(n+1)(n+1-u)} + \ln(\xi^2) - 2(\psi(n+1) - \psi(n+2-u)) \right] \right\} \quad (104)$$

This is identical to (103).

Using shift identities for the digamma functions, $2\psi(n+1) = \psi(n+1) + \psi(n+2) - \frac{1}{n+1}$ and $2\psi(n+2-u) = \psi(n+1-u) + \psi(n+2-u) + \frac{1}{n+1-u}$, we arrive at our final result

$$B^T(u, \mathbf{r}_1\mu, \mathbf{r}_2\mu) = \frac{\sin(\pi u)}{\pi} \left(\frac{4e^{\frac{5}{3}}}{r_{>}^2 \mu^2} \right)^u \left\{ u\Gamma^2(-u) - \sum_{n=0}^{\infty} \frac{(\xi^2)^{(n+1)} \Gamma(n+1-u)\Gamma(n+2-u)}{\Gamma(n+1)\Gamma(n+2)} \right. \\ \left. \times [\psi(n+2-u) + \psi(n+1-u) - \psi(n+1) - \psi(n+2) + \ln(\xi^2)] \right\}. \quad (105)$$

B B^L in coordinate space

The calculation of the coordinate expression for B^L is slightly simpler than that of B^T and uses the same techniques.

We start from (65) for the longitudinal contribution and note that its contribution to the $m=0$ subtraction term vanishes:

$$\mathcal{K}_{\mathbf{x}z\mathbf{y}} B^L(u, \mathbf{r}_1\mu, \mathbf{r}_2\mu) = -e^{\frac{5}{3}u} \frac{\sin \pi u}{\pi} \int_0^\infty \frac{dm^2}{m^2} \left(\frac{m^2}{\mu^2} \right)^{-u} \mathcal{K}_{\mathbf{x}z\mathbf{y}}^{L,m}. \quad (106)$$

Abbreviating $f(u) = -e^{\frac{5}{3}u} \frac{\sin \pi u}{\pi}$ and using the parameter the appropriate parameter representation for the K_0 factors this turns into

$$= \frac{f(u)}{(2\pi)^2} \int_0^\infty \frac{dm^2}{m^2} \left(\frac{m^2}{\mu^2} \right)^{-u} (-m^2) \int_0^\infty dt_1 e^{-t_2 m^2 - \frac{(r_1^2/4)}{t_1} t_1^{-d/2} \pi^{d/2}} \int_0^\infty dt_2 e^{-t_2 m^2 - \frac{(r_2^2/4)}{t_2} t_2^{-d/2} \pi^{d/2}}$$

For the remainder of the calculation we present only minimal comments.

–separate off the m integral–

$$= -\frac{f(u)}{(2\pi)^2} \pi^d \int_0^\infty dt_1 \int_0^\infty dt_2 e^{-\frac{(r_1^2/4)}{t_1} t_1^{-d/2}} e^{-\frac{(r_2^2/4)}{t_2} t_2^{-d/2}} \int_0^\infty \frac{dm^2}{m^2} \left(\frac{m^2}{\mu^2}\right)^{-u} m^2 e^{-(t_1+t_2)m^2}$$

–the m integral requires $\text{Re}(u) < 1$ –

$$= -\frac{f(u)}{(2\pi)^2} (\mu^2)^u \pi^d \int_0^\infty dt_1 \int_0^\infty dt_2 e^{-\frac{(r_1^2/4)}{t_1} t_1^{-d/2}} e^{-\frac{(r_2^2/4)}{t_2} t_2^{-d/2}} (t_1 + t_2)^{u-1} \Gamma(1-u) \quad (107)$$

–use MB to factor $(t_1 + t_2)^{u-1}$ –

$$= -\frac{f(u)}{(2\pi)^2} (\mu^2)^u \Gamma(1-u) \pi^d \int_0^\infty dt_1 \int_0^\infty dt_2 e^{-\frac{(r_1^2/4)}{t_1} t_1^{-d/2}} e^{-\frac{(r_2^2/4)}{t_2} t_2^{-d/2}} \\ \times \frac{1}{2\pi i} \int_\gamma d\nu \frac{\Gamma(-(u-1)+\nu) \Gamma(-\nu)}{\Gamma(-(u-1))} \frac{t_1^\nu}{t_2^{-(u-1)+\nu}} \quad (108)$$

–separate the t integrals and perform them ($\text{Re}(-d/2+\nu) < -1$ and $\text{Re}(-d/2+u-1)-\nu < -1$)–

$$= -\frac{f(u)}{(2\pi)^2} (\mu^2)^u \pi^d \frac{1}{2\pi i} \int_\gamma d\nu \Gamma(-(u-1)+\nu) \Gamma(-\nu) \\ \times (r_1^2/4)^{1-\frac{d}{2}+\nu} \Gamma\left(\frac{d}{2}-1-\nu\right) (r_2^2/4)^{-\frac{d}{2}+u-\nu} \Gamma\left(\frac{d}{2}-u+\nu\right) \quad (109)$$

–rearrange to expose convergence of the MB integral–

$$= -\frac{f(u)}{(2\pi)^2} (\mu^2 r_2^2/4)^u (r_1^2/4)^1 \pi^d \left(\frac{r_1^2 r_2^2}{4 \ 4}\right)^{-\frac{d}{2}} \\ \times \frac{1}{2\pi i} \int_\gamma d\nu \Gamma(-(u-1)+\nu) \Gamma\left(\frac{d}{2}-u+\nu\right) \Gamma(-\nu) \Gamma\left(\frac{d}{2}-1-\nu\right) \left(\frac{r_2^2}{r_1^2}\right)^{-\nu} \quad (110)$$

–evaluate MB independently for both cases $r_2 > r_1$ and $r_1 > r_2$, find sums of residues to agree, set $d = 2$ to obtain the final result–

$$= -\frac{\sin(\pi u)}{\pi} \frac{1}{r_>^2} \left(\frac{4 e^{-\frac{5}{3}}}{\mu^2 r_>^2}\right)^{-u} \sum_{n=0}^{\infty} \left(\frac{\Gamma(n+1-u)}{\Gamma(n+1)}\right)^2 (\xi^2)^n (\ln(\xi^2) - 2\psi(n+1) + 2\psi(n+1-u)) \quad (111)$$

C Pole and renormalon structure of B^T

To expose the pole structure of B^T we find it easiest to start from (72b) and rewrite it as

$$\begin{aligned} B^T(u, r_1\mu, r_2\mu) &= \left(\frac{4e^{-\frac{5}{3}}}{r_{>}^2\mu^2} \right)^{-u} \frac{\sin(\pi u)}{\pi} \frac{u(1-u) \left(\Gamma(1-u)\Gamma(-u) \right)^2}{\Gamma(2(1-u))} {}_2F_1 \left(\begin{matrix} 1-u, -u \\ 2(1-u) \end{matrix} \middle| 1-\xi^2 \right) \\ &= - \sum_{n=0}^{\infty} \frac{(1-\xi^2)^n}{\Gamma(n+1)} \left(\frac{4e^{-\frac{5}{3}}}{r_{>}^2\mu^2} \right)^{-u} \frac{1}{\Gamma(u)} \frac{\Gamma(1-u+n)}{\Gamma(2(1-u)+n)} \Gamma(2-u)\Gamma(-u+n) \end{aligned} \quad (112)$$

Here all is regular but the factor $\Gamma(2-u)\Gamma(n-u)$ which will cause at most double poles at positive integers $u = m = 1, 2, \dots$. In the following we will encounter Laurent expansions around given pole locations and use the abbreviation $\epsilon = u - m$.

- Double poles arise via combined divergence in $\Gamma(2 - (m + \epsilon))\Gamma(n - (m + \epsilon))$. For a fixed pole location $u = m = 2, 3, \dots, \infty$ the second factor appears to contribute as long as $n \leq m$. The Laurent expansion around $u = m$ in these cases can generically be written as

$$\begin{aligned} &2(-1)^{m-n} \left(\frac{4e^{-\frac{5}{3}}}{r_{>}^2\mu^2} \right)^{-m} \frac{(1-\xi^2)^n}{\Gamma(n+1)} \frac{\Gamma(2m - (n+1))}{\Gamma(m)\Gamma(m-1)\Gamma(m-n)\Gamma(m+1-n)} \left\{ \frac{1}{\epsilon^2} \right. \\ &+ \left[-\ln \left(\frac{4e^{-\frac{5}{3}}}{r_{>}^2\mu^2} \right) - \Psi(m-1) - \Psi(m) - \Psi(m-n) - \Psi(m+1-n) + 2\Psi(2m - (n+1)) \right] \frac{1}{\epsilon} \\ &\left. + \mathcal{O}(\epsilon^0) \right\} \end{aligned} \quad (113)$$

We note that coefficient of the double pole also vanishes for $n = m$ so that the sum of the double pole terms may be expressed as

$$\begin{aligned} B_{\text{double pole}}^T &= \sum_{m=2}^{\infty} \sum_{n=2}^{m-1} \frac{(1-\xi^2)^n}{\Gamma(n+1)} \\ &\times \left(\frac{4e^{-\frac{5}{3}}}{r_{>}^2\mu^2} \right)^{-m} \frac{\Gamma(2m - (n+1))}{\Gamma(m)\Gamma(m-1)\Gamma(m-n)\Gamma(m+1-n)} \frac{2(-1)^{m-n}}{(u-m)^2} \end{aligned} \quad (114)$$

- As is obvious from the Laurent expansion in (113) we inherit single poles at the double pole locations. Additional single poles arise when
 - only the first of the factors contributes a pole, i.e. for $n > m \geq 2$, (the coefficients here vanish, however, where $n \leq 2(m-1)$)
 - or where only the second of the factors does contribute, i.e. for $2 > m \geq n$ (this is limited to $m = 1, n = 0, 1$):

The Laurent expansion around any of these additional single poles is given by

$$(-1)^m \left(\frac{4e^{-\frac{5}{3}}}{r_{>}^2 \mu^2} \right)^{-m} (1 - \xi^2)^n \frac{\Gamma(1 - m + n)}{\Gamma(n + 1)\Gamma(n + 2 - 2m)\Gamma(m - 1)} \frac{1}{\epsilon} + \mathcal{O}(\epsilon^0) \quad (115)$$

Adding all these leads to the following sum of single pole contributions which mark the power correction to to B^T

$$\begin{aligned} B_{\text{single pole}}^T &= \left(\frac{4e^{-\frac{5}{3}}}{r_{>}^2 \mu^2} \right)^{-1} \frac{-2 + (1 - \xi^2)}{u - 1} \\ &+ \sum_{m=2}^{\infty} \sum_{n=2(m-1)}^{\infty} \frac{(-1)^m (1 - \xi^2)^n}{u - m} \frac{\Gamma(1 - m + n)}{\Gamma(n + 1)} \left(\frac{4e^{-\frac{5}{3}}}{r_{>}^2 \mu^2} \right)^{-m} \frac{\Gamma(1 - m + n)}{\Gamma(n - 2(m - 1))\Gamma(m - 1)} \\ &+ \sum_{m=2}^{\infty} \sum_{n=2}^{m-1} \frac{(1 - \xi^2)^n}{\Gamma(n + 1)} \frac{2(-1)^{m-n}}{(u - m)} \\ &\times \frac{d}{dm} \left\{ \left(\frac{4e^{-\frac{5}{3}}}{r_{>}^2 \mu^2} \right)^{-m} \frac{\Gamma(2m - (n + 1))}{\Gamma(m)\Gamma(m - 1)\Gamma(m - n)\Gamma(m + 1 - n)} \right\} \quad (116) \end{aligned}$$

As a power correction each of the terms at fixed m comes with an a priori unknown coefficient.

D Pole and renormalon structure of B^L

$$\begin{aligned} \mathcal{K}_{\mathbf{xyz}\mathbf{y}} B^L(u, \mathbf{r}_1 \mu, \mathbf{r}_2 \mu) &= + \frac{\sin(\pi u)}{\pi} \frac{1}{r_{>}^2} \left(\frac{4e^{-\frac{5}{3}}}{r_{>}^2 \mu^2} \right)^{-u} \frac{(\Gamma(1 - u))^4}{\Gamma(2(1 - u))} {}_2F_1 \left(\begin{matrix} 1 - u, 1 - u \\ 2(1 - u) \end{matrix} \middle| 1 - \xi^2 \right) \\ &= + \sum_{n=0}^{\infty} \frac{(1 - \xi^2)^n}{\Gamma(n + 1)} \frac{1}{r_{>}^2} \left(\frac{4e^{-\frac{5}{3}}}{r_{>}^2 \mu^2} \right)^{-u} \frac{1}{\Gamma(u)} \frac{\Gamma(1 + n - u)}{\Gamma(2(1 - u) + n)} \Gamma(1 - u) \Gamma(1 - u + n) \quad (117) \end{aligned}$$

Renormalon poles again appear at $u = m = 1, 2, 3, \dots$, with everything regular but the factor $\Gamma(1 - u)\Gamma(1 - u + n)$.

- Double poles at m arise where both $\Gamma(1 - (m + \epsilon))\Gamma(n + 1 - (m + \epsilon))$ diverge, i.e. for $1 \leq m \leq n + 1$. The Laurent expansion around these pole locations $u = m$ is

$$\begin{aligned} &2(-1)^{m-n} \frac{1}{r_{>}^2} \left(\frac{4e^{-\frac{5}{3}}}{r_{>}^2 \mu^2} \right)^{-m} \frac{(1 - \xi^2)^n}{\Gamma(n + 1)} \frac{\Gamma(2m - (n + 1))}{(\Gamma(m))^2 (\Gamma(m - n))^2} \\ &\times \left\{ \frac{1}{\epsilon^2} + \left[-\ln \left(\frac{4e^{-\frac{5}{3}}}{r_{>}^2 \mu^2} \right) - 2\Psi(m - 1) - 2\Psi(2(m - 1)) + 2\Psi(m) \right] \frac{1}{\epsilon} + \mathcal{O}(\epsilon^0) \right\} \quad (118) \end{aligned}$$

so that the double pole part of the longitudinal contribution may be written as

$$\mathcal{K}_{\mathbf{xzy}} B_{\text{double pole}}^L = - \sum_{m=1}^{\infty} \sum_{n=0}^{m-1} \frac{2(-1)^{m-n} (1-\xi^2)^n}{(u-m)^2 \Gamma(n+1)} \frac{1}{r_{>}^2} \left(\frac{4e^{-\frac{5}{3}}}{r_{>}^2 \mu^2} \right)^{-m} \frac{\Gamma(2m-(n+1))}{(\Gamma(m))^2 (\Gamma(m-n))^2} \quad (119)$$

- As for B^T , we inherit single poles at the double pole locations. Additional single poles arise when only the first factor in $\Gamma(1-(m+\epsilon))\Gamma(n+1-(m+\epsilon))$ diverges, i.e. for $1 \leq m < n+1$. The Laurent expansion around these new pole locations reads

$$+(-1)^m \frac{1}{r_{>}^2} \left(\frac{4e^{-\frac{5}{3}}}{r_{>}^2 \mu^2} \right)^{-m} (1-\xi^2)^n \frac{(\Gamma(n+1-m))^2}{\Gamma(n+1)(\Gamma(m))^2 \Gamma(n+2-2m)} \frac{1}{\epsilon} + \mathcal{O}(\epsilon^0) \quad (120)$$

Some of the residues vanish (where $2m > n+2$).

Combining the two contributions leads to an expression for the single pole part of B^L of the form

$$\begin{aligned} \mathcal{K}_{\mathbf{xzy}} B_{\text{single pole}}^L = & - \sum_{m=1}^{\infty} \sum_{n=m}^{\infty} \frac{-(-1)^m}{u-m} \frac{1}{r_{>}^2} \left(\frac{4e^{-\frac{5}{3}}}{r_{>}^2 \mu^2} \right)^{-m} \frac{(1-\xi^2)^n}{\Gamma(n+1)} \frac{(\Gamma(n+1-m))^2}{(\Gamma(m))^2 \Gamma(n+2-2m)} \\ & - \sum_{m=1}^{\infty} \sum_{n=0}^{m-1} \frac{2(-1)^{m-n} (1-\xi^2)^n}{u-m} \frac{1}{\Gamma(n+1)} \frac{d}{r_{>}^2 dm} \left\{ \left(\frac{4e^{-\frac{5}{3}}}{r_{>}^2 \mu^2} \right)^{-m} \frac{\Gamma(2m-(n+1))}{(\Gamma(m))^2 (\Gamma(m-n))^2} \right\} \quad (121) \end{aligned}$$

E Principal value definition of the perturbative sum

The small ξ^2 series differ strongly from the $1-\xi^2$ series so that we will deal with them separately.

- Closer inspection of (64) via (72a) and (74b) reveals, that the double poles in the obstructing terms have their origin in a u derivative of a Γ function, i.e. they arise from differentiating simple poles. To make this manifest we rewrite (72a) and (74a) as

$$\begin{aligned} B^T(u, \mathbf{r}_1 \mu, \mathbf{r}_2 \mu) = & \left(\frac{r_{>}^2 \mu^2 e^{\frac{5}{3}}}{4} \right)^u \left\{ \frac{\Gamma(1-u)}{\Gamma(1+u)} \right. \\ & + \sum_{n=1}^{\infty} (-1)^{n+1} (\xi^2)^n \frac{\Gamma(1-u+n)}{n \Gamma^2(n) \Gamma(1+u-n)} (\Psi(1+n) + \Psi(n) - \ln \xi^2) \\ & \left. + \sum_{n=1}^{\infty} (-1)^{n+1} (\xi^2)^n \frac{2 \frac{d}{du} \Gamma(1-u+n) + \Gamma(n-u)}{n \Gamma^2(n) \Gamma(1+u-n)} \right\} \quad (122a) \end{aligned}$$

$$\begin{aligned} \mathcal{K}_{\mathbf{xzy}} B^L(u, \mathbf{r}_1 \mu, \mathbf{r}_2 \mu) = & - \frac{1}{r_{>}^2} \left(\frac{\mu^2 r_{>}^2 e^{\frac{5}{3}}}{4} \right)^u \sum_{n=0}^{\infty} \frac{(\xi^2)^n}{(-1)^n \Gamma(u-n) (\Gamma(n+1))^2} \\ & \times \left[\Gamma(n+1-u) (\ln(\xi^2) + 2\psi(n+1)) + 2 \frac{d}{du} \Gamma(n+1-u) \right] \quad (122b) \end{aligned}$$

The double pole contributions arise from factor $\frac{d}{du}\Gamma(1-u+n)$ and as such they can be converted into single poles under the Borel integral by a partial integration in the expression for R , Eq. (64). For this, we note that boundary terms of the partial integration in (64) vanish to display the results separately for R^T and R^L as

$$\begin{aligned}
R^T(\mathbf{r}_1\Lambda, \mathbf{r}_2\Lambda,) &= \frac{1}{\beta_0} \int_0^\infty du T(u) \left(\frac{\mu^2}{\Lambda^2}\right)^{-u} B^T(u, \mathbf{r}_1\mu, \mathbf{r}_2\mu) \\
&= \frac{1}{\beta_0} \int_0^\infty du T(u) \left(\frac{4e^{-\frac{5}{3}}}{r_{>}^2\Lambda^2}\right)^{-u} \left\{ \frac{\Gamma(1-u)}{\Gamma(1+u)} \right. \\
&\quad + \sum_{k=1}^\infty (-1)^{k+1} \frac{(\xi^2)^k}{k\Gamma^2(k)} \left[\frac{\Gamma(1-u+k)}{\Gamma(1+u-k)} (\Psi(1+k) + \Psi(k) - \ln \xi^2) + \frac{\Gamma(k-u)}{\Gamma(1+u-k)} \right. \\
&\quad \left. \left. + \frac{2\Gamma(1-u+k)}{\Gamma(1+u-k)} \left(\ln \left(\frac{4e^{-\frac{5}{3}}}{r_{>}^2\Lambda^2} \right) - \frac{T'(u)}{T(u)} + \Psi(1+u-k) \right) \right] \right\} \quad (123a)
\end{aligned}$$

and

$$\begin{aligned}
\mathcal{K}_{\mathbf{xzy}} R^L(\mathbf{r}_1\Lambda, \mathbf{r}_2\Lambda,) &= \frac{1}{\beta_0} \int_0^\infty du T(u) \left(\frac{\mu^2}{\Lambda^2}\right)^{-u} \mathcal{K}_{\mathbf{xzy}} B^L(u, \mathbf{r}_1\mu, \mathbf{r}_2\mu) \\
&= -\frac{1}{\beta_0} \int_0^\infty du T(u) \frac{1}{r_{>}^2} \left(\frac{4e^{-\frac{5}{3}}}{r_{>}^2\Lambda^2}\right)^{-u} \sum_{n=0}^\infty \frac{\Gamma(n+1-u) (\xi^2)^n}{(-1)^n \Gamma(u-n) (\Gamma(n+1))^2} \\
&\quad \times \left[\ln(\xi^2) - 2\psi(n+1) + 2 \left(\ln \left(\frac{4e^{-\frac{5}{3}}}{r_{>}^2\Lambda^2} \right) - \frac{T'(u)}{T(u)} - \psi(u-n) \right) \right]. \quad (123b)
\end{aligned}$$

- The single pole expressions given above converge only very slowly near $\xi = 1$. To circumvent this we also present single pole expressions based on (72b) and (74b). For the transverse contributions we write

$$\begin{aligned}
R^T(\mathbf{r}_1\Lambda, \mathbf{r}_2\Lambda,) &= \frac{1}{\beta_0} \int_0^\infty du T(u) \left(\frac{\mu^2}{\Lambda^2}\right)^{-u} B^T(u, \mathbf{r}_1\mu, \mathbf{r}_2\mu) \\
&= \frac{1}{\beta_0} \int_0^\infty du T(u) \left\{ \left(\frac{\mu^2}{\Lambda^2}\right)^{-u} B^T(u, \mathbf{r}_1\mu, \mathbf{r}_2\mu) - \left[\left(\frac{\mu^2}{\Lambda^2}\right)^{-u} B^T(u, \mathbf{r}_1\mu, \mathbf{r}_2\mu) \right]_{\text{double pole}} \right\} \\
&\quad + \frac{1}{\beta_0} \int_0^\infty du T(u) \left[\left(\frac{\mu^2}{\Lambda^2}\right)^{-u} B^T(u, \mathbf{r}_1\mu, \mathbf{r}_2\mu) \right]_{\text{double pole}} \quad (124a)
\end{aligned}$$

where B^T is taken from (72b) and the double pole part of the integrand is derived in Ap-

pendix C. It is given by

$$\left[\left(\frac{\mu^2}{\Lambda^2} \right)^{-u} B^T(u, \mathbf{r}_1\mu, \mathbf{r}_2\mu) \right]_{\text{double pole}} = \sum_{m=2}^{\infty} \sum_{n=2}^{m-1} \left(\frac{4e^{-\frac{5}{3}}}{r_{>}^2 \Lambda^2} \right)^{-m} \frac{(1-\xi^2)^n 2(-1)^{m-n}}{\Gamma(n+1) (u-m)^2} \times \frac{\Gamma(2m-(n+1))}{\Gamma(m)\Gamma(m-1)\Gamma(m-n)\Gamma(m+1-n)} \quad (124b)$$

The first term can now be integrated with a principal value prescription (it only contains single poles) while (for one loop running) the last term is given a meaning via integration by parts and gives only a boundary contribution. To this end we recall that for one loop running we may set $T(u) \rightarrow 1$, $T'(u) \rightarrow 0$ and identify $\ln(\mu^2/\Lambda^2) = \frac{\pi}{\beta_0 \alpha_s(\mu^2)}$:

$$\frac{1}{\beta_0} \int_0^{\infty} du T(u) \left[\left(\frac{\mu^2}{\Lambda^2} \right)^{-u} B^T(u, \mathbf{r}_1\mu, \mathbf{r}_2\mu) \right]_{\text{double pole}} \quad (124c)$$

$$\xrightarrow{T(u) \rightarrow 1} - \sum_{m=2}^{\infty} \sum_{n=2}^{m-1} \left(\frac{4e^{-\frac{5}{3}}}{r_{>}^2 \Lambda^2} \right)^{-m} \frac{(1-\xi^2)^n 2(-1)^{m-n}}{\Gamma(n+1) m} \frac{\Gamma(2m-(n+1))}{\Gamma(m)\Gamma(m-1)\Gamma(m-n)\Gamma(m+1-n)}$$

We have checked that this result matches with a very costly evaluation of R^T via (123). R^L can be treated analogously

$$R^L(\mathbf{r}_1\Lambda, \mathbf{r}_2\Lambda,) = \frac{1}{\beta_0} \int_0^{\infty} du T(u) \left(\frac{\mu^2}{\Lambda^2} \right)^{-u} B^L(u, \mathbf{r}_1\mu, \mathbf{r}_2\mu)$$

$$= \frac{1}{\beta_0} \int_0^{\infty} du T(u) \left\{ \left(\frac{\mu^2}{\Lambda^2} \right)^{-u} B^L(u, \mathbf{r}_1\mu, \mathbf{r}_2\mu) - \left[\left(\frac{\mu^2}{\Lambda^2} \right)^{-u} B^L(u, \mathbf{r}_1\mu, \mathbf{r}_2\mu) \right]_{\text{double pole}} \right\}$$

$$+ \frac{1}{\beta_0} \int_0^{\infty} du T(u) \left[\left(\frac{\mu^2}{\Lambda^2} \right)^{-u} B^L(u, \mathbf{r}_1\mu, \mathbf{r}_2\mu) \right]_{\text{double pole}}, \quad (125a)$$

where now (see App. D)

$$\mathcal{K}_{\mathbf{xzy}} \left[\left(\frac{\mu^2}{\Lambda^2} \right)^{-u} B^L(u, \mathbf{r}_1\mu, \mathbf{r}_2\mu) \right]_{\text{double pole}} = - \sum_{m=1}^{\infty} \sum_{n=0}^{m-1} \frac{2(-1)^{m-n} (1-\xi^2)^n}{(u-m)^2 \Gamma(n+1)} \frac{1}{r_{>}^2} \left(\frac{4e^{-\frac{5}{3}}}{r_{>}^2 \Lambda^2} \right)^{-m} \times \frac{\Gamma(2m-(n+1))}{(\Gamma(m))^2 (\Gamma(m-n))^2} \quad (125b)$$

and to one loop accuracy

$$\begin{aligned} \mathcal{K}_{xyz} \frac{1}{\beta_0} \int_0^\infty du T(u) \left[\left(\frac{\mu^2}{\Lambda^2} \right)^{-u} B^L(u, \mathbf{r}_1 \mu, \mathbf{r}_2 \mu) \right]_{\text{double pole}} \\ \xrightarrow{T(u) \rightarrow 0} + \sum_{m=1}^\infty \sum_{n=0}^{m-1} \frac{2(-1)^{m-n} (1-\xi^2)^n}{m} \frac{1}{\Gamma(n+1)} \frac{1}{r_{>}^2} \left(\frac{4e^{-\frac{5}{3}}}{r_{>}^2 \Lambda^2} \right)^{-m} \frac{\Gamma(2m - (n+1))}{(\Gamma(m))^2 (\Gamma(m-n))^2}. \end{aligned} \quad (125c)$$

The expressions on the r.h.s. of all the Borel integrals shown in this section are in general well defined with any arbitrary contour connecting 0 to ∞ in the complex plane that avoids the poles of the integrand on the real axis. All such expressions share the same perturbative expansion (be they partially integrated or not!). The uncertainty introduced by this freedom of choice in the contour is qualitatively determined by the size of residues of these poles. An important consistency condition for using the partially integrated version to study non-perturbative corrections is therefore that the residues of the integrand remain the same as in the original version (64). This is a generic consequence of the fact that $\Gamma(2-u+k)$ (the function contributing the poles) has no logarithmic terms in its Laurent expansions. Appendices C and D contain an explicit discussion of the pole part of B^T and B^L .

References

- [1] L. D. McLerran and R. Venugopalan, *Computing quark and gluon distribution functions for very large nuclei*, *Phys. Rev.* **D49** (1994) 2233–2241, [[hep-ph/9309289](#)].
- [2] L. D. McLerran and R. Venugopalan, *Gluon distribution functions for very large nuclei at small transverse momentum*, *Phys. Rev.* **D49** (1994) 3352–3355, [[hep-ph/9311205](#)].
- [3] L. D. McLerran and R. Venugopalan, *Green's functions in the color field of a large nucleus*, *Phys. Rev.* **D50** (1994) 2225–2233, [[hep-ph/9402335](#)].
- [4] Y. V. Kovchegov, *Non-abelian Weizsaecker-Williams field and a two-dimensional effective color charge density for a very large nucleus*, *Phys. Rev.* **D54** (1996) 5463–5469, [[hep-ph/9605446](#)].
- [5] Y. V. Kovchegov, *Quantum structure of the non-abelian Weizsaecker-Williams field for a very large nucleus*, *Phys. Rev.* **D55** (1997) 5445–5455, [[hep-ph/9701229](#)].
- [6] J. Jalilian-Marian, A. Kovner, L. D. McLerran, and H. Weigert, *The intrinsic glue distribution at very small x* , *Phys. Rev.* **D55** (1997) 5414–5428, [[hep-ph/9606337](#)].
- [7] C. S. Lam and G. Mahlon, *Color neutrality and the gluon distribution in a very large nucleus*, *Phys. Rev.* **D61** (2000) 014005, [[hep-ph/9907281](#)].
- [8] C. S. Lam and G. Mahlon, *Longitudinal resolution in a large relativistic nucleus: Adding a dimension to the mclerran-venugopalan model*, *Phys. Rev.* **D62** (2000) 114023, [[hep-ph/0007133](#)].

- [9] C. S. Lam and G. Mahlon, *Non-gaussian correlations in the McLerran-venugopalan model*, *Phys. Rev.* **D64** (2001) 016004, [[hep-ph/0102337](#)].
- [10] Y. Y. Balitsky and L. N. Lipatov *Sov. J. Nucl. Phys.* **28** (1978) 822.
- [11] L. N. Lipatov *Sov. J. Nucl. Phys.* **23** (1976) 642.
- [12] E. A. Kuraev, L. N. Lipatov, and V. S. Fadin, *Multi - reggeon processes in the yang-mills theory*, *Sov. Phys. JETP* **44** (1976) 443–450.
- [13] E. A. Kuraev, L. N. Lipatov, and V. S. Fadin, *The Pommeranchuk singularity in non-Abelian gauge theories*, *Sov. Phys. JETP* **45** (1977) 199–204.
- [14] L. N. Lipatov *Sov. Phys. JETP* **63** (1986) 904.
- [15] J. Jalilian-Marian, A. Kovner, A. Leonidov, and H. Weigert, *The BFKL equation from the Wilson renormalization group*, *Nucl. Phys.* **B504** (1997) 415–431, [[hep-ph/9701284](#)].
- [16] J. Jalilian-Marian, A. Kovner, A. Leonidov, and H. Weigert, *The Wilson renormalization group for low x physics: Towards the high density regime*, *Phys. Rev.* **D59** (1999) 014014, [[hep-ph/9706377](#)].
- [17] J. Jalilian-Marian, A. Kovner, and H. Weigert, *The Wilson renormalization group for low x physics: Gluon evolution at finite parton density*, *Phys. Rev.* **D59** (1999) 014015, [[hep-ph/9709432](#)].
- [18] J. Jalilian-Marian, A. Kovner, A. Leonidov, and H. Weigert, *Unitarization of gluon distribution in the doubly logarithmic regime at high density*, *Phys. Rev.* **D59** (1999) 034007, [[hep-ph/9807462](#)].
- [19] A. Kovner, J. G. Milhano, and H. Weigert, *Relating different approaches to nonlinear QCD evolution at finite gluon density*, *Phys. Rev.* **D62** (2000) 114005, [[hep-ph/0004014](#)].
- [20] H. Weigert, *Unitarity at small Bjorken x* , *Nucl. Phys.* **A703** (2002) 823–860, [[hep-ph/0004044](#)].
- [21] E. Iancu, A. Leonidov, and L. D. McLerran, *Nonlinear gluon evolution in the color glass condensate. I*, *Nucl. Phys.* **A692** (2001) 583–645, [[hep-ph/0011241](#)].
- [22] E. Ferreiro, E. Iancu, A. Leonidov, and L. McLerran, *Nonlinear gluon evolution in the color glass condensate. II*, *Nucl. Phys.* **A703** (2002) 489–538, [[hep-ph/0109115](#)].
- [23] I. Balitsky, *Operator expansion for high-energy scattering*, *Nucl. Phys.* **B463** (1996) 99–160, [[hep-ph/9509348](#)].
- [24] I. Balitsky, *Operator expansion for diffractive high-energy scattering*, [hep-ph/9706411](#).
- [25] I. Balitsky, *Factorization and high-energy effective action*, *Phys. Rev.* **D60** (1999) 014020, [[hep-ph/9812311](#)].
- [26] Y. V. Kovchegov, *Small- x F_2 structure function of a nucleus including multiple pomeron exchanges*, *Phys. Rev.* **D60** (1999) 034008, [[hep-ph/9901281](#)].

- [27] Y. V. Kovchegov, *Unitarization of the BFKL pomeron on a nucleus*, *Phys. Rev.* **D61** (2000) 074018, [[hep-ph/9905214](#)].
- [28] A. H. Mueller, *Soft gluons in the infinite momentum wave function and the BFKL pomeron*, *Nucl. Phys.* **B415** (1994) 373–385.
- [29] A. H. Mueller and B. Patel, *Single and double BFKL pomeron exchange and a dipole picture of high-energy hard processes*, *Nucl. Phys.* **B425** (1994) 471–488, [[hep-ph/9403256](#)].
- [30] A. H. Mueller, *Unitarity and the BFKL pomeron*, *Nucl. Phys.* **B437** (1995) 107–126, [[hep-ph/9408245](#)].
- [31] Z. Chen and A. H. Mueller, *The dipole picture of high-energy scattering, the BFKL equation and many gluon compound states*, *Nucl. Phys.* **B451** (1995) 579–604.
- [32] A. H. Mueller and G. P. Salam, *Large multiplicity fluctuations and saturation effects in onium collisions*, *Nucl. Phys.* **B475** (1996) 293–320, [[hep-ph/9605302](#)].
- [33] K. Golec-Biernat, L. Motyka, and A. M. Stasto, *Diffusion into infra-red and unitarization of the BFKL pomeron*, *Phys. Rev.* **D65** (2002) 074037, [[hep-ph/0110325](#)].
- [34] K. D. Anderson, D. A. Ross, and M. G. Sotiropoulos, *Running coupling and borel singularities at small x* , *Nucl. Phys.* **B515** (1998) 249–268, [[hep-ph/9705466](#)].
- [35] M. Ciafaloni and G. Camici, *Energy scale(s) and next-to-leading BFKL equation*, *Phys. Lett.* **B430** (1998) 349–354, [[hep-ph/9803389](#)].
- [36] V. S. Fadin and L. N. Lipatov, *BFKL pomeron in the next-to-leading approximation*, *Phys. Lett.* **B429** (1998) 127–134, [[hep-ph/9802290](#)].
- [37] Y. V. Kovchegov and A. H. Mueller, *Running coupling effects in BFKL evolution*, *Phys. Lett.* **B439** (1998) 428–436, [[hep-ph/9805208](#)].
- [38] S. J. Brodsky, V. S. Fadin, V. T. Kim, L. N. Lipatov, and G. B. Pivovarov, *The QCD pomeron with optimal renormalization*, *JETP Lett.* **70** (1999) 155–160, [[hep-ph/9901229](#)].
- [39] R. D. Ball and S. Forte, *All order running coupling BFKL evolution from GLAP (and vice-versa)*, *Nucl. Phys.* **B742** (2006) 158–175, [[hep-ph/0601049](#)].
- [40] G. Altarelli, R. D. Ball, and S. Forte, *Resummation of singlet parton evolution at small x* , *Nucl. Phys.* **B575** (2000) 313–329, [[hep-ph/9911273](#)].
- [41] M. Ciafaloni, D. Colferai, and G. P. Salam, *Renormalization group improved small- x equation*, *Phys. Rev.* **D60** (1999) 114036, [[hep-ph/9905566](#)].
- [42] M. Ciafaloni, D. Colferai, G. P. Salam, and A. M. Stasto, *Renormalisation group improved small- x green’s function*, *Phys. Rev.* **D68** (2003) 114003, [[hep-ph/0307188](#)].
- [43] R. S. Thorne, *The running coupling BFKL anomalous dimensions and splitting functions*, *Phys. Rev.* **D64** (2001) 074005, [[hep-ph/0103210](#)].
- [44] E. Iancu, K. Itakura, and S. Munier, *Saturation and BFKL dynamics in the hera data at small x* , *Phys. Lett.* **B590** (2004) 199–208, [[hep-ph/0310338](#)].

- [45] K. Rummukainen and H. Weigert, *Universal features of JIMWLK and BK evolution at small x* , *Nucl. Phys.* **A739** (2004) 183–226, [[hep-ph/0309306](#)].
- [46] I. I. Y. Bigi, M. A. Shifman, N. G. Uraltsev, and A. I. Vainshtein, *The pole mass of the heavy quark. Perturbation theory and beyond*, *Phys. Rev.* **D50** (1994) 2234–2246, [[hep-ph/9402360](#)].
- [47] B. H. Smith and M. B. Voloshin, *Normalization of QCD corrections in top quark decay*, *Phys. Lett.* **B340** (1994) 176–180, [[hep-ph/9405204](#)].
- [48] M. Beneke and V. M. Braun, *Naive nonAbelianization and resummation of fermion bubble chains*, *Phys. Lett.* **B348** (1995) 513–520, [[hep-ph/9411229](#)].
- [49] P. Ball, M. Beneke, and V. M. Braun, *Resummation of $(\beta_0\alpha_s)^n$ corrections in QCD: Techniques and applications to the τ hadronic width and the heavy quark pole mass*, *Nucl. Phys.* **B452** (1995) 563–625, [[hep-ph/9502300](#)].
- [50] Y. L. Dokshitzer, G. Marchesini, and B. R. Webber, *Dispersive Approach to Power-Behaved Contributions in QCD Hard Processes*, *Nucl. Phys.* **B469** (1996) 93–142, [[hep-ph/9512336](#)].
- [51] G. Grunberg, *On power corrections in the dispersive approach*, *JHEP* **11** (1998) 006, [[hep-ph/9807494](#)].
- [52] E. Gardi and G. Grunberg, *Power corrections in the single dressed gluon approximation: The average thrust as a case study*, *JHEP* **11** (1999) 016, [[hep-ph/9908458](#)].
- [53] E. Gardi, *Suppressed power corrections for moments of event-shape variables in e^+e^- annihilation*, *JHEP* **04** (2000) 030, [[hep-ph/0003179](#)].
- [54] M. Cacciari and E. Gardi, *Heavy-quark fragmentation*, *Nucl. Phys.* **B664** (2003) 299–340, [[hep-ph/0301047](#)].
- [55] E. Gardi and L. Magnea, *The C parameter distribution in e^+e^- annihilation*, *JHEP* **08** (2003) 030, [[hep-ph/0306094](#)].
- [56] I. I. Balitsky and A. V. Belitsky, *Nonlinear evolution in high-density QCD*, *Nucl. Phys.* **B629** (2002) 290–322, [[hep-ph/0110158](#)].
- [57] E. Gotsman, E. Levin, U. Maor, and E. Naftali, *A modified Balitsky-Kovchegov equation*, *Nucl. Phys.* **A750** (2005) 391–405, [[hep-ph/0411242](#)].
- [58] E. Iancu, A. Leonidov, and L. McLerran, *The colour glass condensate: An introduction*, [hep-ph/0202270](#).
- [59] E. Iancu and R. Venugopalan, *The color glass condensate and high energy scattering in QCD*, [hep-ph/0303204](#).
- [60] H. Weigert, *Evolution at small x_{bj} : The Color Glass Condensate*, *Prog. Part. Nucl. Phys.* **55** (2005) 461–565, [[hep-ph/0501087](#)].
- [61] J. Jalilian-Marian and Y. V. Kovchegov, *Saturation physics and deuteron gold collisions at RHIC*, *Prog. Part. Nucl. Phys.* **56** (2006) 104–231, [[hep-ph/0505052](#)].

- [62] K. Golec-Biernat and M. Wüsthoff, *Saturation effects in deep inelastic scattering at low Q^2 and its implications on diffraction*, *Phys. Rev.* **D59** (1999) 014017, [[hep-ph/9807513](#)].
- [63] K. Golec-Biernat and M. Wüsthoff, *Saturation in diffractive deep inelastic scattering*, *Phys. Rev.* **D60** (1999) 114023, [[hep-ph/9903358](#)].
- [64] A. M. Stasto, K. Golec-Biernat, and J. Kwiecinski, *Geometric scaling for the total γ^*p cross-section in the low x region*, *Phys. Rev. Lett.* **86** (2001) 596–599, [[hep-ph/0007192](#)].
- [65] R. Baier, A. Kovner, and U. A. Wiedemann, *Saturation and parton level Cronin effect: Enhancement vs suppression of gluon production in pA and AA collisions*, *Phys. Rev.* **D68** (2003) 054009, [[hep-ph/0305265](#)].
- [66] D. Kharzeev, Y. V. Kovchegov, and K. Tuchin, *Cronin effect and high- p_t suppression in pA collisions*, *Phys. Rev.* **D68** (2003) 094013, [[hep-ph/0307037](#)].
- [67] J. Jalilian-Marian, Y. Nara, and R. Venugopalan, *The cronin effect, quantum evolution and the color glass condensate*, *Phys. Lett.* **B577** (2003) 54–60, [[nucl-th/0307022](#)].
- [68] J. L. Albacete, N. Armesto, A. Kovner, C. A. Salgado, and U. A. Wiedemann, *Energy dependence of the Cronin effect from non-linear QCD evolution*, *Phys. Rev. Lett.* **92** (2004) 082001, [[hep-ph/0307179](#)].
- [69] **BRAHMS** Collaboration, I. Arsene *et. al.*, *On the evolution of the nuclear modification factors with rapidity and centrality in $d + Au$ collisions at $\sqrt{s_{NN}} = 200\text{ GeV}$* , [nucl-ex/0403005](#).
- [70] M. Hentschinski, H. Weigert, and A. Schafer, *Extension of the color glass condensate approach to diffractive reactions*, *Phys. Rev.* **D73** (2006) 051501, [[hep-ph/0509272](#)].
- [71] V. M. Braun, G. P. Korchemsky, and D. Mueller, *The uses of conformal symmetry in QCD*, *Prog. Part. Nucl. Phys.* **51** (2003) 311–398, [[hep-ph/0306057](#)].
- [72] M. Braun, *Structure function of the nucleus in the perturbative QCD with $N_c \rightarrow \infty$ (BFKL pomeron fan diagrams)*, *Eur. Phys. J.* **C16** (2000) 337–347, [[hep-ph/0001268](#)].
- [73] M. A. Kimber, J. Kwiecinski, and A. D. Martin, *Gluon shadowing in the low x region probed by the LHC*, *Phys. Lett.* **B508** (2001) 58–64, [[hep-ph/0101099](#)].
- [74] N. Armesto and M. A. Braun, *Parton densities and dipole cross-sections at small x in large nuclei*, *Eur. Phys. J.* **C20** (2001) 517–522, [[hep-ph/0104038](#)].
- [75] E. Levin and M. Lublinsky, *Parton densities and saturation scale from non-linear evolution in dis on nuclei*, *Nucl. Phys.* **A696** (2001) 833–850, [[hep-ph/0104108](#)].
- [76] M. Lublinsky, *Scaling phenomena from non-linear evolution in high energy DIS*, *Eur. Phys. J.* **C21** (2001) 513–519, [[hep-ph/0106112](#)].
- [77] J. L. Albacete, N. Armesto, J. G. Milhano, C. A. Salgado, and U. A. Wiedemann, *Numerical analysis of the Balitsky-Kovchegov equation with running coupling: Dependence of the saturation scale on nuclear size and rapidity*, [hep-ph/0408216](#).

- [78] A. H. Mueller and D. N. Triantafyllopoulos, *The energy dependence of the saturation momentum*, *Nucl. Phys.* **B640** (2002) 331–350, [[hep-ph/0205167](#)].
- [79] E. Iancu, K. Itakura, and L. McLerran, *Geometric scaling above the saturation scale*, *Nucl. Phys.* **A708** (2002) 327–352, [[hep-ph/0203137](#)].
- [80] S. J. Brodsky, G. P. Lepage, and P. B. Mackenzie, *On the elimination of scale ambiguities in perturbative quantum chromodynamics*, *Phys. Rev.* **D28** (1983) 228.
- [81] S. J. Brodsky, J. R. Ellis, E. Gardi, M. Karliner, and M. A. Samuel, *Pade approximants, optimal renormalization scales, and momentum flow in Feynman diagrams*, *Phys. Rev.* **D56** (1997) 6980–6992, [[hep-ph/9706467](#)].
- [82] S. J. Brodsky, E. Gardi, G. Grunberg, and J. Rathsmann, *Disentangling running coupling and conformal effects in QCD*, *Phys. Rev.* **D63** (2001) 094017, [[hep-ph/0002065](#)].
- [83] M. Neubert, *Scale setting in qcd and the momentum flow in feynman diagrams*, *Phys. Rev.* **D51** (1995) 5924–5941, [[hep-ph/9412265](#)].
- [84] Y. L. Dokshitzer, G. Marchesini, and B. R. Webber, *Dispersive approach to power-behaved contributions in QCD hard processes*, *Nucl. Phys.* **B469** (1996) 93–142, [[hep-ph/9512336](#)].
- [85] B. Lautrup, *On high order estimates in qed*, *Phys. Lett.* **B69** (1977) 109–111.
- [86] G. 't Hooft, *Can we make sense out of 'quantum chromodynamics'?*, . Lectures given at Int. School of Subnuclear Physics, Erice, Sicily, Jul 23 - Aug 10, 1977.
- [87] A. H. Mueller, *On the structure of infrared renormalons in physical processes at high-energies*, *Nucl. Phys.* **B250** (1985) 327.
- [88] G. Parisi, *Singularities of the borel transform in renormalizable theories*, *Phys. Lett.* **B76** (1978) 65–66.
- [89] F. David, *On the ambiguity of composite operators, I.R. renormalons and the status of the operator product expansion*, *Nucl. Phys.* **B234** (1984) 237–251.
- [90] V. I. Zakharov, *QCD perturbative expansions in large orders*, *Nucl. Phys.* **B385** (1992) 452–480.
- [91] M. Beneke, *Renormalons*, *Phys. Rept.* **317** (1999) 1–142, [[hep-ph/9807443](#)].
- [92] M. Beneke and V. M. Braun, *Renormalons and power corrections*, [hep-ph/0010208](#).
- [93] G. Grunberg, *Renormalization group improved perturbative QCD*, *Phys. Lett.* **B95** (1980) 70.
- [94] G. Grunberg, *The Renormalization scheme invariant Borel transform and the QED renormalons*, *Phys. Lett.* **B304** (1993) 183–188.
- [95] E. Gardi and R. G. Roberts, *The interplay between Sudakov resummation, renormalons and higher twist in deep inelastic scattering*, *Nucl. Phys.* **B653** (2003) 227–255, [[hep-ph/0210429](#)].

- [96] E. Gardi, G. P. Korchemsky, D. A. Ross, and S. Tafat, *Power corrections in deep inelastic structure functions at large Bjorken x* , *Nucl. Phys.* **B636** (2002) 385–417, [[hep-ph/0203161](#)].
- [97] V. M. Braun, E. Gardi, and S. Gottwald, *Renormalon approach to higher-twist distribution amplitudes and the convergence of the conformal expansion*, *Nucl. Phys.* **B685** (2004) 171–226, [[hep-ph/0401158](#)].
- [98] M. Beneke and V. M. Braun, *Naive nonAbelianization and resummation of fermion bubble chains*, *Phys. Lett.* **B348** (1995) 513–520, [[hep-ph/9411229](#)].
- [99] E. Gardi, G. Grunberg, and M. Karliner, *Can the QCD running coupling have a causal analyticity structure?*, *JHEP* **07** (1998) 007, [[hep-ph/9806462](#)].
- [100] D. V. Shirkov and I. L. Solovtsov, *Analytic model for the QCD running coupling with universal $\bar{\alpha}_s(0)$ value*, *Phys. Rev. Lett.* **79** (1997) 1209–1212, [[hep-ph/9704333](#)].
- [101] J. R. Andersen and E. Gardi, *Taming the $B \rightarrow X_s \gamma$ spectrum by dressed gluon exponentiation*, *JHEP* **06** (2005) 030, [[hep-ph/0502159](#)].
- [102] A. Hebecker and H. Weigert, *Small- x parton distributions of large hadronic targets*, *Phys. Lett.* **B432** (1998) 215–221, [[hep-ph/9804217](#)].
- [103] Y. Kovchegov and H. Weigert, *Triumvirate of Running Couplings in Small- x Evolution*, *In preparation* (2006).
- [104] M. Abramowitz and I. A. Stegun, *Handbook of Mathematical Functions with Formulas, Graphs, and Mathematical Tables*. Dover, New York, ninth Dover printing, tenth GPO printing ed., 1964.
- [105] D. J. Broadhurst, *Large n expansion of qed: Asymptotic photon propagator and contributions to the muon anomaly, for any number of loops*, *Z. Phys.* **C58** (1993) 339–346.
- [106] C. N. Lovett-Turner and C. J. Maxwell, *All orders renormalon resummations for some QCD observables*, *Nucl. Phys.* **B452** (1995) 188–212, [[hep-ph/9505224](#)].
- [107] M. Y. Kalmykov, *Gauss hypergeometric function: Reduction, ϵ -expansion for integer/half-integer parameters and Feynman diagrams*, *JHEP* **04** (2006) 056, [[hep-th/0602028](#)].
- [108] E. Remiddi and J. A. M. Vermaseren, *Harmonic polylogarithms*, *Int. J. Mod. Phys.* **A15** (2000) 725–754, [[hep-ph/9905237](#)].
- [109] V. A. Smirnov, *Evaluating Feynman integrals*, . Berlin, Germany: Springer (2004) 244 p.